Three papers on Aeolian Sand Transport

Pages 2-32
A fully predictive model for aeolian sand transport
L.C. van Rijn, G. Strypsteen, 2020
Coastal Engineering Vol. 156, 103600

Pages 33-55
A fully predictive model for aeolian sand transport, Part 2: Description and calibration of models and effect of moisture and coarse materials
L.C. van Rijn, 2022
Coastal Engineering Vol. 171, 104052

Pages 56-78
A fully predictive model for aeolian sand transport, Part 3: Verification and application of model for natural beaches
L.C. van Rijn, 2022
Coastal Engineering Vol. 171, 104051

A FULLY PREDICTIVE MODEL FOR AEOLIAN SAND TRANSPORT

by L.C. van Rijn[1] and G. Strypsteen[2]
[1]LVRS-consultancy, Domineeswal 6, 8356D Blokzijl, The Netherlands; info@leovanrijn-sediment.com
[2]Construction TC, Dept. Of Civil Engineering, Bruges Campus, KU Leuven, Spoorwegstraat 12,
B-8200, Bruges, Belgium. glenn.strypsteen@kuleuven.be

Keywords: predictive model for wind-blown sand; supply-limiting effects on wind-blown sand

Abstract
This paper presents the development, calibration and verification of a fully predictive model for wind-blown dry sand. The model is based on the modification of the well-known Bagnold equation by including the threshold shear velocity, which is also slightly modified to ensure a smoother transition from the non-transport regime to the transport regime. The sand transport rate is related to the static and dynamic grain roughness by using a semi-empirical roughness predictor, which is calibrated based on sand transport data from wind tunnel experiments with a flat mobile sand surface. The model input for dry sand is the wind velocity at one height above the surface and the sand characteristics (d_{50}, d_{90}). The effects of moisture, vegetation and shells on the sand transport process are included by fairly simple expressions which are acting on the shear velocity, the threshold value and the transport rate. In all, 105 high-quality data sets have been used for verification of the proposed predictive model. About 73% of the predicted values are within a factor of 2 of measured values of the transport rate.

1 Introduction

Restoration and maintenance of coastal beach and dune systems require knowledge of aeolian transport processes for the prediction of the system response to wind forces over short to long-term time scales. Accurate aeolian sand transport equations are of utmost importance for modern geomorphology and coastal engineering practices.
Many aeolian equations are available for the prediction of the transport of loose grains along a surface of dry and clean sand without vegetation. Extensive overviews have been given by Nickling and Davidson-Arnott (1990), Kok et al. (2012) and Valance et al. (2015). Most equations are strongly dependent on the bed-shear velocity (u_*) to the power 2 or 3 and to lesser extent on the grain size and composition. One or more empirical coefficients are included based on calibration using data from wind tunnel and field experiments. Although sand transport by wind is easily observable, reliable and accurate data sets of sand transport rates are still scarcely available due to measuring difficulties. Mostly, relatively simple mechanical trapping systems are being used, but reported efficiencies are often below 50%, differing from site to site and sometimes even unknown (Sherman et al., 2014). Hence, corrections are not always possible resulting in biased calibration data. Using such data sets imply that the calibrated models are inadequate yielding poor model performance.
Sherman et al. (1998, 2013) have shown that many models substantially overpredict the measured sand transport rates of high-quality data sets. Similar results were obtained by Horikawa et al. 1986; Dong et al., 2002 and Liu et al., 2006.
Reasons for discrepancies are discussed in detail by Sherman et al. (2013). Important sources of error are the grain size and composition of the bed (uniform versus graded), horizontally non-uniform sand surface conditions related to grain size, relief, crusting and shells, moisture variations and saturation length scales. However, the major source of error most likely is the bed-shear velocity and associated bed roughness height. This latter parameter consists of several contributions, being the static and dynamic grain roughness, form-related roughness if bed forms (ripples) are present and roughness of isolated elements resting on the surface (shells, pebbles, stones, etc). It is common practice to determine the bed shear velocity from the slope of measured velocity profile data using κ=0.4 (Von Karman coefficient). These shear velocities may be significantly too large

as discussed by Li et al. (2010). High concentrations of saltating particles may lead to the damping of turbulence which can be expressed as a reduction of the κ-coefficient (range of 0.25 to 0.4 based on Li et al., 2010). Similar effects have been extensively observed and described for sediment-laden water flows (Van Rijn 1993). Taking this effect into account, the bed-shear velocities are substantially reduced resulting in smaller predicted sand transport rates (less over-prediction, Sherman et al., 2013). A problem of the methods proposed by Li et al. (2010) and Sherman et al. (2013) is that the modified κ-coefficient is related to the sand transport rate, which is a priori unknown and thus requiring iterative computations. Another problem of the model application proposed by Sherman et al. (2013) is the use of measured bed-shear velocities requiring detailed wind velocity measurements at different levels above the sand surface. Most accurate estimates of the bed-shear velocity even require the use of sophisticated anemometers to measure the instantaneous horizontal and vertical wind velocity components to derive the Reynold stress term. As such, this method is in no way predictive. In principle for engineering practices, it must be possible to get a reasonable estimate of the aeolian stand transport rates at a particular site based on wind velocity data from a nearby meteorological station and available grain size data from local samples.

This paper describes the development of a fully predictive sand transport equation (Section2) based on the work of Bagnold (1936, 1941) in combination with a roughness predictor (Section 3) to achieve a 'best practice' engineering model for wind-blown sand. High-quality data sets have been used for model calibration and verification of the proposed model (Sections 4). The effects of moisture, shells and vegetation is extensively studied to derive simple coefficients for the predictive transport model (Section 5). Applications of the model for sand transport at the beach parallel to the shoreline and normal to the dune crest are given in Section 6.

2. Sand transport model for saturated conditions

2.1 Modified Bagnold-equation for sand transport

Sand transport commences as soon as the threshold shear velocity is exceeded. Bagnold (1941), Kok et al. (2012) and Valance et al. (2015) and many others have discussed the dominant modes of wind-blown transport. The transport of sand particles in the size range of 100 to 500 μm is dominated by the saltation type of transport (small ballistic type of hops). Very small particles (fine fraction) ranging from 63 to 100 μm are transported in suspension by turbulent eddies. The largest particles (coarse fraction) ranging from 500 to 2000 μm are transported by sliding and rolling as surface creep. The combined transport of particles by rolling, sliding and small hops (saltations) can be defined as bed load transport of particles in more or less continuous contacts with the bed. Bed load transport of particles in a thin transport layer is the dominant mode of wind-blown transport for sand particles (100 to 300 μm). Observations in wind tunnels and in nature show that most of the transport occurs in a thin layer (< 0.05 m) above the sand surface (Ho, 2012). In this thin transport layer, the particle velocity (averaged over the layer thickness) is almost insensitive to the external wind velocity above the transport layer and is approximately equal to 3 to 4 times the critical bed shear velocity ($u_p \cong$ 3 to 4 $u_{*,th}$). Particle concentration is so high that the wind velocity is strongly reduced to a value of the order of 0.8 to 1.2 m/s (Kok et al., 2012). An increase of the wind velocity results in an increase of the particle concentration which in turn leads to a decrease of the wind flow speed close to the bed such that the new equilibrium particle velocity remains almost unchanged (Valance et al., 2015).

Above the saltation layer, the suspended particle concentrations are smaller and the air flow is almost unaffected by the presence of the particles. As a result, the particle velocity above the saltation layer increases with increasing wind velocity (Valence et al., 2016).

Many researchers have proposed models for aeolian sand transport under ideal conditions with uniform and steady wind obeying the law of the wall; with almost uniform (size, composition) and dry sand on a horizontal sand surface without vegetation and other obstacles. Uncertainties related to non-ideal conditions as present at field sites are discussed by Sherman et al. (2013). One of the first models for ideal conditions has been formulated by Bagnold (1936) and is most widely used. Sherman et al. (1998, 2013), Strypsteen (2019) and Strypsteen et al. (2019) have shown that the Bagnold-model performs reasonably well in predicting sand transport of high-quality

data sets, but the original equation tends to systematically overpredict (factor 2 to 3). This can be improved by the inclusion of a threshold value. Herein, only the Bagnold-model with minor modifications is proposed to be used as a predictive model.

In most general form, the sand transport in both water and air can be described as: $\phi = \alpha\ D_*^{\beta}\ (\theta-\theta_{th})^{\gamma}$ with $\phi = q_s/[\rho_s\ (s-1)^{0.5}\ g^{0.5}\ d_{50}^{1.5}]$= dimensionless sand transport; $D_* = [(s-1)g/\upsilon^2]^{1/3}\ d_{50}$= dimensionless grain size, and $\theta = u_*^2/[(s-1)gd_{50}]$= dimensionless shear stress; α, β and γ= coefficients.
Based on this, the modified Bagnold-equation for the transport of dry sand can be derived (see Strypsteen et al., 2019), which reads as:

Saturated/equilibrium transport: $q_{s,eq} = \alpha_B\ \alpha_{ad}\ \alpha_{shell}\ (d_{50}/d_{50,ref})^{0.5}\ (\rho_{air}/g)\ [(u_*)^3 - (u_{*,th})^3]$ (2.1)

Critical shear stress: $u_{*,th} = \alpha_w\ \alpha_{slope}\ u_{*,th,B}$ (2.2a)

$u_{*,th,B} = \alpha_{th}\ [(\rho_s/\rho_{air}-1)\ g\ d_{50}]^{0.5}$ for $d_{50} > 100\ \mu m$ (2.2b)

$u_{*,th,B} = \alpha_{th}\ u_{*,th,100\ um}$ for $32 < d_{50} < 100\ \mu m$ (2.2c)

Shear stress: $u_* = \kappa\ \alpha_{veg}\ u_w/\ln(30z_{wind}/k_s)$ (2.3)

with: $q_{s,eq}$ = mass flux of sediment at equilibrium conditions (saturated transport, kg/m/s); d_{50} = particle size (m); $d_{50,ref}$ =reference particle size = ($250\ 10^{-6}$ m; 250 μm); ρ_{air} = density of air ($\cong$1.2 kg/m^3); ρ_s = density of sediment ($\cong$2650 kg/m^3); $s=\rho_s/\rho_{air}$= relative density, υ=kinematic viscosity coefficient (m^2/s), g = acceleration of gravity (m/s^2); u_* = surface shear velocity due to wind forces (m/s); $u_{*,th}$=surface shear velocity at initiation of motion; threshold shear velocity (m/s); k_s= equivalent roughness length scale of Nikuradse (m); u_w = wind velocity at height z_{wind} above the surface (m/s); κ= constant of Von Karman (=0.4 for conditions without transport); α_B= Bagnold-coefficient for dry sand $\cong$ 1.5 for uniform sand; $\cong$1.8 for naturally graded sand; $\cong$2.8 for widely graded sand (Bagnold, 1941); herein the value of 2 is used as default value: α_B= 2; α_{ad}= adjustment coefficient related to fetch (maximum 1); α_{shell} = reduction coefficient related to the presence of shells; α_{th}= 0.11 based on data of Shao-Lu (2000) and Han et al. (2011); $\cong$ 0.1 based on Bagnold (1941); α_{slope} = coefficient for sand grains at a sloping surface; α_w= moisture coefficient (=1 for dry sand); α_{veg}= vegetation coefficient (=1 for conditions without vegetation). The effects of moisture (α_w), vegetation (α_{veg}), shells (α_{shell}) are discussed in Section 5. Strypsteen et al. (2019) have shown that the predictive ability of the modified Bagnold-equation (2.1) with α_B = 2 is excellent.

2.2 Threshold shear velocity

The value of the wind-induced stress at which saltation is initiated is known as the static fluid threshold shear stress. This threshold value depends not only on the properties of the fluid, but also on the gravitational and interparticle cohesion forces that oppose the fluid lifting. The fluid threshold is different from the dynamic or impact threshold, which is the lowest wind stress at which saltation can be sustained after it has been initiated. The impact threshold is smaller than the fluid threshold because the transfer of momentum to the surface through particle impacts is more efficient than through drag (Kok et al., 2012). Herein, only the dynamic threshold shear velocity based on Equation (2.2) is used with α_{th}= 0.11 based on data of Shao-Lu (2000) and Han et al. (2011) whereas $\alpha_{th} \cong 0.1$ based on Bagnold (1941). Experimental data (Kok et al., 2012) show that the measured threshold shear velocities of very fine sediments between 20 and 100 μm are scattered with values between 0.15 and 0.25 m/s. Equation (2.2b) underpredicts the measured threshold values of particles between 20 and 100 μm and therefore the shear velocity of fine sediment is herein assumed to be constant and equal to the threshold shear velocity of 100 μm-sand yielding a constant value of 0.16 m/s (Equation 2.2c).
When a grain is resting on a sloping surface (dune front), the threshold shear velocity is different from that on a horizontal surface. The threshold value increases for upsloping wind flow and decreases for downsloping wind flow. A simple and fairly accurate method is the method of Dey (2003), which has been slightly improved (Van

Rijn 2006): $\alpha_{slope}= u_{*,th,slope}/u_{*,th,B} = [(1+\beta/\varphi)^{0.75}(1+\gamma/\varphi)^{0.37}]^{0.5}$ with β=longitudinal slope angle (positive for upsloping wind flow), γ= lateral slope angle (positive for upsloping flow) and φ= angle of repose (see also Section 6).

2.3 Effect of shear velocity and grain size on sand transport

The results of the modified Bagnold equation based on equations (2.1 and 2.2) are compared to the measured sand transport rates for dry sand (three diameters:0.44, 0.3 and 0.145 mm, see Section 4.2) of the wind tunnel experiments of Belly (1964), see **Figure 2.1**. Using the default coefficient α_B=2 (other coefficients=1) and the measured shear velocities, the measured transport rates are underpredicted by a factor of about 1.5 for 0.44 mm-sand and 0.3 mm-sand and overpredicted by a factor of 1.5 for 0.145 mm-sand (Figure 2.1), which is a fairly good result for a sand transport predictor. It is noted that the original Bagnold model (1941) without the threshold-modification produces equally well results for the data set of Belly (1964). Bagnold(1954) proposed to use $(u_*-u_{*,th})^3$ as the driving term, but this yields transport values which are much too small (Strypsteen et al, 2019).

Equation (2.1) was also fitted to the three data sets by varying the α_B-coefficient resulting in α_B =3.5 (R^2=0.82) for 0.44 mm and 0.3 mm-sand and α_B =1.5 (R^2=0.9) for 0.145 mm-sand. This confirms that Equation (2.1) with default settings underpredicts for coarser sand (0.44 mm and 0.3 mm) and overpredicts for finer sand (0.145 mm).

To show that the cubic power relationship between transport and shear velocity is a reasonable approach, the function $q_{s,}= \alpha [(u_*)^3- (u_{*,th})^3]^{\beta}$ was fitted to three datasets resulting in β-values between 0.95 and 1.1 with $R^2 \cong 0.9$. This confirms that the cubic relationship (β=1) is a good approach.

The measured sand transport rates of the three sands with diameters of 0.44, 0.3 and 0.145 mm show that the transport rate of 0.3 mm is smaller than that of 0.44 mm-sand for u_*>0.5 m/s, but larger for u_*<0.5 m/s. The modified Bagnold equation shows a similar effect for u_*<0.45 m/s, but in a minor way. This effect with smaller and larger transport rates is caused by including the threshold shear velocity in Equation (2.1) and cannot be represented by the original Bagnold model without threshold parameter. The measured sand transport rates of 0.145 mm-sand are much smaller (factor 2 to 3) than those of 0.44 mm and 0.3 mm-sand. The decrease of the transport rate for decreasing grain size is also shown by the Bagnold equation, but the effect is too small for fine sand of 0.145 mm.

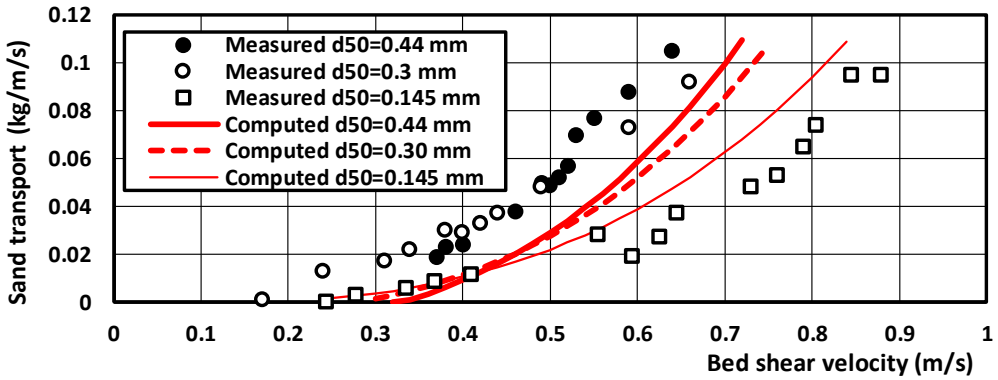

Figure 2.1 *Wind transport of dry, loose sand particles based on modified Bagnold-equation (α_B=2) for sand with d_{50}=0.44, 0.3 and 0.145 mm; data of Belly (1964)*

2.4 Adjustment length scale

Equilibrium sand transport may differ from the actual transport due to: i) limited fetch length and ii) horizontal variations of roughness, moisture, shells, vegetation and grain size/composition (see overview of Delgado-Fernandez, 2010). Fetch length (F_w) is the distance over which wind blows along the sand surface. Adjustment length (L_{ad}) is the distance which is required for approaching equilibrium (saturated) transport. This length scale is also known as the critical fetch length ($F_{w,cr}=L_{ad}$). When transport conditions change due to horizontal variation of sand and surface conditions, the transport rate adjusts/adapts to the new conditions within the adjustment

distance, which depends on the thickness of the sand transport layer, the wind speed and the mixing capacity (turbulence and roughness) and wind speed. Two types of upwind supply conditions are possible: underload or overload conditions. A typical example of underload conditions (supply-limited conditions) is the entrainment of sand by onshore wind at the lower beach (underload) as long as the fetch length is smaller than the adjustment length ($F_w<L_{ad}$). An example of overload conditions is the transition from an upwind site with a rough bed (high shear velocity) to a flat, smooth downwind surface (lower shear velocity) or the transition to a more sheltered site.

The adjustment length for dry sand conditions can be derived from laboratory and field experiments. Experiments in wind tunnels with dry, loose sand surfaces have shown that the transport layer including the saltation layer and the suspended layer is of the order of 0.1 to 0.5 m for low to high wind velocities and grain diameters between 0.2 and 0.45 mm. Most of the transport takes place in the near-bed layer of about 0.05 m (Han et al, 2011; Yang et al. 2019). The adjustment of the boundary layer flow over a rough surface can be described by $\delta \cong 0.2x^{0.6}$ (Granger et al., 2006). Hence, the adjustment length scale for the air flow to adjust over the height of the transport layer of δ=0.5 m is about 5 to 10 m. Given near-surface wind speeds of the order of 5 m/s, the adjustment time scale is about 1 to 2 s. Basically, the adjustment length scale to approach equilibrium conditions in air and in water (Van Rijn 1987) depends on the shear velocity (u_*), the particle diameter (d_{50}) or fall velocity (w_s) expressing the gravity effect and the thickness of the transport layer (δ_s). A classic problem in water is the adjustment of sand transport in a channel with a fine sand bed downstream of a rigid bed channel. The adjustment from zero transport at the entrance of the sand bed to the new equilibrium sand transport value takes about 50 to 100 times the water depth (Van Rijn 1987). Hence, a conservative estimate for sand transport in water and air is: L_{ad}=100 δ_s (Van Rijn 1987). The thickness of the transport layer (δ_s) in air is assumed to be equal to the saltation height of the sand particles and scales with the particle size (d_{50}), and the excess shear velocity ($u_*-u_{*,th}$). Based on analysis of the data of Yang et al. (2019), a tentative relationship similar to that for the saltation height in water (Van Rijn 1987) is:

$$\delta_{sal}=\alpha_s (d_{ref}/d_{50}^{0.5}) (u_*-u_{*,th})/g^{0.5} \quad (2.4)$$

with α_s =150 and d_{ref}=0.00025 m. Data are given in Table 2.1. Equation (2.1) has the correct dimension of length and shows a decreasing thickness of the transport layer for increasing particle size.

The adjustment length is:

$$L_{ad}=100\, f_{moist}\, \delta_{sal} = 1.5\, 10^4\, f_{moist}\, (d_{ref}/d_{50}^{0.5})(u_*-u_{*,th})/g^{0.5} \quad (2.5)$$

with: f_{moist}=moisture effect factor (f_{moist}=1 for dry sand and >1 for moist sand depending on the moisture content). Data of the adjustment length for dry sand conditions can be derived from the wind tunnel data of Han et al. (2012) and Yang et al. (2019); the field data of Davidson-Arnott et al. (2008) at a Canadian beach with sand of 0.26 mm; the field data of Jackson and Cooper (1999) at Benone beach, Northern Ireland and the data of Zhang et al. (2012) and Dong et al. (2012) in China deserts. The observed values are in the range of 10 to 100 m for dry sand. Table 2.1 shows computed and measured values of the saltation height and saturation length for a particle of 0.0003 m (0.3 mm) with threshold shear velocity $u_{*,th}$= 0.28 m/s.

Shear velocity u_* (m/s)	Saltation height δ_{sal} (m)		Saturation length L_{ad} (m)	
	Computed	Observed	computed	observed
0.4	0.08	0.1-0.2	8	≅10 (wind tunnel)
0.6	0.23	0.2-0.3	23	≅10-50
0.8	0.36	0.3-0.4	36	≅50-100 (field)

Table 2.1 *Saltation height and saturation length for dry sand particles of 0.3 mm*

Equilibrium sand transport conditions also depend on various limiting effects (small or wide grain size composition; moisture content; armor effects). The equilibrium transport of moist sand is smaller than that of

dry sand (see α_w-coefficient of Equation 2.2a). Similarly, the adjustment length scale for dry sand conditions is different from that for moist sand conditions (f_{moist}> 1). The moisture effect factor (f_{moist}) is unknown at present, but is most likely of the order of 1.5 to 2. Research on this is highly recommended. A consequence of this detailed approach is that the behavior of the limiting factors must be part of the transport prediction model (process-based approach, see De Vries et al. (2014), De Vries and Hoonhout (2017) and Hoonhout and De Vries (2019).

A simple approach to deal with adjustment effects in overload and underload conditions is given by:

$$q_{s,x}=q_{s,eq,up} - (x/L_{ad})^{0.6} (q_{s,eq,up}- q_{s,eq,down}) \quad (2.6)$$

with: $q_{s,x}$= actual transport at location x, $q_{s,eq,up}$= equilibrium transport at upwind location (x=0) and $q_{s,eq,down}$= equilibrium transport at downwind location ($x=L_{ad}$). For underload conditions due to limited fetch ($x=L_{fetch}$ and $q_{s,eq,up}$=0), this yields: $q_{s,x}=\alpha_{ad}\, q_{s,eq,down}$ with $\alpha_{ad}= (L_{fetch}/L_{ad})^{0.6}$ and α_{ad} =1 for $L_{fetch} > L_{ad}$.
The power of the adjustment process is taken as 0.6 similar to that of air flow layer adjustment (Granger et al., 2006). The adjustment process proceeds in a progressive way; the sand transport is about 70% of the equilibrium value after 50% of the total adjustment length (L_{fetch}/L_{ad}=0.5). If the dry zone of the beach is wider than about 100 m, the adjustment coefficient can be safely neglected. Research is recommended to improve the proposed equations (2.4) and (2.5).

3. Effective bed roughness

3.1 Influencing parameters

The wind velocity in the near-bed region strongly depends on the effective or equivalent bed roughness (k_s) as defined by Nikuradse (Nikuradse 1933, Van Rijn 2011). This roughness length is defined as the equivalent grain roughness replacing any type of roughness yielding the same overall bed roughness (same velocity profile).
It is most logic to assume that the effective roughness (k_s) of the sandy beach surface is related to the:

- grain roughness effects of static and saltating particles (Owen, 1964; Farrell and Sherman, 2016; Field and Pelletier 2018);
- height of the micro bed morphology (ripples), (Pelletier and Field 2016, Field and Pelletier, 2018);
- size of shells or shell fragments/clusters which are sometimes abundantly available, particularly at nourished beaches.

The effective roughness length of an irregular sand surface is strongly related to the presence of flow separation, as controlled by the slopes, curvature and height of the irregularities. Bed irregularities generate additional near-bed turbulent velocity fluctuations (turbulence) enhancing sand transport. In areas with abundant sand supply, the height and wavelength of aeolian ripples may increase with increasing shear velocity and grain size. Little is known about the relative contribution of saltation processes and ripple formation to changes in roughness length (Field and Pelletier, 2018).
Most likely, the static and dynamic grain roughness are the most important components, but the role of form roughness is not yet fully clear. Both effects can be separated by the method of shear partitioning resulting in: $\tau=\tau^{/}+\tau^{//}$ with $\tau^{/}$= grain-related shear stress and $\tau^{//}$=form drag-related shear strss. Bed-load transport in water flow is mostly related to $\tau^{/}$, whereas suspended load transport is affected by both components ($\tau^{/}+\tau^{//}$).
The field data sets of Sherman et al. (2013), described as a data set closely approaching ideal conditions for dry and unvegetated sand, are herein used to determine the roughness required for perfect agreement of measured and computed sand transport rates using the modified Bagnold-equations (2.1) and (2.2) with α_B=2 and α_{th}=0.11 (and $\alpha_{ad}= \alpha_{shell}= \alpha_w=\alpha_v$=1). Thus, it is assumed that the Bagnold equation is perfect and that discrepancies are only related to the uncertainties of the bed-shear velocity. The bed shear velocity is computed by using: $u_*=\kappa u_w/\ln(30z/k_s)$ with: u_w= measured wind velocity at height z=2 m above the surface, κ=0.4 and $k_{s,perfect}$=roughness height giving perfect agreement of measured and computed sand transport rates. The $k_{s,perfect}$ values were determined by trial and error until perfect agreement of measured and computed transport rates is

obtained. This procedure was repeated using a smaller and larger transport coefficients α_B=1.5 and α_B=2.5 (range given by Bagnold) resulting in larger and smaller $k_{s,perfect}$ values (uncertainty range).

Figure 3.1 shows the ratio of the $k_{s,perfect}$ and $k_{s,measured}$ and the uncertainty range as function of the measured wind velocity at 2 m above the surface. Most values are smaller than 0.3, which suggest that the effective roughness required for sand transport is only a fraction of the overall roughness. When this effect is neglected and the overall roughness (measured shear velocity u_*) is used, the Bagnold-equation systematically overpredicts the measured sand transport rates of Sherman et al. (2013) by a factor of 2 to 5. Thus, most likely, the static and dynamic grain roughness (related to τ') rather than the overall roughness are the dominant components for sand transport, similar to that for sand transport by flowing water (Van Rijn 1993). In **Section 3.4** a roughness predictor will be derived for the static and dynamic grain roughness.

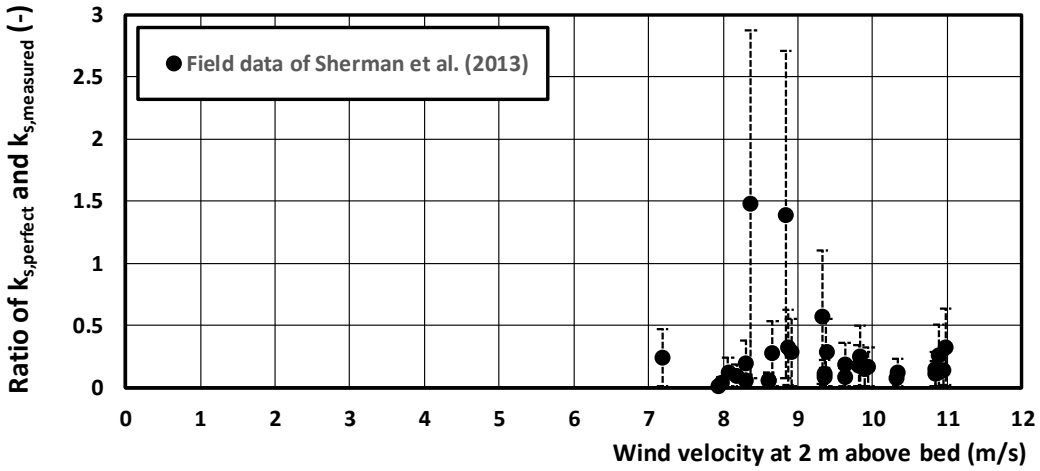

Figure 3.1 *Ratio of $k_{s,perfect}$ and $k_{s,measured}$ as function of the wind velocity*

3.2 Flat bed

Xian et al. (2002) studied the aerodynamic roughness length (z_o) values of various types of flat surfaces of coarse materials in a wind tunnel and in the Gobi desert in China. The desert surface is mostly flat, unvegetated and covered with gravel. The field results show that the effective bed roughness is of the order of 5 to 10d for the gravel-type surfaces and about 100d for sand-type surfaces with d= average height of roughness elements. The relatively large roughness values of the sand surfaces are most likely caused by the larger roughness elements (cobbles) resting on the bed. Wind tunnel experiments with various types of roughness elements were conducted. The main findings are: i) the effective bed roughness of crushed gravel, oblate shingle and cobblestone is related to largest diameter (d_{max}); ii) the roughness increases for increasing percentage of cover; iii) the shape of the roughness elements has not much effect on bed roughness.

Dong et al. (2002) performed wind tunnel experiments to determine the aerodynamic roughness length of spherical roughness elements of different size and cover at free-stream wind velocities in the range of 4 to 22 m/s. The aerodynamic roughness was found to increase with increasing cover values of 1% to 50 % and was about constant for cover values > 50%. If only a few isolated gravel particles are present (cover< 1%), the measured bed roughness is almost completely determined by the roughness of the surrounding bottom (cement floor).

Zhang et al. (2004) studied the surface roughness of cultivated soil by performing wind tunnel tests with five artificially prepared soil surfaces. Soil samples were taken from farmland in the semi-arid region of northwest China. The soil characteristics are: 36% sand, 53% silt and 11% clay. Five surface soil samples with depth of 15 cm were taken in tray-type sample boxes (50 cm × 30 cm × 15 cm). The diameters of the largest clods (D_{max}) were

in the range of 1.5 to 50 mm. The effective roughness of a flat bed with about 20% to 40% of large clods was found to be in the range of 0.4 to 1.3 D_{max}.

Summarizing the results of Xian et al. (2002), Dong et al. (2002) and Zhang et al. (2004), it can be concluded that the static bed roughness of a flat, horizontal bed is related to the largest diameters of the roughness elements (pebbles, gravel, sand) on the surface. In the case of a flat sandy surface, the d_{90} is a good measure to represent the roughness of the surface. This is also valid for a subaqueous sand surface (Van Rijn 1993). A few isolated extremely large roughness elements (cover < 1%) have almost no effect on the overall bed roughness.

3.3 Bed irregularities and bed forms

Owen (1964) has found that the effective bed roughness of natural sandy surfaces with small-scale bed irregularities can be represented by:

$$z_o=\alpha_o\, u_*^2/2g \quad \text{and} \quad k_s=30z_o=30\alpha_o\, u_*^2/2g \tag{3.1}$$

with: α_o= coefficient ($\cong$0.01). Thus, the bed roughness increases for increasing bed-shear velocity, either due to the increasing dynamic grain roughness (more saltating grains) and/or due to increasing bed forms (growing ripples). At very high wind velocities, the ripples will most likely disappear again (Belly, 1964).

Hsu (1974) analyzed various field data sets from a variety of environments with particles sizes between 0.2 and 0.3 mm, including those over beaches, tidal flats, and small dune fields in Barbados, Ecuador, Florida, and Texas and in the Libyan desert. Based on these results, he proposed:

$$u_*=0.037\, U_{10m} \text{ and } u_*=0.044\, U_{2m} \tag{3.2}$$

with: U_{2m}= wind velocity at z=2 m above bed and U_{10m}= wind velocity at z=10 m above bed.

Using: $U_{wind,z} = (u_*/\kappa)\ln(z/z_o)$ with κ=0.4 and z=2 m yields $U_{2m}/u_*=(1/\kappa)\ln(2/z_o)$ which is equivalent to

$$z_o=2/\exp(\kappa\, U_{2m}/u_*) \text{ or } k_s= 30z_o = 60/\exp(\kappa\, U_{2m}/u_*). \tag{3.3}$$

This gives: k_s= 0.0067 m (6.7 mm) for $u_*=0.044\, U_{2m}$ and κ=0.4. This roughness height of k_s=6.7 mm is much larger than the grain size of the beaches involved and is a measure of the thickness of the layer with intense sand transport producing roughness. As bed form data are not reported by Hsu, it is not clear whether the effect of bed forms on the bed roughness is very small or that bed forms were just absent.

Sherman (1992) and Sherman and Farrell (2008) proposed the following equation for natural sandy beds in wind tunnel and field conditions:

$$z_{o,dynamic}= z_{o,static} + (C_m/g)(u_*-u_{*,th})^2 \text{ and } k_{s,dynamic}= k_{s,static} + (30C_m/g)(u_*-u_{*,th})^2 \tag{3.4}$$

with: c_m=coefficient and $k_{s,static}= 2d_{50}$. They found $C_m \cong 0.012$ for wind tunnel data sets and $C_m \cong 0.13$ for field data sets. Limiting the maximum shear velocity u_* to less than 1.0 m/s, they found C_m = 0.023 for the wind tunnel data sets and $C_m \cong 0.15$ for the field data sets. Thus, the field and wind tunnel values are significantly different from each other by an order of magnitude. Field and Pelletier (2018) found C_m=0.063 based on their field data. Using: $C_m \cong 0.1$ for field sites, u_*=0.5 m/s and $u_{*,cr}$=0.25 m/s, it is found that $k_{s,dynamic} \cong$ 150 mm, which is so high that it can only be caused by form-related roughness. The precise types of beds are not described but most likely, the grain-related bed roughness is dominant in wind tunnel experiments, whereas the bed roughness in field conditions is dominated by small-scale bed forms (ripples).

Strypsteen et al. (2017) and Strypsteen (2019) measured wind velocities (8 points up to 2.5 m above the bed) in 2016 at two Belgian beaches Mariakerke and Koksijde with sand in the range of 0.2 to 0.35 mm. The beach of Mariakerke (d_{50}=0.31 mm) is somewhat flatter and contains some shell fragments due to regular nourishments, but the measurements were performed in in the dry upper beach zone with minor shells. The bed roughness derived from the velocity profile data is relatively small < 10 mm, as bed ripples were not present. The beach of Koksijde consists of sand (d_{50}=0.21 mm) with small-scale bed irregularities (ripples) and many shell hash and fragments with height of the order of 30 mm. The bed roughness is relatively high with values up to 100 mm due to the presence of bed ripples and patches of shells.

Lancaster and Baas (1998) measured the bed roughness of a smooth, bare, wind-rippled sand surface at the western part of the former delta of the Owen River in eastern California, USA. The surface sand at this site is coarse (median particle size of 500 to 1000 μm). The largest relief is of the order of 150 mm. Bed form dimensions are not given, but most likely the ripple heights are in the range of 50 to 100 mm. It was found that:

k_s= 27 mm for wind conditions below the threshold condition (no sand transport) and k_s= 38 mm for wind conditions with sand transport (saltating grains). These relatively large roughness values are most likely caused by the presence of bed forms.

Pelletier and Field (2016) studied the roughness length of the microtopography of desert-type surface (sites in southwestern US, 2015). The roughness length scale was quantified by the H_{RMSE}, the root-mean-squared values of the surface elevations, which varied in the range of 0.55 to 36 mm. The dominant wave lengths (0.03 to 3 m) were also measured and the average slope S_{av} was computed over a horizontal scale of 0.01 m. The surfaces (30x30 m) studied were predominantly crusted and devoid of vegetation. No sediment transport was present, not even during fast winds. Wind speeds were measured to determine the u_* and z_o-values. Herein, it is assumed that the height (Δ_{ib}=crest to trough height) of the dominant bed irregularities is about 3 H_{rmse}. Using $\Delta_{ib}=3H_{rmse}$, the ratio k_s/Δ_{ib} is found to be in the range of 0.04 to 7 depending on the bed slope/steepness. The effective bed roughness $k_{s,ib}$ of the irregular bed elevations can be represented by simple expressions, as follows:

Linear slope effect: $k_{s,ib}= 20\ \Delta_{ib}\ S$ (3.5a)

Quadratic slope effect: $k_{s,ib}= 150\ \Delta_{ib}\ S^2$ (3.5b)

with: Δ_{ib} = height of dominant bed irregularities; S= slope/steepness of dominant bed irregularities ($S \cong \Delta_{ib}/\lambda_{ib}$); λ_{ib} = length of dominant bed irregularities.

Equations (3.5a,b) are shown in **Figure 3.2**. As can be seen, the effective bed roughness of the irregular bed elevations is strongly dependent on the bed slope. For steep bed slopes of about 0.15, the effective bed roughness is of the order $k_{s,ib} \cong 5\Delta_{ib}$. Equation (3.5a) is the same as that for the flow of water over a rippled bed (see Van Rijn 1993).

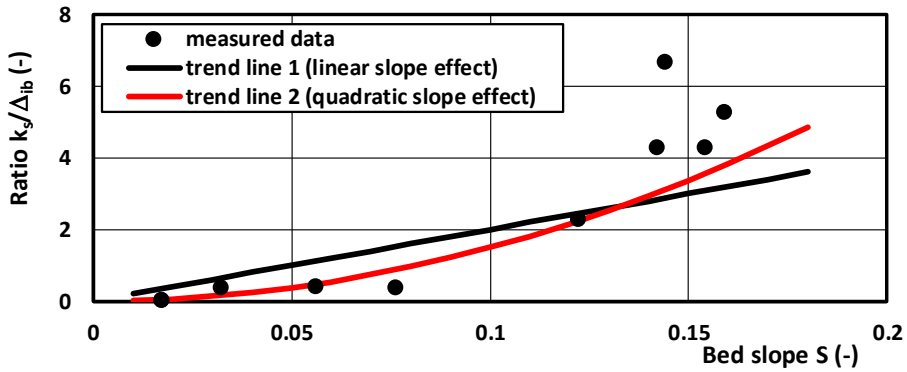

Figure 3.2 *Ratio of $k_{s,ib}/\Delta_{ib}$ as function of the bed slope S; data of Pelletier and Field (2016)*

Field and Pelletier (2018) studied the contributing effects of micro-morphology (ripples) and saltation-related grain roughness to the overall bed roughness. They report field measurements of z_o-values derived from velocity profiles measured over evolving sand ripples in field conditions (Salton Sea dune field near Salton City, California, USA). The ripple field had a bimodal grain-size distribution with the fine fraction ranging from 0.05 to 0.2 mm and the coarse fraction ranging from 0.5 to 1 mm. Wind speeds were close to or exceeded the saltation threshold during the three monitoring periods. The sand ripple height (Δ) and length (λ) were in the range $\Delta \cong$0.01-0.015 m; $\lambda \cong$0.15-0.35 m for smaller shear velocities of 0.2 to 0.3 m/s increasing to $\Delta \cong$0.015-0.03 m; $\lambda \cong$0.3-0.5 m for larger shear velocities of 0.3 to 0.6 m/s. The observations indicate that at low shear velocity ripples can maintain a fairly constant height and spacing while migrating downwind without further growth. The overall k_s-values derived from the data are roughly:

- k_s=0.5 to 5 mm for u_* <0.2 m/s (during conditions with static sand ripples and no saltation);
- k_s=1.5 to 15 mm for u_* =0.2 to 0.4 m/s (during conditions with saltation and evolving sand ripples);
- k_s= 5 to 50 mm for u_* = 0.4 to 0.6 m/s (during conditions with saltation and evolving sand ripples).

The roughness height during periods without saltation (u_*<0.2 m/s;) represents the static grain roughness plus the form roughness of the fairly regular and smooth sand ripples resulting in small roughness values. The measurements indicate that the k_s-values during periods of saltation are much greater (factor 3 or more) than

the values derived for conditions without saltation (static sand ripples). The maximum roughness values at the site with regular ripples of Field and Pelletier (2018) are up to 50 mm, where those of Pelletier and Field (2016) are up to 700 mm for a site with irregular bed forms. Hence, the form roughness of irregular bed forms may be substantially higher (**Figure 3.2**).

3.4 General roughness prediction model

The effective grain roughness of a flat (static) sand bed without any grain movement is related to the size of the largest particles (d_{90}). Van Rijn (1982) studied the effective roughness of flat sand beds in flumes and rivers. The effective bed roughness was found to be in the range of $k_{s,grain}$= 1 to 10 d_{90} with a mean value of $3d_{90}$. The relatively large experimental range expresses the effect of small irregularities related to preparation of laboratory beds. A perfectly flat bed in field conditions does hardly occur. Observations of flat beds often show the presence of small irregularities, isolated larger roughness elements (shells, stones, pebbles, cobbles, vegetation) or the presence of patches with finer and coarser materials in conditions with graded sediments.
Based on the available data (Xian et al. 2002; Dong et al. 2002; Zhang et al, 2004; van Rijn 1993), it is proposed to use $k_s=3d_{90}$ for static grain roughness of relatively fine sands (<0.5 mm) and $k_s=1d_{90}$ for coarse sand (>0.5 mm) and gravels.
The effective grain roughness of a flat, dynamic sand bed with significant sand transport as sheet flow is related to the thickness of the saltation or sheet flow layer, which increases for increasing wind velocities. Observations show that the transport layer is as high as about 0.5 m above the sand surface. However, most of the sand transport occurs in a layer with a thickness of about 50 mm (Yang et al. 2019). The effective roughness of a flat sand surface during conditions with intense sand transport in the upper wind regime is not precisely known, as no field data for this regime are available, but most likely the roughness will be related to the thickness of the saltation layer (10 to 50 mm). Winterwerp et al. (1990) studied the dynamic grain roughness in the upper flow regime with a plane fine sand bed in a water flume and flow velocities up to 2 m/s resulting in a dynamic grain roughness of about 10 mm ($\cong 30\ d_{90}$). Similar experiments have not yet been done for aeolian transport. Therefore, generally accepted relationships to describe the effective bed roughness of a flat dynamic sand bed in the upper transport regime are not yet available.
Small-scale bed forms (ripples) or bed irregularities with height scales of 0.01 to 0.1 m and length scales of 0.1 to 1 m are mostly generated in the lower wind regime (< 10 m/s) and are gradually smoothed out in the transitional (10 to 15 m/s) and upper wind regimes (> 15 m/s; Belly 1964). When ripples are present, the effective bed roughness (form roughness) increases significantly, depending on the height and steepness of the ripples.
The maximum effective bed roughness was found to be of the order of 5 times the bed form height (Pelletier and Field 2016). However, the data of Field and Pelletier (2018) show that the effect of form roughness is very minor with effective bed roughness values up to 50 mm. Based on the work of Owen (1964), Sherman and Farrell (2008) and Strypsteen (2019), the effective bed roughness (k_s) is in the range of 10 to 100 mm. As bed form information is lacking, it is not clear whether these roughness values are caused by the drag of saltating particles, the form drag of the bed forms or both. The form roughness of ripples leads to: i) smaller wind velocities in the near-bed layer, ii) larger shear velocities and iii) more turbulence (larger fluctuations). Larger shear velocities and more turbulence most likely lead to more saltating particles (larger concentrations), but smaller velocities lead to smaller transport rates. Overall, the sand transport may be slightly increased by the effect of form roughness (presence of ripples). Wind-driven sand transport is more intensively related to shear stresses acting on the static and dynamic grains and to lesser extent related to form drag, similar as in water flow (Van Rijn 1993).
A major drawback of the roughness predictors proposed by Owen (1964) and Sherman and Farrell (2008) is that the bed roughness (k_s) is related to the overall bed-shear velocity u_*, which depends on the bed roughness (k_s) itself. Hence, an iterative method is required to determine the k_s-value.

Herein, a simple and straightforward roughness predictor is proposed which primarily depends on the static and dynamic grain roughness parameters. Various transport regimes with different roughness parameters are distinguished based on the transport stage parameter T which is defined (see Van Rijn 1984, 1993) as the grain-

related bed-shear stress minus the threshold bed-shear stress divided by the threshold bed-shear stess: $T=(\tau_{grain,}-\tau_{th})/\tau_{th}$. The transport regimes and associated bed roughness parameters are:

- Premature transport stage with rolling, sliding and hopping particles (T<0.5): mostly static grain roughness related to the larger particles (d_{90}) of the sand surface;
- Lower transport stage with saltating particles and evolving bed ripples (0.5<T<1): dynamic grain roughness produced by small-scale vortices in the lee of the saltating particles due to the wind-particle velocity differences;
- Transitional transport stage with saltating particles and smoothed-out ripples (1<T<5): dynamic grain roughness in combination with gradually disappearing form-related roughness;
- Upper transport regime with a thin sheet flow layer of saltating particles in contact with the surface and suspended transport layer (T>5): dynamic grain roughness.

It is proposed to represent the effective bed roughness for sand transport in the lower, transitional and upper regime by the following expressions.

$$k_s = k_{s,ir} + k_{s,grain,\,st} + k_{s,grain,\,dyn} \quad (3.6a)$$

$$k_s = k_{s,ir} + d_{90} + \alpha_1\,\gamma_r\,d_{50}\,T^{\alpha 2} \quad (3.6b)$$

$$T = [(u_{*,grain,st})^2 - (u_{*,cr})^2]/(u_{*,cr})^2 \quad (3.6c)$$

$$u_{*,grain,st} = \kappa U_{w,z}/(\ln(30z_w/d_{90}) \quad (3.6d)$$

$$u_{*} = \alpha_{veg}\,\alpha_{slope}\,\kappa\,U_{w,z}/(\ln(30z_w/k_s) \quad (3.6e)$$

with: $k_{s,ir}$= roughness due to irregularities (shells, stones, etc) producing additional turbulence (m); T= transport stage parameter (-); $k_{s,grain,st}$= bed roughness height due to static grains (m); $k_{s,grain,dyn}$= bed roughness height due to dynamic grains (m); d_{90}= grain diameter (90% smaller); κ=0.4; α_1 and α_2= coefficients; γ_r = 1+1/T= ripple enhancement coefficient for the lower wind transport regime with values between 1 and 3 depending on the ripple steepness (-). The γ_r-coefficient is related to the T-parameter in a way that the effect reduces for increasing T-values as the ripples are gradually smoothed out. The default coefficients α_1 and α_2 are found to be α_1 = 15 and α_2= 1 for the data sets of Han et al. (2011) and Yang et al. (2019), see Section 4.3.

The d_{90} is roughly equal to d_{90}=2 to 3d_{50} for fairly uniform (narrow-graded) sand and may be as large as about d_{90}=10d_{50} for very wide-graded sand mixtures. When relatively large shells and other roughness elements are present on a flat sand bed, the effective roughness will increase considerably due to generation of extra turbulence depending on the size and cover of the roughness elements resulting in an increase of the sand transport capacity. The static roughness of shells may be in the range of 1 to 5 mm for small to large shells with a cover percentage of 5% to 10% (McKenna et al., 2012). The roughness of shells can be neglected for cover percentages < 5% (see Dong et al., 2002; McKenna et al., 2012). The bed roughness related to irregularities is most likely somewhat larger for coarse sand surfaces than for fine sand surfaces. Equation (3.6) produces dynamic grain roughness values in the range of 5 to 10 mm for wind speeds of 10 to 15 m/s, which is of the right order of magnitude compared to the field data of Davidson-Arnott et al. (2005) and Strypsteen (2019) for a flat bed without much irregularities (no shells, no ripples). Equation (3.6) is a first attempt to better describe the dynamic grain roughness related to the saltation process. Detailed experiments in wind tunnels are highly recommended to improve the coefficients involved. It is noted that the bed roughness for sand transport may be substantially smaller than the bed roughness for the large-scale wind flow which is dominantly affected by macro-scale bed features (dunes, objects, etc.).

4. Sand transport for saturated conditions based on predicted shear velocity

4.1 Roughness predictor

To compute the sand transport rate (Equation 2.1), the bed shear velocity (u_*) and thus the bed roughness height (k_s) are required as input parameters. If measured velocity profile data are available, these parameters can be derived from the measured data. However, the shear velocity derived from the slope of the measured velocity profile is not representative for sand transport if bed forms are present.

If only one wind velocity from a nearby weather station is available, the bed roughness parameter (k_s) and hence the effective shear velocity for sand transport must be predicted. Various expressions are available to predict the k_s-value (Equations 3.2 to 3.4). A major drawback of these equations is that the bed roughness (k_s) is related to u_*, which depends on the bed roughness (k_s) itself. Hence, an iterative method is required to determine the k_s-value. A non-iterative prediction method is given by Equation (3.6).

4.2 Data sets used

Various data sets (see **Table 4.1**) from wind tunnel experiments and field sites have been used for calibration and verification of the predictive model. Only data sets with fully-developed sand transport and shear velocities which are more than 5% larger than the threshold shear velocity have been selected ($u_* > 1.05\ u_{*,th}$). The data sets of Mariakerke contain some shell (< 5%), but this is neglected.

Data set	**Number of data points**	**Wind velocity (m/s)**	**Grain size**		**Roughness of irregularities $k_{s,ir}$ (mm)**
			d_{50} (mm)	**d_{90} (mm)**	
Wind tunnel experiments (Belly 1964)	36	5-12 z=0.3 m	0.44, 0.3, 0.145	$3d_{50}$	0
Wind tunnel experiments (Han et al. 2011)	6	10-20 z=0.6 m	0.203	$2d_{50}$	0
Wind tunnel experiments (Yang et al. 2019)	8	8-22 z=0.3 m	0.455	$2d_{50}$	0
Inch spit beach, Ireland (Sherman et al. 1998, 2013)	17	5-10 z=2 m	0.17	$3d_{50}$	1 (minor shell < 2%)
Esponsende site, North Portugal (Sherman et al., 2013)	12	10-14 z=2 m	0.27-0.35	$3d_{50}$	2
Jericoacoara site, 500 m from shoreline, north-eastern coast of Brazil (Sherman et al., 2013)	15	13-17 z=2 m	0.22-0.44	$3d_{50}$	2
Mariakerke beach Belgium (Strypsteen et al., 2019)	14	6-11 z=2 m	0.31	$3d_{50}$	2 (some shell < 5%)
Koksijde beach Belgium (Strypsteen et al., 2019)	11	8-12 z=2 m	0.22	$3d_{50}$	15 (many patches of shells and shell hash; 10%-15%)

Table 4.1 *Grain size and roughness input parameters of calibration and verification data*

Wind tunnel experiments USA by Belly (1964)

Belly (1964) has performed detailed wind tunnel experiments with sand diameters of 0.44, 0.3 and 0.145 mm. Sand transport rates were measured in tests with and without sand feed. The wind velocity was measured by a pitot tube mounted in the wind tunnel (length=30 m; width=1.2 m; height=0.8 m). The wind tunnel had a sand feed system at the entrance. The sand bed had a length of 20 m and thickness of about 0.05 m. Sand transport was measured by a trap sampler at the end of the sand bed. The sand transport data of Belly are given in tables for 0.44 mm-sand (26 data points) and 0.145 mm-sand (15 data points). The plots of Belly for 0.44 m-sand only shows 13 data points, which are herein used (extracted from the plots). The data for 0.3 mm-sand were also

extracted from plots (11 data points) given by Belly. The measured wind velocities for 0.3-mm sand are not given by Belly (1964), and have therefore been derived by the authors from the plot of u_* against $u_{wind,at\ 1\ foot}$ using the data of 0.455 mm-sand. Ripples were observed for wind velocities in the range of 7 to 10 m/s. Ripples were smoothed out for velocities > 10 m/s. The measured wind velocity at 0.3 m above the surface was used as input data for the Bagnold-equation.

Wind tunnel experiments China by Han et al. (2011)

Han et al. (2011) studied the effect of moisture content on sand transport in a wind tunnel (length=37m, width=1.2m, height=1.2 m). Sand trap measurements were done at the end of a sand tray with length of 4 m. The bed consisted of sand with d_{50}=0.203 mm. The sand trap (efficiency of 90% for particles >0.1 mm) had a height of 0.6 m and was sectionalized in 60 openings with height of 10 mm and width of 5 mm. The lowest opening was flush with the sand surface. The wind velocity was measured at z=0.6 m above the flat sand surface using a Pitot-tube method. The moisture content (ratio of mass of water and mass of dry sand x100%) of the sand bed was varied in the range of 0.14% to 2.7%. The moisture content of the sand bed was prepared just before the experiment using distilled water. Each experiment was run over only 90 s to prevent a change of the moisture content. Five bed surface samples were taken after each experiment to determine the moisture content again. The measured results show that most of the sand transport is taken place in a layer with height of about 0.2 to 0.5 m above the sand surface depending on the wind velocity (10 to 20 m/s). The moisture content (w) has almost no effect on the height of the transport layer. The sand transport rate is not affected by moisture for w<0.25%. These values for w<0.25% are used by the authors.

Wind tunnel experiments China by Yang et al. (2019)

Yang et al. (2019) studied the grain size distribution of the saltating particles for wind velocities in the range of 8 to 22 m/s. The sand used was typical dune sand collected from the southern margin of the Tengger Desert in China. The mean sand grain size is 0.455 mm. Before performing the wind-blown sand experiments, free-stream wind velocities were determined at a height of 0.3 m above the center line of the working section of the wind tunnel using a pitot tube. The sand beds were 1 m wide, 0.1 m deep and 8 m long, and this ensured that the sand flux was close to the saturation state at all measured wind velocities. The sand in the bed was replaced for each experiment. A segmented sand trap with height of 0.5 m was used to collect the sand grains in the saltation layer and was located on the center line at 12 m downward from the entrance of the working section of the tunnel. The duration of each experiment was in the range of 480 to 10 sec for the wind velocity range of 8 to 22 m/s.

Field experiments at Inch Spit beach in Ireland, Sherman et al. (1998)

The Inch Spit data were obtained along the beach and back beach profile seaward of the foredune in April 1994. The Inch site is part of a morphodynamically dissipative system in Dingle Bay, on the south-western coast of Ireland. Fetch distances perpendicular to the shoreline varied from 100 to almost 250 m, depending on the tide and wave conditions. Blowing sand was captured using Leatherman/Rosen type cylindrical traps with openings 40 mm wide and 450 mm high, and the bottom of the opening flush with the sand surface. The data used herein refer to the mean values of tower 1 and 2 (situated in the upper beach area with relatively dry sand without vegetation).

Field experiments at three sites of Sherman et al. (2013)

Data were obtained from field experiments conducted at three sites (Inch Spit, Ireland, Esposende, Portugal and Jericoacoara, Brazil). The Inch site (April 1994) is part of a morphodynamically dissipative beach system in Dingle Bay, on the south-western coast of Ireland. The field site at Esposende, along the northern coast of Portugal, was near the downwind end of a parabolic dune trough (May and June 2006). The upwind surface was flat and unobstructed and almost horizontal near the sand traps. During the experiments the sand surface was dry, and winds blew parallel to the trough with a fetch of approximately 80 m. Blowing sand was trapped using vertical arrays of hose-type traps. Samples for grain size analyses were obtained from sand caught in the traps.

Located on the north-eastern coast of Brazil, the Jericoacoara site was also near the downwind end of a parabolic dune trough, but at a location approximately 500 m from the shoreline. The upwind surface was flat and unobstructed, with a fetch of approximately 100 m, and the surface was almost horizontal near the traps. During the experiments, the wind blew parallel to the trough and the surface sediments were dry. Sand transport rates were measured with vertical hose-type trap arrays and grain size samples were obtained from the trapped sands. In order to estimate shear velocity using the cup anemometer data, wind speeds were averaged over time intervals coincident with those for sand trap data. The number of data was reduced to 32 data sets (5 for Inch Spit; 12 for Esposende and 15 for Jericoacoara) by selecting: i) only those wind profiles with a best-fit line R^2 exceeding 98%, ii) only those data for which the sand moisture content was less than 2% and iii) data sets with sand transport rates larger than about 0.3 g/m/s (1 kg/m/hour).

Field experiments Koksijde and Mariakerke beaches 2016-2018, Belgium

Strypsteen (2019) and Strypsteen et al. (2019) conducted field experiments at the beaches of Mariakerke and Koksijde in Belgium. The beach of Mariakerke (d_{50}=0.31 mm) is fairly flat and contains some shell fragments due to regular nourishments. The measurements were performed in the dry upper beach zone without much shells. The bed roughness (k_s) is smaller than 10 mm. The beach of Koksijde consists of sand (d_{50}=0.21 mm) with small-scale bed irregularities (ripples) and many shell fragments with height of the order of 30 mm. The bed roughness (k_s) is relatively high with values up to 45 mm. Wind-induced sand transport was measured by using MWAC-sand traps and streamer type traps on top of each other.

4.3 Model calibration

Basically, the calibration of the α_1 and α_2 coefficient of Equation (3.6) require measured data of bed roughness and sand transport for a flat sand bed under controlled conditions. The best data sets available are those of Han et al. (2011) and Yang et al. (2019), although only measured data of wind velocities and sand transport rates are given. Measured shear velocity values are not reported in their papers. Using Equation (3.6) with γ_r = 1 (no bed forms and $d_{90}=2d_{50}$ in combination with Equation (2.2), the coefficients α_1 and α_2 of Equation (3.6) are found to be α_1 =15 and α_2= 1, giving the best overall agreement between measured and predicted sand transport rates.

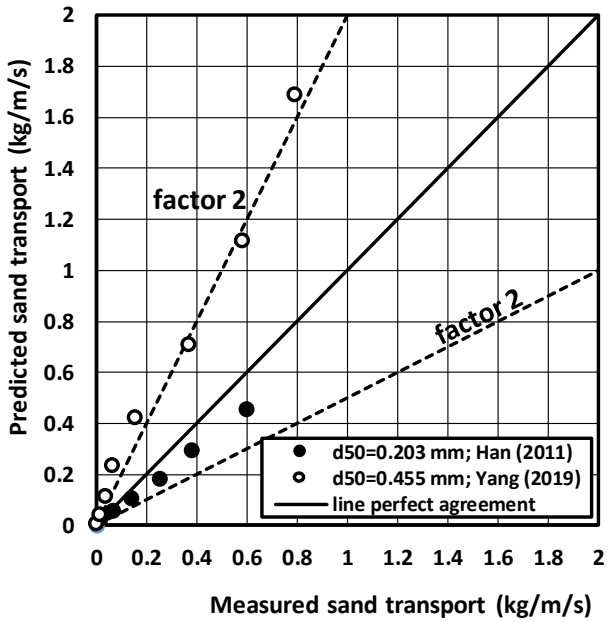

Figure 4.1 *Comparison of measured and computed sand transport; α_B=2; α_{th}=0.11; $d_{90}=2d_{50}$ data of Han et al. (2018) and Yang et al. (2019)*

The sand transport rates for 0.2 mm-sand of Han et al. (2011) are very well represented by the model, but the transport rates for the 0.455 mm-sand of Yang et al. (2019) are systematically overpredicted by a factor of 2 (**Figure 4.1)**. The predicted grain roughness values are in the range of 3 to 20 mm depending on the wind velocity between 8 and 22 m/s. These values cannot be checked as measured values of the roughness are not given by Han et al. (2011) and Yang et al. (2019). However, the computed roughness values are of the right order of magnitude compared to the range of 1 to 10 mm found by Strypsteen et at. (2019) for the fairly flat beach of Mariakerke (Belgium). More experimental research with flat sand beds in wind tunnels are highly recommended, so that the grain-related roughness can be better determined.

4.4 Model verification

The predictive model consisting of Equations (2.1, 2.2, 2.3, 3.6) has been verified using the data sets of Belly (1964), Sherman et al. (1998, 2013) and Strypsteen et al. (2019). In all, 105 high-quality data sets have been used. The input data are the measured wind velocity at z=2 m, the d_{50} and d_{90}-values, see **Table 4.1.** For all field data, it is assumed that $d_{90}=3d_{50}$. The roughness related to background irregularities is varied between 1 and 15 mm depending on the presence of shells and other irregularities. No information is available for the field sites of Portugal and Brazil. As relatively coarse sand is present at these sites, the background roughness is set to 2 mm. The background roughness is set to 2 mm for the data of Mariakerke beach where minor shells and other irregularities were observed and to 15 mm for the data of Koksijde beach where large patches of shells and shell fragments/hash were observed. McKenna et al. (2012) found k_s-values in the range of 1 to 6 mm for a surface with many shells in a wind tunnel. In field conditions these values will somewhat larger due the presence of shell clusters.

The computation procedure of the predictive model for dry sand is as follows: 1) specify wind velocity u_w at one height; 2) specify d_{50} and d_{90} of sand; 3) specify background roughness of irregularities $k_{s,ir}$ (if present); 4) compute static grain roughness by Eq. (3.6d); 5) compute threshold shear velocity by Eq. (2.2); 6) compute T-parameter by Eq. (3.6c); 7) compute bed roughness k_s by Eq. (3.6b), 8) compute shear velocity u_* by Eq. (3.6e); 9) compute sand transport by Eq.(2.1). Other parameters are: κ=0.4; ρ_{air}=1.2 kg/m³; ρ_{sand}=2650 kg/m³;α_B=2; α_{cr}=0.11; $d_{50,ref}$=0.00025 m.

Figure 4.2 (right) shows a plot of measured and computed transport rates for all available 105 data points. The computed transport rates are based on the measured shear velocities. About 58% of the predicted data are within a factor of 2 of the measured values. The measured transport rates are significantly overpredicted for the field data of Sherman et al. (1998, 2013). The measured wind tunnel data of Belly (1964) show considerable scatter (over- and underprediction).

Figure 4.2 (left) shows a similar plot of measured and computed sand transport rates, but now the predictive model is used. Most (72%) of the predicted data are within a factor of 2 of the measured values. The overprediction is substantially reduced and the scatter within the data of Belly (1964) is also reduced. Similar scores were obtained by Van Rijn (1984; 2007) for sand transport by water flow. Given all variabilities and non-uniformities involved and the problem of measuring under extreme wind conditions, it may be almost impossible to predict the sand transport rate with a score of 100% within a factor of 2. The predicted values are sometimes much too large at conditions near the threshold value, which is an inherent effect of a deterministic approach. This is, however, not so important for engineering practice as the transport rates involved are very small. The predicted values are somewhat too small for higher wind velocities. The model underprediction may be related to the underprediction of the dynamic grain roughness ($k_{s,grain,dyn}$), as only a few laboratory data of Han et al. (2011) and Yang et al. (2019) were used to calibrate the dynamic grain roughness (Equation 3.6). This can be improved by using results from new wind tunnel tests with flat mobile beds (future research). According to Sherman et al. (2013), the measured transport rates at their field sites may be slightly too small, as minor moisture may have been present in the sand surface raising the threshold values slightly. Most likely, measured transport in field conditions are somewhat too small rather than too large given the relatively low efficiencies of most trap samplers. Sherman et al. (2013) noticed significant overprediction (factor 2 to 3) of the original

Bagnold-equation with measured shear velocities as input (κ=0.4). The overprediction is substantially reduced by using smaller bed-shear velocities taking only grain-related roughness into account (Equation 3.6).

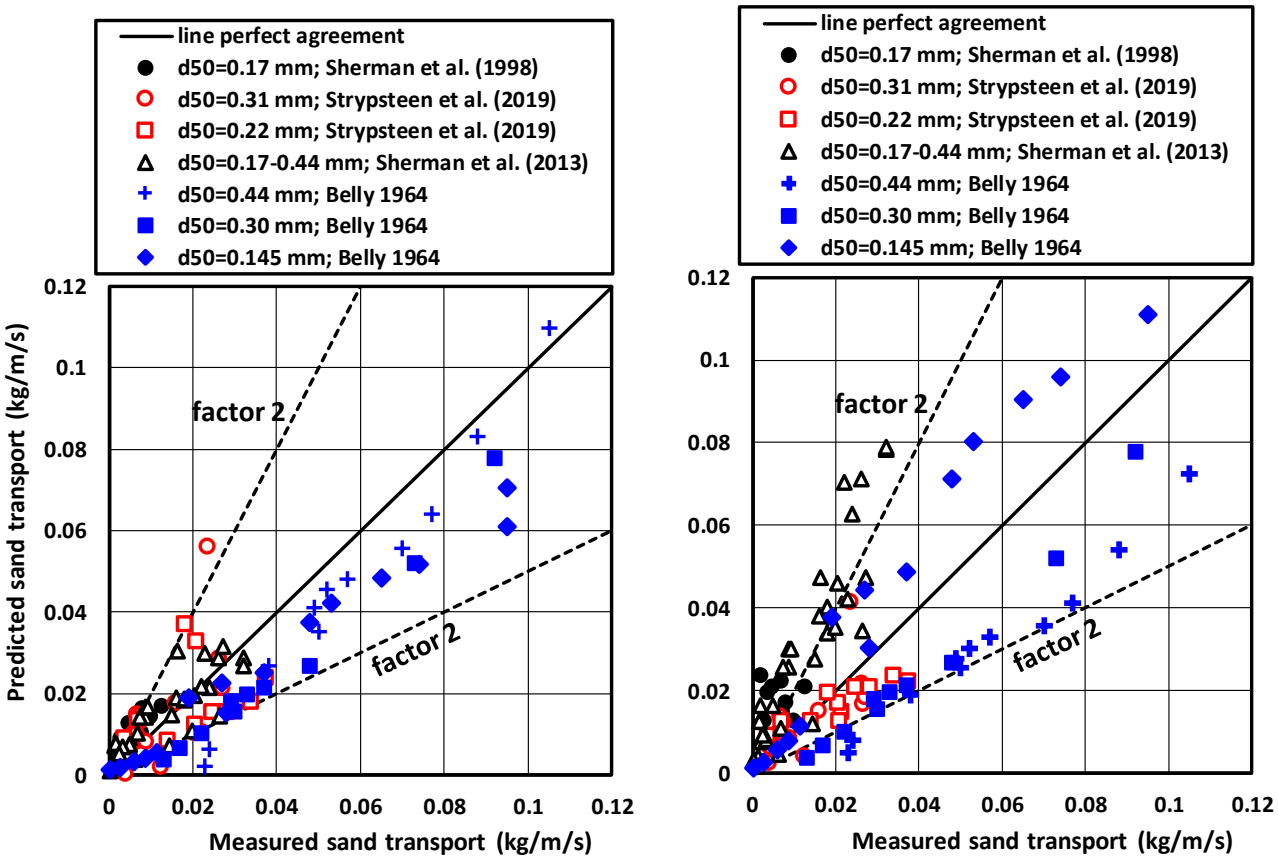

Figure 4.2 *Comparison of measured and computed sand transport;*
Left: based on predicted shear velocities; Right: based on measured shear velocities

5. Other effects

5.1 General

A fully predictive model must include the effects of sloping surfaces, varying moisture contents, vegetation and shells. Herein, it is proposed to represent these effects by simple coefficients acting on the bed-shear velocity, the threshold velocity or on the sand transport rate. The proposed coefficients are derived from reliable data in the opinion of the authors and can be seen as a first estimate for engineering purposes. Further research is required to improve and extend the knowledge. Some processes can be studied in wind tunnels (effect of bed slope, moisture and shells), but other processes can be better studied at field sites (vegetation, saturation). Given time and budget, the proposed coefficients can be gradually improved as more data become available.

5.2 Moisture content

Wind-induced sand transport is strongly affected (reduction factor of 2 to 10) by moisture content and related cohesion/adhesion effects, particularly for lower wind velocities < 20 m/s (Hotta et al., 1984). Moisture contents up to 8% had much less effect (< factor 2) for high wind velocities in the range of 20 to 30 m/s in a wind tunnel (Hotta et al., 1984).

Cohesion and adhesion between particles increase the surface resistance against erosion (threshold shear velocity). Cohesion and adhesion effects may result from the presence of moisture, salt, algae, clay, organic matter and calcareous materials. Even low levels of moisture may effectively reduce the transport rate of dry sand. However, intensive rainfall may also increase the sand transport rate by splash effects promoting saltation

processes. Moisture content (w) may be the direct result of precipitation, water spray, wave uprush near the water line or capillary action (adhesive forces; surface tension forces).

Moisture fraction is generally defined as: w= mass water of sample/mass dry sand of sample (moisture content is moisture fraction x 100%). Moisture content of a saturated sample can be computed by the expression $w_{saturated}=[\varepsilon/(1-\varepsilon)][\rho/\rho_s]x100\%$ with ε= porosity factor (0.35-0.45 for sand); ρ= water density ($\cong$1000 kg/m³); ρ_s= sand density ($\cong$2650 kg/m³), yielding $w_{saturated}$= 20%-30%. Generally, moisture contents are in the range of 0 to 10%, as the pores are not fully saturated with water.

Let us assume that a sand particle with diameter D is covered by a thin water film with thickness δ except at the particle contact points; any other pore water is absent.

The volume of the water film is: $V_{wf} = 1.33\pi\ [(0.5D+\delta)^3-(0.5D)^3]$ and the mass is: $M_{wf}=\rho V_{wf}$.

The volume of the sand particle is: $V_{sand}=1.33\pi(0.5D)^3$ and the mass is $M_{sand}=\rho_s V_{sand}$.

The mass ratio of water and dry sand defined as the moisture fraction is:

$w= M_{wf}/M_{sand}= \rho[(0.5D+\delta)^3-(0.5D)^3]/[\rho_s(0.5D)^3]$.

Using: D=200 μm for sand, δ=0.01D=2 μm, it follows that: $w \cong 0.025$ (2.5%).

Thus, a thin water film with thickness equal to 2 μm surrounding a sand particle of 200 μm yields a moisture content of about 2.5%. A water film of 1 μm yields a moisture content of 1%. Dry sand has a moisture content < 0.25% (Han et al., 2011). In conditions with a moisture content > 2.5%, the sand transport rate is strongly reduced to a very small value. In conditions with w=10% (near the water line), the surface is so saturated that aeolian transport reduces to almost zero even under very strong winds.

Various authors have studied the influence of moisture on the threshold shear velocity of sand particles by wind in wind tunnel conditions (Chepil, 1956; Belly, 1964; Hotta et al., 1984; Saleh and Fryrear, 1995; Cornelis and Gabriels, 2003 and Han et al., 2011) and in field conditions (Davidson-Arnott et al., 2005, 2008; Udo et al., 2008).

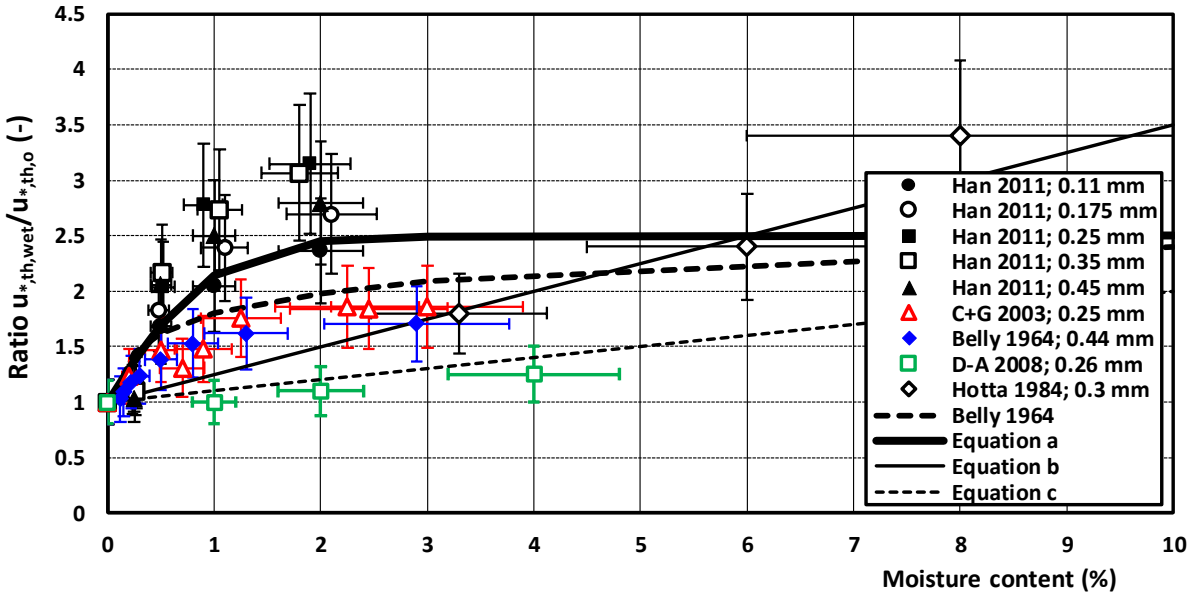

Figure 5.1 *Threshold shear velocity as function of particle diameter and moisture content; laboratory data (Han et al. 2011; Cornelis and Gabriels 2008; Belly 1964) and field data (Davidson-Arnott et al. 2008)*

Available laboratory data of Belly (1964), Hotta et al. (1984), Cornelis and Gabriels (2003) and Han et al. (2011) are shown in Figure 5.1. The effect of moisture is negligibly small for moisture content < 0.25% (Han et al. 2011). The threshold shear velocity increases for increasing moisture content. Sand with w=0.5% has a significant higher threshold shear velocity (factor 1.5 to 2) than that of dry sand. The scatter and error ranges are relatively large, which is most likely caused by the different definitions and measuring method used by the various researchers. The wind tunnel data of Belly refer to the upper 1 mm of the surface, as he used a moist air flow. The wind

tunnel data of Hotta et al. refer to a layer of 5 mm as samples with thickness of 5 mm were taken from the surface. The wind tunnel data of Cornelis and Gabriels and Han et al. refer to a layer of 1 to 3 mm. A basic problem is the rapid decrease of the moisture content due to the blowing wind, even for very short run times (< 2 min, Cornelis and Gabriels, 2003). Davidson-Arnott et al. (2008) report an increase of the threshold wind speed and shear velocity of only 20% for 0.26 mm-sand in the case of an increase of the moisture content from 1 to 4% in field conditions, see Figure 5.1. Udo et al. (2008) found an increase of a factor of 2 for 0.18 mm-sand in the case of an increase of the moisture content from 0 to 10%. The field results show a large discrepancy compared to those for wind tunnel conditions. Most likely, this is caused by the thickness of the top layer in which the moisture content is measured. The field data are valid for a top layer with a thickness of about 20 mm, whereas the laboratory data refer to the topmost layer of 1 to 5 mm. The moisture content of the thin top layer of 1 to 5 mm in field conditions will be much lower than the average value over a layer of 20 mm. The field experiments (Davidson-Arnott, 2008) also show that the moisture content at a certain location and thus the critical shear velocity can change rapidly over a period of minutes to hours due to drainage and/or drying by wind and sun. Large variations of the critical wind speeds were observed: $u_{w,min}$= 5 m/s (lowest wind speed with sediment transport) and $u_{w,max}$= 9 m/s (highest wind speed without sediment transport) mainly due to variations of the moisture content. Davidson-Arnott et al. (2008) have also found that the transport above a flat, hardpacked (damp) surface can be relatively high if there is a drier surface upwind of the damp surface. Based on this, the wind-driven sediment transport is highly variable in space and usually intermittent in time, depending on moisture conditions. Delgado-Fernandez (2011) found that the moisture conditions of natural beaches can be crudely classified into three categories: a) dry with w_{20mm}<2% and a fully developed saltation system; b) medium with w_{20mm}=2 to 10% and restricted sand transport and c) wet with w_{20mm}>10% and sand transport is completely prevented.

The effect of the moisture content on the threshold shear velocity is herein represented by: $u_{*,th,wet}=\alpha_w u_{*,th,B}$ with

$$\alpha_{w,2mm} = 1+2\tanh(w_{2mm}) \quad (3.7a)$$

$$\alpha_{w,5mm} = 1+0.25w_{5mm}) \quad (3.7b)$$

$$\alpha_{w,20mm}= 1+0.1w_{20mm} \quad (3.7c)$$

with: w_{2mm}= moisture content in upper 2 mm of surface (in %), w_{5mm}= moisture content in upper 5 mm of surface and w_{20mm}=moisture content in upper 20 mm of surface. Equations (3.7a,b.c) and that of Belly are shown in **Figure 5.1**. Equation (3.7a) and that of Belly (1964) are both in reasonable agreement with the laboratory results, but largely overpredict for field conditions. Equation (3.7b) is very close to the data and the empirical equation of Hotta et al. (1984). Equation (3.7c) represents the field data of Davidson-Arnott (2008) and is advised for field conditions provided that the moisture content of the topmost 20 mm is measured (input value). Application of Equation (3.7c) requires input data of the moisture content of the topmost 20 mm of the sand bed, either from measurements or from a prediction model for the moisture content. Brakenhoff et al. (2019) have studied the moisture content in cross-shore direction from the low tide water line to the upper dry beach and developed a prediction model for the surface moisture content calibrated with data from a mesotidal beach in The Netherlands. The length of the intertidal beach was about 60 m. Their results show that the lower 30% of the intertidal beach is always saturated with water and w_{20mm}> 20%. Higher up the tidal beach up to the high tide line, the moisture content is between 5% and 20% depending on the tidal stage; drying rates were found to be 50% in 2.5 hours. Above the high tide line, the moisture content decreased from about 5% at the high tide line to about 2% at about 30 m beyond the high tide line in conditions without rainfall. This latter zone is the transition zone to the dry beach, where the moisture content solely depends on precipitation (rainfall). In the Netherlands, there is a total rainfall time of about 500 hours or about 20 days per year in which windblown transport in the 'dry' beach zone is almost absent (wet conditions w_{20mm}>10%), about 45 days with restricted conditions (medium w_{20mm}=2% to 10%) and 300 days with dry conditions (w_{20mm}<2%). Drying times of the topmost layer of 3 mm after rainfall are found to be fairly short in

summer time (< 3 hours, Hotta et al., 1984). This means that effect of precipitation on wind transport in the dry beach zone is meaningful, but not dominant. Most of the time (at least 80%), the dry beach zone is really dry.
De Vries et al. (2014) have found that the transition zone of about 30 m seaward and landward of the high tide line in which the moisture content reduces from about 5% to 2% is an important source of sand for the gradual pickup (entrainment) of sand, as other supply-limiting factors (shells, vegetation) are absent in that zone. The pickup process will continue in the dry beach zone if supply-limiting factors are absent (shell lag deposits, vegetation).

5.3 Shells

Shells (calcium carbonate) can protect the beach surface against erosion of the sand particles. Large percentages of shell are mostly found on the upper part of natural beaches outside the wave action zone and on beaches with nourished sand. Literature on this topic is rather scarce and mostly qualitative. The two main effects of shells on the sand transport process are: i) shells cover a certain area of the bed which is not available for sand particle erosion and ii) sand particles in the direct vicinity of shells are less exposed to the wind forces (hiding effect). Observations in wind tunnels and field conditions show that shells of different sizes tend to interlock and form clusters (spatial organization; Mckenna et al., 2012; Strypsteen 2019). At the Dutch sand motor site (see Section 6.1) with shell cover values up to 20%, sufficient sand particles were winnowed from the shelly bed to give appreciable erosion and deposition volumes of sand. Based on these observations, it is herein assumed that the effects of shells on the sand transport process can be best represented for engineering purposes by a simple reduction coefficient acting on the transport rate. This coefficient is derived from the experiments in wind tunnels (Van der Wal, 1999 and McKenna et al. 2012). It is realized that this approach only gives the transport-limiting effect.
Van der Wal (1999) studied the effect of shells on the wind-induced transport rate of beach sand. Beach sand samples were taken from 5 sites along the Dutch coast and tested in a wind tunnel. The d_{50} varied in the range of 0.21 to 0.35 mm. The percentage of shells (> 2 mm) varied in the range 1 to 30%. A tray with (length=1.22m; width=0.33 m; height=0.03m) was filled with weighed oven-dried sand and placed in the middle of the test section. The sample surface was smoothed and levelled to the tray edges. The wind speed was gradually increased over one minute to about 11 m/s and kept at this speed for another minute. Then, the wind speed was gradually returned to zero over one minute. After the experiment, the sand was reweighed. The percentage of sand blown off during the test was calculated for each of the experiments. The transport rate was reduced by a factor of 1.5 for samples with a percentage of shells of 10% and by a factor of 3 for samples with a percentage of shells of 20% to 30%. Shell pavements were formed during the wind tunnel experiments with shell-rich beach samples.
McKenna et al. (2012) conducted a wind tunnel study on the effect of various types of shells on the erosion of a sand bed with a total area of about 10 m^2. Wind velocities were in the lower range of 8 to 12 m/s (BF<7). Three types of shells were used: crushed shells with cover percentages between 12% and 22% (heights 1.1 to 1.6 mm); small shells < 12.7 mm with cover percentages between 17% and 43% (height 2.6 to 5.7 mm) and large shells > 12.7 mm with cover percentages between 14% and 30% (heights 7 to 9.2 mm). The freestream velocity was gradually increased until the cumulative number of particle counts recorded by a piezoelectric impact sensing device began to increase continuously. A sediment trap at the downwind end was used to collect sand particles eroded from between the shells. The test was terminated when bed the transport rate dropped to a negligible value (<0.05 g/cm/s). It was observed that the shells were organized into chains and clusters with the long axis of many of the shells appearing to be aligned with the wind flow. The threshold wind velocity and shear velocity were found to increase by about 15% to 25% for a cover of 15% and about 35% to 45% for a cover of 43%. The amount of erosion after the test (in kg/m^2) was recorded showing almost no erosion for the largest cover values of 40% both for small and large shells. Erosion is reduced by a factor of 5 to 10 by increasing the cover of shell from about 15% to about 30-40%. Crushed shells are less effective than small/large shells. The sand transport is estimated to be reduced by about 40% for a cover of 15% and about 95% for a cover of 40%.
Important parameters appear to be the fetch length and the uniformity of the shell cover. In wind tunnel experiments, the fetch length is relatively small (1 to 8 m in the studies discussed herein) and the initial shell

cover is quite uniform in space. In field conditions, the fetch length is often larger than 50 m and the shells are not uniformly distributed over the beach surface. Shell clusters are pronounced features at natural beaches (Strypsteen 2019). McKenna et al. (2012) have observed in their wind tunnel experiments that the shells are not operating independently, but rather display some degree of spatial organization resulting in shell clusters of partly interlocking shells of different sizes. Shells are sometimes rolling coming to rest against others downwind resulting in clusters. Corridors of lower shell coverage are generated at the sand surface. This justifies the use of a simple transport limiting coefficient for engineering practices. Herein, the reduction effects based on the tests of Van der Wal (1999) and Mckenna et al. (2012) are simply represented in Equation (2.1) by a reduction factor acting on the transport rate:

$$\alpha_{shell}=(1-2p_{shell}/100)^2 \quad (3.8)$$

with p_{shell}=percentage of shell (<30%). The sand transport rate as affected by shells was not measured directly in the studies considered herein (van der Wal, 1999; Mckenna et al., 2012; Hoonhout and De Vries, 2017) and thus Equation (3.8) could not be tested against measured transport rates. Equation (3.8), which is only valid for a shell cover < 30%, is herein used as a transport-limiting factor acting on the sand transport rate to obtain a quick engineering scan of the effect of shells in reducing sand transport on nourished shelly beaches. The gradual development of an armor layer in time cannot be represented in this way, as it requires a more detailed approach. Basically, the simulation of sand transport in conditions with a relatively wide grain size distribution (d_{90}/d_{10}> 10) and significant shell cover values (10% to 30%) requires an approach with multiple fractions including a book-keeping process for each grid cell and vertical sand layer. Hiding and exposure effects must be included as well as roughness variation effects (Raupach 1992; Van Rijn 2007). The present model can be extended to a fractional approach (Van Rijn 2007). Using such an approach, the changes in surface conditions can be simulated both in space and time. Hoonhout and De Vries (2017) used a fractional model to study the windblown sand transport at a large-scale mega-nourishment (sand motor in The Netherlands). They found that the intertidal zone and the transition zone where shells were absent were the dominant sources of sand for windblown sand. The dry beach plain with abundant shell cover (5% to 15%) developed a beach armor layer suppressing the pickup of sand particles to some degree. However, such an approach is far more complex with many coefficients and calibrations involved and may be a bridge too far for engineering purposes (see detailed discussion by McKenna et al., 2012). In section 6.1 it is shown that Equation (3.8) predicts meaningful results for the Dutch sand motor site which is a shelly beach plain/nourishment site. Model improvements based on detailed research in wind tunnels and at field sites focusing on the sand transport processes with wide grain size distributions including/excluding shells are highly recommended.

5.4 Vegetation

Wind-blown sand transport is substantially reduced if numerous roughness elements are present on a sand surface, as shown in a fundamental study by Gillies et al. (2006). Sand transport was measured between plastic buckets (4 different configurations) resting on a flat horizontal sand surface. Results of these tests indicate that sediment transport rates through patches of roughness are controlled by the roughness density depending on the dimensions (width, height) and number of elements. Sand transport reductions based on comparison with upwind trap results were as large as 90%.

The effects of vegetation on wind-blown sand can be described as (Wolfe and Nickling 1993): i) vegetation extracts momentum from the air flow resulting in larger roughness; ii) vegetation elements are obstacles for saltating sand grains and iii) vegetation reduces part of the surface where sand transport takes place. Vegetation is herein identified as grass-type plants with a maximum height of about 0.5 m. The shear velocity can be determined from wind velocity measurements outside the roughness layer (say 2 times the plant height) to eliminate the local velocity variations occurring between the plants. Both the shear velocity and the overall effective bed roughness will increase due to the presence of the vegetation.

Two approaches are possible to account for the effect of vegetation on the sand transport rate by : i) increase of the threshold value as the sand grains are hiding between the vegetation and the application of the total bed-shear velocity for sand transport (Musick and Gillette, 1990; Raupach et al., 1993; Musick et al., 1996;) and ii)

reduction of bed-shear velocity acting on the sand grains between the vegetation and the application of the standard threshold shear velocity (Raupach 1992).

The latter approach requires partitioning of the bed shear stress ($\tau=\tau^{/}+\tau^{//}$) into a component related to grain roughness ($\tau^{/}$) and another component related to form drag of the vegetation ($\tau^{//}$). The stress component $\tau^{/}$ represents the averaged stress on the exposed grain surface. This approach has been formulated and tested in great detail by Raupach (1992), Brown et al. (2008), Shao et al. (2015). Raupach assumed that the surface consists of randomly distributed cylinders uniform in size, each having a frontal area of a_f and n is the number density (number unit area) of the roughness elements (roughtons). The frontal area index of the roughtons is $\lambda=n\, a_f$. The ratio of roughton basal area to frontal area is $\sigma=a_b/a_f$ and the exposed percentage of the surface subject to wind velocity is $p_s=(1-\sigma\lambda)100$ and the cover percentage $p_v=\sigma\lambda 100$. The shear stress on the exposed surface can be expressed as: $\tau^{/}/\tau=[1-\sigma\lambda]^{-1}\ [1+\beta\lambda]^{-1}$ with $\beta=C_r/C_s$ and C_s= frictional drag coefficient and C_r= pressure drag coefficient. Raupach et al. (1993) formulated a correction factor for the threshold friction velocity in the presence of roughness elements: $u_{*,cr}=u_{*,cr,o}\ [(1-m\sigma\lambda)(1+m\beta\lambda)]^{0.5}$ with m=coefficient$\cong$0.5.

The approach of Raupach is most scientific, but it contains many coefficients and parameter to be specified as the vegetation roughness is of complex nature with many influential parameters (stem diameter, stem height, number of stems per bundle or plant; bundle porosity, bundle configuration, heterogenous clustering, etc.). Herein, a simpler approach is proposed for engineering practices by using a correction coefficient (α_v) based on percentage of cover and the vegetation height and acting on the shear velocity (see Equation 2.3).

Various researchers have studied the effect of vegetation on wind-blown sand transport in wind tunnels (Buckley, 1987; Burri et al., 2011; Youssef et al., 2012; Hesp et al., 2019) and at field sites (Wasson and Nanninga, 1985; Lancaster and Baas 1998; Arens et al., 2001; Hupy 2003; Hesse and Simpson, 2006; Davidson-Arnott et al., 2012).

Buckley (1987) studied the effect of sparse vegetation on wind-blown dune sand (0.15 mm) in a wind tunnel. Three plant types (F,G,R) with heights of the order of 10 cm were used, corresponding to characteristic shapes of common small herbaceous dune plants. Cover percentages were in the range of 0 to 20%. Sand transport was measured with three vertical profile traps 50 cm downstream of the vegetated area.

The reduction of sand transport rate at constant wind velocity of 10 to 15 m/s for plant type F was as large as 90% for a cover of 20%, see **Figure 5.2**.

Lancaster and Baas (1998) studied the effect of vegetation on the bed roughness and the sand transport process at the western part of the former delta of the Owen River in eastern California, USA. The surface sand at the site is coarse (median particle size of 0.5 to 1 mm). The sand sheets are vegetated with salt grass with a cover that ranges from zero to about 30 per cent and which increases northwards. The sand flux measured at 0.1 to 0.2 m above the bed was largest at the sites A and B with a vegetation cover < 5%. The sand flux strongly decreases for increasing values of the vegetation cover. **Figure 5.2** shows the normalized sand flux values (ratio of local transport and upwind transport) for increasing cover values. A vegetation cover of 10% already gives a reduction of 50%. The reduction is about 90% for a cover of about 25%.

Arens et al. (2001) studied the effect of vegetation density on aeolian sediment transport and deposition in the area of foredunes (12 m high) at the Holland coast near the Hague. The seaward front of the foredune was partitioned into three plots, each 100 m long along the foredune and 10 m wide over the cross-shore. The plots were planted with 4, 2 and 1 bundles of reed stems per m^2. Each bundle consisted of 15 stems; bundle diameter is 0.17 m; porosity of bundle is about 50%. The number of bundles is 1 per m^2 at distance of 1 m (plot N1), 2 per m^2 at distance of 0.7 m (plot N2) and 4 per m^2 at distance of 0.5 m (Plot N4). The height of the stems was approximately 0.5 m immediately after planting and gradually decreased due to sand burial. Analysis of all sand trap data (wind velocity between 10 and 12 m/s) shows sand transport reductions from 40% to almost 100%, see **Figure 5.2**. Also noticed was gradual deposition starting at the first row of the reed bundles and slowly evolving into bed forms as a result of the reduction of sand transport within the vegetated area. This was also observed by Hesp et al. (2019) with artificial plants (h=22 cm) in a wind tunnel and at field sites. Bed form heights were largest for the highest cover value of 40-50%.

Burri et al. (2011) performed a wind tunnel study of wind-blown sand with live plant canopies: three canopy densities (cover 4%, 16% and 47%) of Perennial Ryegrass (h=6 cm) and bare sand surfaces ($d_{50}\cong$0.6 mm). The

sand transport decreased by about 90% for cover of 16% and by about 100% for cover of 47%, see **Figure 5.2**. The sand transport increased by about 20% for the lowest cover of 4%, which is attributed to the increase of local shear stress due to flow acceleration around the plants and due to extra lee turbulence produced by the plants. Furthermore, the grasses were observed to trigger erosion by oscillating movements at the sand surface. Davidson-Arnott et al. (2012) reported a 99%-reduction of sand transport at a vegetated foredune (stations 6 and 10) with cover percentages of 15 to 25% compared with sand transport at the beach (stations 1, 3, 4; d_{50}=0.26 mm) during an event with wind velocities of about 10 to 11 m/s. Sand transport reduced from about 50±30 kg/m/hr to about 0.35±0.25 kg/m/hr. These results are in line with the values presented in **Figure 5.2**.

All available data are shown in **Figure 5.2**. It can be clearly seen that high reed bundles (h=50 cm) of Arens et al. (2001) have a greater reducing effect on the sand transport rate than the lower plants (h=10 cm) used by Buckley (1987) and Lancaster and Baas (1998). Hupy (2003) found that sand transport was much larger in areas of loose sand and at sites directly downwind from loose sand than in areas containing heavy crusting, gravel, or a forb/grass cover. Differences between sites with gravel surfaces and those with forb/grass cover were, however, insignificant. Thus, the cover percentage seems to be the dominant factor rather than the type of cover. Hesse and Simpson (2006) also conclude that sand movement along desert dunes is primarily controlled by vegetation cover. Sand movement responds to short-term variations in vegetation cover (including crust). A simple threshold of vegetation cover below which sand transport begins was not found.
The data of **Figure 5.2** can be crudely represented by an engineering expression:

$$\alpha_{veg}=[1-(\Delta_v/\Delta_{v,minimum})^{0.5}p_{veg}/100]^2 \qquad (3.9)$$

with: p_{veg}=percentage of vegetation cover (<30%); Δ_{veg} = height of vegetation which is of order of 0.1 to 0.5 m; $\Delta_{veg,mimimum}$ = minimum height of vegetation (about 0.1 m). Equation (3.9) valid for wind velocities up to about 15 m/s (measured at about 1 to 4 m above surface) shows reasonable agreement with the available data with vegetation cover up to 30%. The agreement is not perfect, but the general trends are well represented. During extreme wind velocities in the range of 15 to 30 m/s, other effects come into play (destruction of vegetation, exposed root systems), which are herein neglected. More field research is required to extend the knowledge of the vegetation effects, particularly for higher wind velocities.

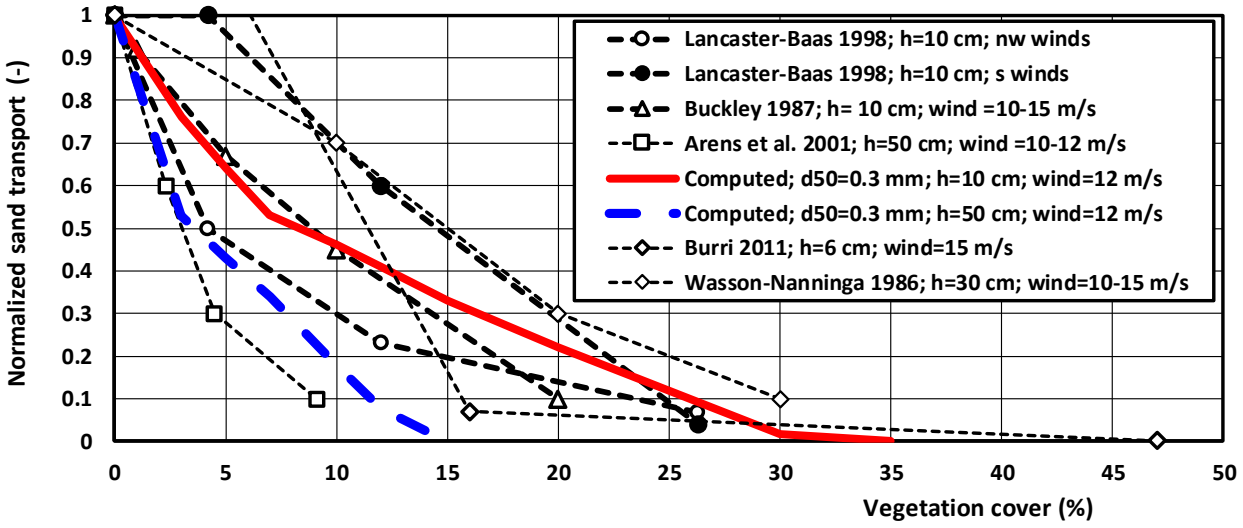

Figure 5.2 *Normalized sand flux as function of vegetation cover based on various field data*

6. Example applications of the predictive sand transport model

The proposed model can be applied in a rather straightforward way for loose, dry sand without shells and vegetation. For moist beach and dune systems including shells and vegetation, the estimation of these parameters requires detailed attention. The percentage of shells can be determined from samples taken over the upper 20 cm of the sand surface at the site or from samples taken at the offshore borrow (source) area in the case of beach nourishment. Vegetation height and cover can be estimated from sites similar to the site studied. Guidelines for the estimation of moisture can be given by distinguishing three ranges (Delgado-Fernandez, 2011): i) almost dry sand for moisture values w_{20mm}< 2% during 70% to 80 % of the time, ii) transition range with a drying sand surface and w_{20mm}=2% to 10% during 3 hours after each rainfall event and iii) wet sand for w_{20mm}> 10% during rainfall conditions preventing sand transport.
Two example cases are studied: i) sand transport at a horizontal beach parallel to the shoreline with effects of moisture and vegetation and ii) sand transport from the beach normal to the dune crest.

6.1 Sand transport at beach parallel to shoreline

The predictive model for wind-blown sand transport has been used to predict the sand transport rate for a range of conditions. **Figure 6.1** shows computed values for dry sand with d_{50}=0.3 mm and d_{90}=0.5 mm. The predicted transport rates for dry sand (solid bold curve) show a continuously increasing transport rate for increasing wind velocity. The effects of moisture (Equation 3.7c) and vegetation cover (Equation 3.9) are also shown. The moisture content increases the threshold shear velocity significantly and reduces the dynamic grain roughness (smaller T-parameter and thus smaller $k_{s,grain}$), resulting in almost zero transport for a wind velocity of 8.5 to 14.5 m/s for w_{20mm}-values of 2% to 10% of the topmost 20 mm of the beach sand surface.

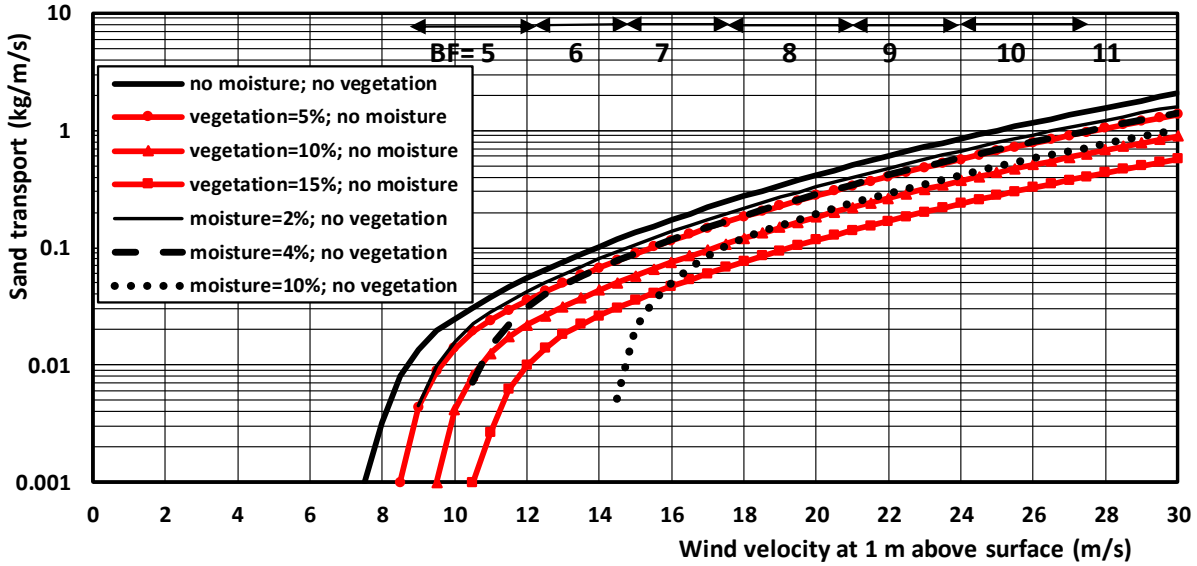

Figure 6.1 *Wind transport of sand based on predictive model (modified Bagnold-equation) (d_{50}=0.3 mm; d_{90}=0.5 mm; α_B= 2; α_{th}= 0.11)*

Once, the threshold value is exceeded the transport rate is much smaller. The reduction effects are largest for wind velocities < 18 m/s. The reduction effect diminishes for higher wind velocities further away from the threshold value. For a high wind velocity of 30 m/s (Beaufort scale 11), the reduction effect is about 20% for w_{20mm}=2% to about 50% for w_{20mm}=10%.
Vegetation (plant height=0.3 m) with covers of 5% to 15% reduces the effective shear velocity of the wind resulting in almost zero transport for wind velocities smaller than 6.5 to 8.5 m/s. Vegetation has a strong effect

on the sand transport rate for wind velocities < 12 m/s. A vegetation cover of 15% consisting of plants of 0.3 m high reduces the sand transport rates by a factor of 2 to 3 for wind velocities > 12 m/s.

A very interesting test case for the predictive model is the windblown sand transport at the Dutch sand motor site, which is a mega-nourishment of about 21 Mm³ (De Vries and Hoonhout, 2018; Hoonhout and De Vries 2019). The dominant wind direction is parallel to the foredunes. Measured deposition/erosion volumes are 300,000±100,000 m^3 for a period of 4 years (2011-2015) in the windblown beach plain area. Based on this, the annual-mean sand transport is about 75,000±25,000 m³/year. The beach width normal to the coast is about 750 m in the middle zone of the site resulting in an annual-mean sand transport rate per unit width of about 100±35 m³/m/year passing from the updrift half on the southwest side to the downwind half on the northeast side of the beach plain area. The large beach plain at a level of 5 m above mean sea level consists of shelly sand with d_{50}=0.335 mm and a shell cover in the range of 5% to 15%. The tidal range is about 2 m. The dominant wind direction is from southwest approximately parallel to the foredune row. During about 30% of the time, the wind speeds are below 8 m/s (BF3) without transport. During 70% of the time, the annual-mean wind speed representative for sand transport is about 10 to 11 m/s (BF5) at a height of 10 m above the beach surface. Table 6.1 shows measured and computed annual-mean transport values for three cases. The computed value is about 50% too large for ideal conditions with dry sand, no shells and no moisture. Fairly accurate results are obtained for a shell cover of 10% and minor moisture of 1% to 2% (supply limiting factors). Most likely, shells are more important than moisture effects, as the beach plain is very flat and infiltration of rainfall is rapid due to the relatively high beach level. Hoonhout and De Vries (2019) have used a much more complex sand transport model (Aeolis) including beach armoring due to presence of shells and a beach drying model in the intertidal zone. Detailed model calibration was required to represent the measured erosion and deposition patterns in the windblown zone. They used the term $(u_*-u_{*,th})^3$ in the Bagnold-equation, which yields much too small transport rates (Strypsteen 2019; Strypsteen et al. 2019). As windblown transport rates were not successfully measured by mechanical traps at the sand motor site, the coefficients of the transport model could not be calibrated separately. The transport model and the detailed beach armoring model were all calibrated in one procedure, which may easily obscure the deficiencies of each component. It is concluded that the sand motor data with a shell cover < 15% and mostly dry sand can be represented by a fairly simple model approach as proposed in this paper.

Table 6.1 *Measured and computed sand transport rates; sand motor site The Netherlands*

Cases	Computed annual-mean sand transport (m³/m/year)	Measured annual-mean sand transport (m³/m/year)
1. Wind speed= 10-11 m/s; dry sand d_{50}=0.335mm; d_{90}=1-3 mm; no shells; no moisture	140±70	100±35
2. Wind speed= 11 m/s dry sand d_{50}=0.335mm; d_{90}=2 mm; shells=5%-15%; no moisture	130±30	
3. Wind speed= 10-11 m/s; moist sand d_{50}=0.335mm; d_{90}=2 mm; shells=10%; moisture w_{20mm}=1%-2%	60±30	

6.2 Sand transport normal to dune

Wind flow from the beach across the foredune profile involves acceleration and deceleration effects over a varying sand surface, see **Figure 6.2**. If vegetation is present along part of the dune front, the surface roughness may also vary horizontally (non-uniform roughness). The wind speed at the sloping dune surface can be determined by various methods: i) measurements at the sloping surface (wind speed masts); ii) wind flow computations using a mathematical model (open foam CFD-model) and iii) empirical coefficients relating the

local wind speed to the upwind velocity ($u_{w,local}=\alpha_{local}\, u_{w,o}$). Wind normal to the beach accelerates along the slope of the foredune and is maximum at the dune crest level (Arens et al., 1995; Wiggs et al. 1996 and Smyth and Hesp, 2015). The sand transport at the sloping surface of the dune front is affected in various ways: i) increase of the wind velocity enhancing the sand transport rate, ii) increase of the threshold shear velocity for upsloping wind flow reducing the sand transport rate and iii) decrease of the particle velocity during upward part of the saltation trajectory related to the counteracting gravity component reducing the transport rate. Another effect is the generation of upward wind velocities enhancing suspension processes. During strong onshore winds, the upward wind velocities may exceed the fall velocity of grains of 0.2 to 0.3 mm (0.8 to 1.5 m/s). Suspension effects are herein neglected. It is assumed that saltation is the dominant mode of transport.

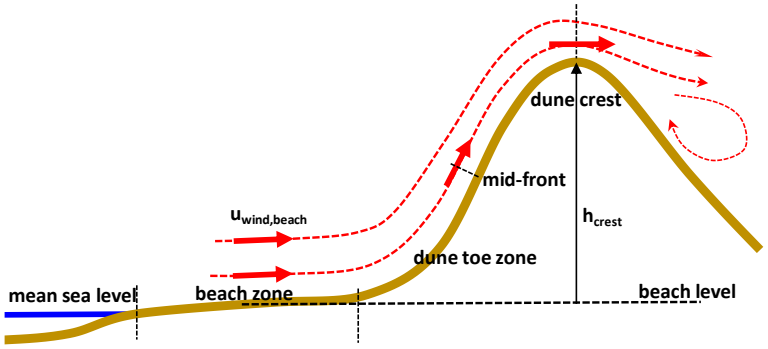

Figure 6.2 *Wind flow normal to dune*

Arens et al. (1995) studied the wind speedup effects at the front of the foredune at three coastal sites (sand of 0.17 to 0.26 mm) in the Netherlands. The dune height was in the range of 6 to 23 m. The beach width was in the range of 80 to 600 m. Three to five masts with cup-anemometers were placed at the beach, in the dune zone (corner zone) and at the dune crest. Wind deceleration occurs in the dune toe zone (corner zone), where the wind speed is reduced by about 10%-20% for small dunes < 10 m high to about 50% for a large dune with height of about 20 m. Wind acceleration is most strong at near the dune crest, where the wind speed is increased by 10% for small dunes up to 50% for larger dunes (20 m). An increase in foredune height up to 10 m leads to an increase of the speed-up near the dune crest of about 50% during onshore wind, but a further increase of foredune height from 10 to 20 m was found to have little effect.

Wiggs et al. (1996) studied the wind velocity distribution across an unvegetated desert dune (10 m high; 100 m long) in Oman and across an artificial dune in a wind tunnel. Both the field and wind tunnel data demonstrate similar patterns of wind and shear velocity over the dune, confirming significant flow deceleration upwind of and at the toe of the dune, acceleration of flow up the windward slope. The field data showed a decrease of the shear velocity at the dune toe, but this was not observed in the wind tunnel based on shear velocity data derived from turbulence measurements. Wind tunnel measurements using a special high-frequency wire probe suggests that the field method of shear velocity derivation is inadequate. The wind tunnel results exhibit no reduction in shear velocity upwind of or at the toe of the dune. Evidence provided by measured Reynolds stress profiles and turbulence intensities measured in the wind tunnel suggest that this maintenance of upwind shear stress may be the result of slightly diverging streamline curvature producing additional turbulence, which are not recorded by the traditional techniques used in the field measurements.

Smyth and Hesp (2015) studied the wind flow over a small artificial dune of sand (0.25 mm) with trapezoidal cross-section made at the landward end of a beach. The dune height is 3 m; the length of the dune front is 4 m; the dune front slope is 1 to 1.5 (angle=34°). A computational fluid dynamic model (CFD) was used to compute the wind flow across the dune and the shear velocity along the surface for an onshore wind velocity of 8 m/s at z=1 m above the beach surface (inlet x=0). The results show a strong reduction (factor 2) in shear velocity at the toe of the dune. The wind velocity strongly (factor 1.5 to 1.7) increases at the crest. The wind velocity and shear velocity decrease again beyond the dune crest. The deceleration and acceleration effects at the toe and near the crest computed by Smyth and Hesp (2015) are much stronger than the effects measured by Arens et al. (1995)

and Wiggs et al. (1996), which is most likely caused by the sharp transitions in the profile of the artificial dune. In field conditions these transitions will be smoother resulting in less strong deceleration/acceleration effects. Furthermore, additional turbulence (slightly diverging streamlines) is produced in the corner zone enhancing the shear stresses.

Given the available information on the velocity distribution along the dune front, the predictive modified Bagnold-equation has been used to compute the sand transport rates at the beach and across the dune front up the crest for wind flow normal to the dune. The upwind velocity is defined at 1 m above the beach level and varied in the range of 7 to 30 m/s. The dune dimensions are taken from the data of Davidson-Arnott et al. (2012). The dune height is 10 m above the beach level; the slope angle in the dune toe zone is about 12° and the slope angle of the dune front is about 22°. The beach and dune sand have d_{50}=0.26 mm; d_{90} is set to 0.5 mm and the angle of repose is set to 35°. The beach width is 30 to 40 m, which may give supply-limited effects for onshore winds. The threshold shear velocity of 0.26 mm-sand is 0.26 m/s at the horizontal beach, 0.29 m/s in the dune toe zone and 0.29 m/s in the crest zone based on Equation (2.2) including slope effect for upsloping flow. It is assumed that the median grain size is about constant along the beach and dune faces based on the detailed sampling analysis work of Hallin et al. (2019) for beaches in Sweden. The sand transport is computed at levels of 2 m and 3 m in the dune toe zone, at 5 m (mid-front), and at the dune crest of 10 m above the beach level. The wind speed modification across the dune profile is derived from the available field and wind tunnel data (Arens et al., 1995; Wiggs et al., 1996) resulting: $u_{wind,local}=\alpha_{local}\, u_{w,o}$ with $\alpha_{2m} \cong 1$ (lower toe zone), α_{3m}=1.2 (upper toe zone), α_{5m}=1.3 (mid-front) and α_{10m}=1.5 (crest).

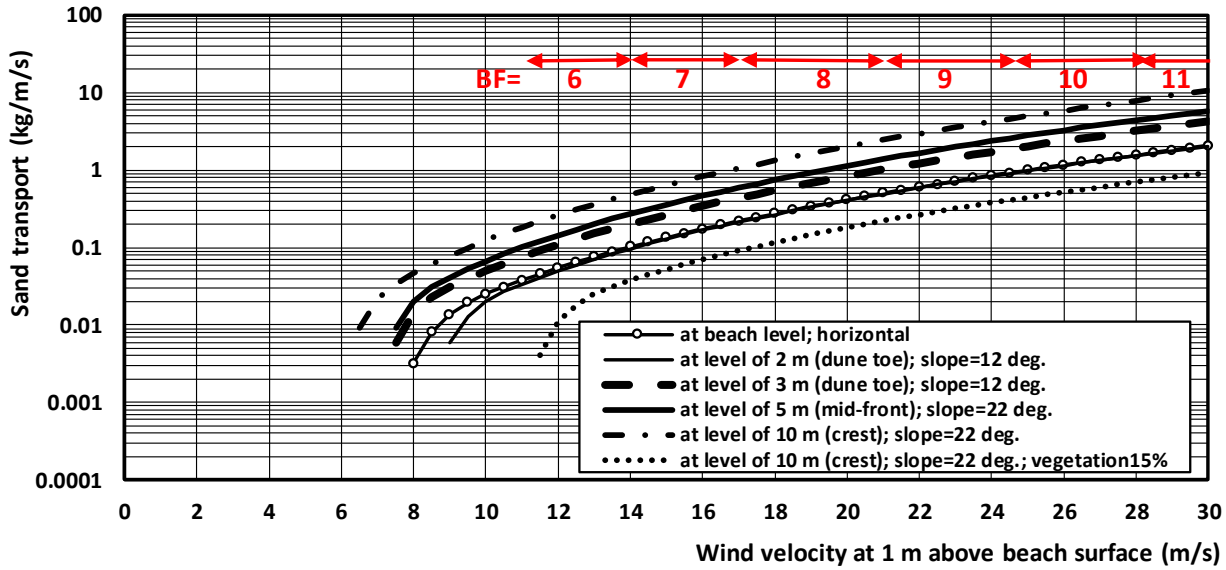

Figure 6.3 *Aeolian sand transport at beach level and at higher levels along dune front; dry sand d_{50}= 0.26 mm; including effects of wind modification, slope on threshold shear velocity and vegetation*

Figure 6.3 shows the computed aeolian sand transport rates at 4 levels for conditions with wind flow normal to the dune front. Supply-limitation effects are neglected. The wind velocity at the horizontal axis is defined at the beach. The sand transport rates (dry sand) at level of 2 m in the dune toe zone is about the same as that on the beach except for relatively small wind speeds < 10 m/s. The sand transport rates at levels of 3 and 5 m are larger (factor 1.5 to 3) than those at level of 2 m. The sand transport rates at level of 10 m (crest) are a factor of 5 larger than those at level of 2 m. The increase of the sand transport rates between levels of 2 and 10 m will lead to erosion if vegetation is absent. The sand transport rates are also computed for conditions with vegetation (plant height=0.3 m; cover=15%) resulting in a significant reduction (factor of 10). These computed results are compared to the measured results of Davidson-Arnott et al. (2012). They report measured transport rates of about 0.0055 kg/m/s at a level of 2 m and 0.02 (±0.005) kg/m/s at levels of 3 to 5 m during oblique onshore winds of about 10 to 11 m/s at dune crest (storm 3-4 May 2010; fairly dry sand as rainfall only occurred on the

evening of 3 May). Assuming a smaller wind velocity of about 8 to 9 m/s at the beach, the predicted sand transport rates are of the order of 0.003 to 0.01 kg/m/s at the beach and about 0.02 to 0.04 kg/m/s at levels of 3 to 5 m, see **Figure 6.3**. These computed values are in very reasonable agreement with the measured values. The measured transport rates at levels of 3 to 5 m are somewhat underpredicted by the model, which may be related to moisture effects (rainfall) and supply-limited effects reducing the (measured) transport rates. Sand transport rates in crest zone with vegetation were also measured by Davidson-Arnott et al. (2012). The vegetation cover of marram grass was highly variable, ranging from about 20% near the crest to about 9% to 40% at a level of about 5 m. The measured sand transport rates in the crest zone (levels of 9 to 10 m) are almost zero (smaller than 0.00015 kg/m/s; factor 50 smaller than at level of 2 m). The model predicts zero transport for a vegetation cover of 15% (plant height=0.3 m) for wind velocities < 11.5 m/s.

The application of the present model to cross-shore windblown sand transport for a beach-dune system is a first and crude attempt to see whether the model predicts meaningful results. Ideally, the model should be coupled to a cross-shore sand transport model for the water system in a time loop-procedure so that the bed morphology from deep water to the foredune row can be simulated in one model. Cohn et al. (2018) have proposed such a coupled model, but our knowledge of shallow-water marine and aeolian processes including precipitation and vegetation needs to be much improved to obtain really accurate morphodynamic predictions. A somewhat different modelling approach at a higher level of aggregation is that of Delgado-Fernandez (2011) and Hallin et al. (2019) which are developed to model the sediment supply and supply limiting conditions from the beach to the dune over longer time scales (months to years). The present model can be easily included in such an approach. However, the upscaling of transport rates to a time scale of months to years may be problematic because of continuous changes of factors such as beach width, slopes, moisture content, shells and vegetation. It may be partly overcome by introducing classes for the moisture content, percentage of shells and vegetation (see Delgado-Fernandez, 2011).

7. Conclusions and recommendations

A fully predictive model for loose, dry sand is proposed, which only requires input from the wind velocity at one height above the surface and characteristic sand diameters (d_{50}, d_{90}). The model is based on the modification of the well-known Bagnold equation by including the threshold shear velocity, which is slightly adjusted to ensure a smoother transition from the non-transport regime to the transport regime. The sand transport rate is related to the static and dynamic grain roughness by using a semi-empirical roughness predictor, which is calibrated based on sand transport data from wind tunnel experiments with a flat mobile sand surface. Analysis of transport data from wind tunnel experiments shows that: 1) the cubic relationship between the transport rate and the shear velocity is a very reasonable approach and 2) the transport decreases for smaller diameters at higher shear velocities (upper regime), but increases slightly for smaller diameters at low shear velocities. This effect is to some extent represented by the modified Bagnold-equation due to the inclusion of a threshold shear velocity. However, the transport of fine sand (0.15 mm) is overpredicted by the Bagnold equation, if the measured shear velocity is used. In all, 105 high-quality data sets of wind tunnel and field experiments have been used for verification of the proposed predictive model. About 73% of the predicted values are within a factor of 2 of measured values of the transport rate. A higher score is hardly possible, given all variabilities and non-uniformities involved (wind field, sand composition, bed relief, surface roughness). The example application related to wind flow and sand transport normal to a foredune shows that the predictive model produces very reasonable results compared to measured sand transport rates across the dune front based on the field data of Davidson-Arnott et al. (2012). The example application related to the erosion of beach sand at the Dutch sand motor shows that the predictive model also produces meaningful results on an annual time scale.

The effects of moisture, vegetation and shells on the sand transport process are included by fairly simple expressions which are acting on the shear velocity, the threshold value and the transport rate. The coefficients were derived from available experiments in wind tunnels and at field sites. Sand transport reduces to almost zero for a moisture content of the topmost 20 mm of the surface exceeding 10%. Similarly, the sand transport is almost completely suppressed for a vegetation cover of about 20% to 30%. Even so, a shell cover of 30% to 40% reduces the sand transport to almost nil. Available data shows that the type of cover is less important.

Sand transport by wind can be compared to that by water by using the T-parameter (Eq. 3.6c). Using $T \cong 5$ (upper transport regime) and d_{50}=0.2 mm, the sand transport rate by wind is about 0.1 kg/m/s whereas that by water flow is of the order of 1 kg/m/s. Suspended sand transport is dominant in water flow whereas, saltation type of transport is dominant in air flow.

To extend the knowledge of the bed roughness and sand transport of sandy beaches, wind tunnel and field experiments are highly recommended. There is pressing need for detailed, short-duration experiments in wind tunnels with a flat, mobile sand surface in the upper transport regime to study the dynamic grain roughness. The effective roughness of a flat sand with and without shells (cover percentage of 3 to 30%) can also be studied in a wind tunnel at low wind velocities without sand transport. The form drag of artificially prepared ripples can also be determined in a wind tunnel. Special field studies focusing on the effect of ripples and shells on sand transport are also highly recommended.

8. References

Arens, S.M., Van kaam-Peters, H.M.E. and Van Boxel, J.H., 1995. Air flow over foredunes and implications for sand transport. Earth Surface Processes and Landforms, Vol. 20, 315-332

Arens, S.M., Baas, A.C.W., Van Boxel, J.H., and Kalkman, C., 2001. Influence of reed stem density on foredune development. Earth Surface Processes and Landforms, Vol. 26, 1161-1176. Doi: 10.1002/esp.257

Bagnold, RA., 1936. The Movement of Desert Sand. Proc. Royal Soc. London, Series A 157, 594-620.

Bagnold, R.A. 1941, 1954. The physics of blown sand and desert dunes. Methuen, New York.

Belly, P.Y., 1964. Sand Movement by Wind. U.S. Army Corps of Engineers, Technical Memorandum No 1, CERC, Washington, DC.

Brakenhoff, L.B., Smit, Y., Donker, J.J.A. and Ruessink, G., 2019. Tide-indiced variability in beach surface moisture: observations and modelling. Earth Surface Processes and Landforms, Vol. 44, 317-330

Brown, S., Nickling, W.G. and Gillies, J.A., 2008. A wind tunnel examination of shear stress partitioning for an assortment of surface roughness distributions. Journal of Geophysical Research Vol. 113. F02S06. Doi: 10.1029/2007JF000790

Buckley, R.C., 1987. The effect of sparse vegetation on the transport of dune sand by wind. Letters to Nature, Vol. 325, 426-428

Burri, K., Lehning, M, Gromke, C, Graf, K., 2011. Aeolian sediment transport over vegetation canopies; a wind tunnel study with live plants. Aeolian Research Vol. 3 (2), 205-213. Doi: 10.1016/j.aeolia.2011.01.003

Chepil, W.S., 1956. Influence of moisture on erodibility of soil by wind. Proc. Soil Sci. Soc. Am., 20, 288–292.

Cohn, N., Hoonhout, B.M., Goldstein, E.B. and De Vries, S., 2019. Exploring marine and aeolian controls on coastal foredune growth using a coupled model. Journal of Marine Science and Engineering, Vol. 7, 1-25, doi:.org/10.3390/jmse7010013

Cornelis, W.M., Gabriels, D., 2003. The effect of surface moisture on the entrainment of dune sand wind: an evaluation of selected models. Sedimentology Vol. 50, 771–790.

Davidson-Arnott, R.G.D., Bauer, B.O., Ollerhead, J., Hesp, P.A., Namikas, S. and Walker, I.J., 2005. Moisture and fetch effects on aeolian sediment transport rates during a fall storm, Greenwich dunes, Prince Edward Island. Canadian Coastal Conference.

Davidson-Arnott, R.G.D., Yang, Y., Ollerhead, J., Hesp., P.A. and Walker, I.J., 2008. The effects of surface moisture on aeolian sediment transport threshold and mass flux on a beach. Earth Surface Processes and Landforms, Vol. 33, 55-74. Doi:10.1002/esp.1527

Davidson-Arnott, R.G.D., Walker, I.J., Hesp, P.A., Ollerhead and Chapman, C., 2012. High-frequency sediment transport responses on vegetated foredune. Earth Surface Processes and Landforms, Vol. 37, 1227-1241

Delgado-Fernandez, I., 2010. A review of the application of the fetch effect to modelling sand supply to coastal foredunes. Aeolian Research Vol. 2 (2-3), 61-70

Delgado-Fernandez, I., 2011. Meso-scale modelling of aelian sediment input to coastal dunes. Geomorphology Vol.130, 230-243

De Vries, S., Arens, S.M., De Schipper, M.A., and Ranasinghe, R., 2014. Aeolian sediment transport on a beach with a varying sediment supply. Aeolian Research Vol. 15, 235-244

De Vries, S. and Hoonhout, B., 2017. Field measurements on spatial variations in aeolian sediment availability at the sand motor mega nourishment. Aeolian Research Vo. 24, 93-104
Dey, S., 2003. Threshold of sediment motion on combined transverse and longitudinal sloping beds. Journal of Hydraulic Research, Vol. 41, No. 4, 405-415.
Dong, Z., Liu, X. and Wang, X., 2002. Aerodynamic roughness of gravel surfaces. Geomorphology Vol 4, 17-31
Dong, Z., Lu, P., Zhang, Z. and Qian, G., 2012. Aeolian transport in the field: a comparison of the effects of different surface treatments. Journal of Geophysical Research Atmosphere, Doi: 10.1029/2012JD017538
Farrell, E.J. and Sherman, D.J., 2016. Process-scaling issues for aeolian transport modelling in field and wind tunnel experiments: roughness length and mass flux distributions. Journal of Coastal Research, SI19, 384-389.
Field, J.P. and Pelletier, J.D., 2018. Controlls on the aerodynamic roughness length and the grain size dependence of aeolian sediment transport. Earth Surface Processes and Landforms Vol. 43, 2616-2626. Doi: 10.1002/esp.4420
Gillies, J.A., Nickling, W.G. and King, J., 2006. Aeolian sediment transport through large patches of roughess in the atmospheric inertial layer. Journal of Geophysical Research Vol. 111, F02006. Doi: 10.1029/2005JF000434
Granger, R.J., Essery, R., Pomeroy, J.W., 2006. Boundary-layer growth over snow and soil patches: field observations. Hydrological Processes 20, 943–951.
Hallin, C., Larson, M., and Hanson, H., 2019. A process-based model for aeolian sediment transport and spatiotemporal varying sediment availability. Journal of Geophysical Research, Earth Surface, Vol. 121, doi:10.1002/2015JF003692
Han, Q., Qu, J., Liao, K., Zhu, S., Zhang, K., Zu, R. and Niu, Q., 2011. A wind tunnel study of aeolian sand transport on a wetted surface using sands from tropical humid coastal southern China. Environmental Earth Sciences, Vol. 64, 1375-1385; DOI 10.1007/s12665-011-0962-7
Hesp, P.A., Dong, Y., Cheng, H., and Booth, J.L., 2019. Wind flow and sedimentation in artificial vegetation: Field and wind tunnel experiments. Geomorhology Vol. 337, 165-182
Hesse, P., and Simpson, R.L., 2006. Variable vegetation cover and episodic sand movement on longitudinal desert sand dunes. Geomorphology Vol. 81, 276-291
Ho, T., 2012. Experimental study of saltating particles in a turbulent boundary layer. Doctoral Thesis, University of Rennes, France
Hoonhout, B. and De Vries, S., 2019. Simulating spatiotemporal aeolian sediment supply at a mega nourishment. Coastal Engineering Vol. 145, 21-35
Horikawa, K., Hotta, S. and Kraus, N.C., 1986. Literature review of sand transport by wind on a dry sand surface. Coastal Engineering 9, 503–526.
Hotta, S., Kubota, S., Katori, S., Horikawa, K., 1984. Sand transport by wind on a wet sand surface. Proceedings 19th Coastal Engineering Conference. ASCE, New York, 1265–1281.
Hsu, S.A., 1974. Computing eolian sand transport from routine weather data. Chapter 94, Proc. International Conference Coastal Engineering, Copenhagen
Hupy, J.P., 2003. Influence of vegetation cover and crust type on wind-blown sediment in a semi-arid climate. Journal of Arid Environments Vol. 58, 167-179
Jackson, D., Cooper, J., 1999. Beach fetch distance and aeolian sediment transport. Sedimentology, 517–522.
Kok, J.F., Parteli, E.J.R., Michaels, T.I. and Karam, D.B.., 2012. The physics of wind-blown sand and dust. Rep. Prog. Phys. Vol. 75, Doi:10.1088/0034-4885/75/10/106901
Lancaster, N. and Baas, A., 1998. Influence of vegetation cover on sand transport by wind; field studies at Owens Lake, California. Earth surface processes and Landforms Vol. 23, 69-82
Li, B., Ellis, J.T. and Sherman, D., 2010. Variability of the apparent Von Karman constant during aeolian transport. Geophysical Letters. Doi. 10.1029/2010GL044068
Liu, X., Dong, Z., Wang, X., 2006. Wind tunnel modeling and measurements of the flux of wind-blown sand. Journal of Arid Environments Vol. 66, 657–672.
McKenna Neuman, C., Li, B. and Nash, D., 2012. Micro-topographic analysis of shell pavements formed by aeolian transport in a wind tunnel simulation. Journal of Geophysical Research Vol. 117, F04003. Doi: 10.1029/2012JF002381

Musick, H.B. and Gillette, D.A. 1990. Field evaluation of relationships between a vegetation structural parameter and sheltering against wind erosion. Land Degradation and Rehabilitation Vol. 2, 87–94.
Musick, H.B., Trujillo, S.M. and Truman, C.R., 1996. Wind-tunnel modelling of the influence of vegetation structure on saltation threshold. Earth Surface Processes and Landforms Vol. 21, 589–605.
Nickling, W.G. and Davidson-Arnott, R.G.D., 1990. Aeolian sediment transport on beaches and coastal dunes. Proc. Canadian Symposium on coastal sand dunes
Owen, P.R., 1964. Saltation of uniform grains in air. Journal of Fluid Mechanics, Vol. 20, 225-242
Pelletier, J.D. and Field, J.P., 2016 Predicting the roughness length of turbulent flows over landscapes with multi-scale microtopography. Earth Surface Dynamics Vol. 4, 391-404. Doi: 10.5194/esurf-4-391-2016
Raupach, M.R., 1992. Drag and drag partition on rough surfaces. Boundary Layer Meteorology Vol. 60, 375–395.
Raupach, M.R., Gillette, D.A., Leys, J.F., 1993. The effect of roughness elements on wind erosion threshold. Journal Geophysical Research Vol. 98, 3023–3029.
Saleh, A. and Fryrear, D.W., 1995. Threshold wind velocities of wet soils as affected by wind-blown sand. Soil Sci., 160, 304–309.
Shao, Y. P. and Lu, H., 2000 A simple expression for wind erosion threshold friction velocity Journal Geophysical Research Vol. 105, 22437–43
Shao, Y. et al., 2015. A tribute to M.R. Raupach for contributions to aeolian fluid dynamics. Aeolian Research Vol. 19, 37-54
Sherman, D.J., 1992. An equilibrium relationship for shear velocity and apparent roughness length in aeolian saltation. Geomorphology, Vol. 5, 419–431.
Sherman, D.J. and Farrell, E.J. 2008. Aerodynamic roughness lengths over movable beds: comparison of wind tunnel and field data. Journal of Geophysical Research: Earth Surface Vol. 113; doi.org/ 10.1029/2007JF000784.
Sherman, D. J., Jackson, D. W. T., Namikas, S. L., and Wang, J., 1998. Wind-blown sand on beaches: An evaluation of models. Geomorphology, Vol. 22(2), 113–133. Doi: 10.1016/S0169-555X(97)00062-7
Sherman, D., Ellis, J.T., Li, B., Farrell, E.J., Maia, P. and Granja, H.M., 2013. Recalibrating aeolian sand transport models. Earth Surface and Landforms, Vol. 38, 169-178. Doi: 10.1002/esp.3310
Sherman, D.J., Swann, C. and Barron, J.D., 2014. A low-cost aeolian sand trap. Aeolian Research, Vol. 13, 31-34.
Strypsteen, G., 2019. Monitoring and modelling aeolian sand transport at the Belgian coast. Doctoral Thesis, KU Leuven, Belgium.
Strypsteen, G., Montreuil, A.L. and Rauwoens, P., 2017. Aeolian sand transport at the Belgian coast; field campaigns and first results. Paper 117. Coastal Dynamics.
Strypsteen, G., Van Rijn, L.C. and Rauwoens, P., 2019. On the relation between predicted and observed aeolian sand transport rates: a field study at the Belgian coast. Submitted to Journal of Aeolian Research
Udo, K., Kuriyama, Y. and Jackson, D.W.T., 2008. Observations of wind-blown sand under various meteorological conditions at a beach. Journal of Geophysical Research Vol. 113, F04008. Doi: 10.1029/2007JF00936
Valance, A., Rasmussen, K.R., Moctar, A.O.E and Dupont, P., 2015. The physics of aeolian sand transport. Comptes Rendus Physique, Elsevier Masson, Vol. 16 (1), 1-13. Doi: 10.1016/j.crhy.2015.01.006
Van der Wal, D. 1999. The impact of the grain-size distribution of nourishment sand on aeolian transport. Journal of Coastal Research Vol. 14 (2), 620-631
Van Rijn, L.C., 1982. Equivalent roughness of alluvial bed. Journal of Hydraulics Division, ASCE, Vol. 108, Hy 10, 1215-1218.
Van Rijn, L.C., 1984. Sediment Transport, Part III: Bed Forms and Alluvial Roughness. Journal of Hydraulic Engineering, ASCE, Vol. 110, No. 12.
Van Rijn, L.C., 1987. Mathematical modelling of morphological processes in the case of suspended sediment transport. Doctoral Thesis, Civil Engineering Department, Delft University of Technology, Delft, The Netherlands
Van Rijn, L.C., 1993. Principles of sediment transport in rivers, estuaries and coastal seas. AquaPublications, The Netherlands (www.aquapublications.nl)
Van Rijn, L.C., 2006. Principles of sediment transport in rivers, estuaries and coastal seas, Part II. AquaPublications, The Netherlands (www.aquapublications.nl)

Van Rijn, L.C., 2007. Unified view of sediment transport by currents and waves, I: Initiation of motion, bed roughness, and bed-load transport. Journal of Hydraulic Engineering, 133(6), 649-667.
Van Rijn, L.C., 2007. Unified view of sediment transport by currents and waves, II: Suspended transport. Journal of Hydraulic Engineering, 133(6), 668-389.
Van Rijn, L.C., 2007. Unified view of sediment transport by currents and waves, III: Graded beds. Journal of Hydraulic Engineering, 133(7), 761-775.
Wasson, R.J. and Nanninga. P.M., 1986. Estimating wind transport of sand on vegetated surfaces. Earth Surface Processes and Landforms. Vol. 11, 505-514
Wiggs, G.F.S., Livingstone, I. and Warren, A., 1996. The role of streamline curvature in sand dune dynamics: evidence from field and wind tunnel measurements. Geomorphology Vol. 17, 29-46
Winterwerp, J.C., De Groot, M.B., Mastbergen, D.R. and Verwoert, H., 1990. Hyper-concentrated sand-water mixture flows over flat bed. Journal of Hydraulic Engineering, ASCE, Vol. 116, No.1
Wolfe, S.A. and Nickling, W.G., 1993. The protective role of sparse vegetation in wind erosion. Progress in Physical Geography 17, 50–68.
Xian, X., Tao, W., Qingwei, S. and Weimin, Z., 2002. Field and wind-tunnel studies of aerodynamic roughness length. Boundary-Layer Meteorology, Vol. 104, 151-163
Yang, Y, Liu, L., Shi, P., Zhang, G., Xiong, Y., Lyu, Y., Guo, L., Liang, B., Zhao, M., Dai, J., Zuo, X, and Han, X., 2019. Aerodynamic grain-size distribution of blown sand. Sedimentology, Vol. 66, 590-603
Youssef, F., Visser, S.M., Karssenberg, D., Erpul, G., Cornelis, W.M., Gabriels, D. and Poortinga, A., 2012. The effect of vegetation patterns on wind-blown mass transport at the regional scale: A wind tunnel experiment. Geomorphology Vol. 159-160, 178-188
Zhang, C.L., Zou, X.Y., Gong, J.R., Liu, J.R. and Liu, Y.Z., 2004. Aerodynamic roughness of cultivated soil and its influences on soil erosion by wind in a wind tunnel. Soil and Tillage Research Vol. 75, 53-59

A FULLY PREDICTIVE MODEL FOR AEOLIAN SAND TRANSPORT, Part 2: Description and calibration of models and effect of moisture and coarse materials.

by L.C. van Rijn[1]
[1]LVRS-consultancy, Domineeswal 6, 8356D Blokzijl, The Netherlands; info@leovanrijn-sediment.com

Keywords: predictive model for wind-blown sand; supply-limiting effects on wind-blown sand

Abstract
This paper presents new research results on the effect of moisture and coarse materials (gravel and shells) on aeolian transport and is a continuation of earlier work. Two mini wind tunnels have been designed and used to study the effect of moisture and coarse materials on the threshold shear velocity and on the sand transport rate at wind velocities in the range of 10 to 16 m/s. Extensive attention was given to the determination of the drying time of the beach surface after a period with rainfall for a range of temperatures and wind conditions. A new equation to include the effects of coarse materials on aeolian sand transport is derived from the mini wind tunnel data. Two prediction methods for aeolian sand transport were evaluated: the modified Bagnold-transport equation and the new VR-transport equation. Both methods include the effects of sand diameter and the threshold shear stress, which is essential for accurate determination of sand transport at low wind speeds. The cessation-related threshold shear velocity produces the best results. The grain-related shear velocity is the basic driving parameter of both prediction methods. The wind tunnel data of Belly (1964) have been used to calibrate the new VR-sand transport equation.

1. Introduction

This paper is a continuation of earlier work on the development of a complete theory for the prediction of aeolian transport including the effects of moisture and coarse materials (Van Rijn and Stryspteen 2020). These latter effects are qualitatively known, but an accurate procedure for quantitative predictions is missing. Another problem is the limited amount of high-quality field data. Although sand transport by wind is easily observable, reliable and accurate data sets of sand transport rates are still scarcely available due to measuring difficulties. Sherman et al. (2013) have presented a high-quality dataset of 32 points of wind-driven sand transport rates, but much more tabulated data based on well-defined parameters can rarely be found in the literature.
In Part 1, Van Rijn and Strypsteen (2020) have modified the well-known Bagnold equation for wind-driven sand transport by including the threshold for initiation of motion and the grain-related shear velocity as the main driving parameter instead of the overall shear velocity. The data set of Sherman et al. (2013) and recent field data from beaches in Belgium (Strypsteen, 2019) were used for verification of the modified Bagnold-equation. Furthermore, the effects of moisture and coarse materials on sand transport were explored based on available data from the literature. Rainfall causing moist sand and coarse materials (gravels and shells) are severe supply-limiting factors on natural sand beaches. Moist sand has a higher threshold shear velocity than dry sand due to cohesive and adhesive forces of very fine particles and water films surrounding the sand particles. Crust forming at the sand surface may also lead to increased threshold values. Coarse materials, shells and shell clusters consisting of interlocking smaller and large shells also protect the sand surface against erosion. Literature on this is scarce and mostly qualitative.
In this Part 2, a new method for aeolian sand transport is developed and calibrated using the wind tunnel data of Belly (1964). The research on the effects of moisture and coarse materials is substantially extended by experimental work (in mini wind tunnels) on dry and moist sand and sand covered with coarse materials. Based on this, existing equations representing the effects of moisture and coarse materials are modified. The new method is verified in Part 3 using old and new field data (beaches in Belgium and The Netherlands).
The applied models for sand transport are presented in Section 2. Laboratory instrumentation is explained in Section 3. The effects of moisture and coarse materials on the sand transport processes are discussed in Sections 4 and 5.

2. Sand transport equations

2.1 Equations

The most classic sand transport equation for wind is that proposed by Bagnold (1941,1954). Van Rijn and Strypsteen (2020) have modified this equation using the grain-related bed-shear velocity as the driving parameter and including the threshold shear velocity for initiation of motion.

Herein, another approach is explored as well. The sand transport of dry sand close to the bed in both water and air can be described by a set of dimensionless parameters (Yalin, 1977; Van Rijn, 1993), being:

- dimensionless sand transport: $\phi=q_{s,eq}/[\rho_s\,(s-1)^{0.5} g^{0.5}\, d_{50}^{1.5}]$; (1)
- dimensionless particle size: $D_*=[(s-1)g/\upsilon^2]^{1/3}\, d_{50}$; (2)
- dimensionless particle mobility parameter (Shields parameter): $\theta = u_{*,gr}^2/[(s-1)gd_{50}]$; (3a)
- dimensionless threshold particle mobility parameter (Shields parameter): $\theta_{th}= u_{*,th}^2/[(s-1)gd_{50}]$; (3b)
- dimensionless sediment density: $s=\rho_s/\rho_{air}$. (4)

with:

$q_{s,eq}$ = equilibrium (saturated) mass sand transport (kg/m/s); ρ_s =sediment density (2650 kg/m³); ρ_{air} =air density (1.2 kg/m³); $s=\rho_s/\rho_{air}$=relative density; d_{50}= median grain size (in m); υ= kinematic viscosity of air ($1.33\cdot10^{-5}$ m²/s for 0 °C and $1.5\cdot10^{-5}$ m²/s for 20 °C); $u_{*,gr}$ = grain-related bed-shear velocity (in m/s) and $u_{*,th}$ = threshold bed-shear velocity (in m/s).

The dimensionless sand transport equation can be formulated as:

$$\phi=\alpha\,[D_*]^{\beta}\,[\theta-\theta_{th}]^{\gamma} \quad (5)$$

with α, β and γ being coefficients. Equation (5) is a universal equation for sand transport in water based on dimensional analysis (Yalin, 1977; Van Rijn, 1993). Herein, it is assumed that Equation (5) is also valid for sand transport in air. Bagnold (1941) for sand transport in air and Meyer-Peter & Müller (1948) for sand transport in water have found that $\gamma \cong 1.5$. Meyer-Peter and Müller (1948) found that bed load transport of very coarse sand particles in water is independent of grain size ($\beta = 0$) for higher stages of flow far beyond initiation of motion. Van Rijn (2007) found that bed load transport of finer sand particles in water is related to $(d_{50})^{0.5}$; thus $\beta = 0.5$. Bagnold (1941) found a similar power for wind-blown sand transport. Thus, the β-parameter is in the range of 0 to 0.5.

Substitution of Equations (1), (3) and (4) in Equation (5) and $s-1 \cong s$ for sand in air gives:

$$q_{s,eq,VR} = \alpha_{VR}\,(\rho_{air}/g)\,(D_*)^{\beta}\,[(u_{*,grain})^2-(u_{*,th})^2]^{1.5} \quad (6a)$$

$$q_{s,eq,VR} = \alpha_{VR}\,\alpha_{ad}\,\alpha_{cf}\,(\rho_{air}/g)\,(D_*)^{\beta}\,[(u_{*,grain})^3-(u_{*,th})^3] \quad (6b)$$

Equation (6a) includes the term $(u_*^2-u_{*,th}^2)^{1.5}$ which can be replaced by the term $(u_*^3-u_{*,th}^3)$ as the error involved is fairly small for wind velocities far beyond initiation of motion. Around threshold conditions, the results of Equation (6b) can deviate significantly, but these transport rates are extremely small and less important in practice. Although there is no physical reason to prefer Equation (6b) above Equation (6a), it has been found that Equation (6b) gives a better overall fit to the transport data of Belly (1964), see Section 2.3. In Part 3, it is shown that Equation (6b) also gives excellent results around threshold conditions. Therefore, Equation (6b) is preferred and used in this study.

The threshold shear velocity is described by the Bagnold-equation, as follows:

Threshold shear velocity:

$$u_{*,th} = \alpha_w\,\alpha_{slope}\,u_{*,th,B} \quad (7a)$$

$$u_{*,th,B} = \alpha_{th}\,[(\rho_s/\rho_{air}-1)\,g\,d_{50}]^{0.5} \quad \text{for } d_{50}> 100\ \mu m \quad (7b)$$

$$u_{*,th,B} = u_{*,th,100\ um} \quad \text{for } 32 < d_{50}< 100\ \mu m \quad (7c)$$

Grain-related shear velocity:

$$u_{*,grain}= \kappa\,\alpha_{veg}\,u_w/\ln(30z_{wind}/k_{s,grain}) \quad (8)$$

with: $u_{*,grain}$ = shear velocity related to the dynamic grains (m/s) as proposed by Van Rijn and Strypsteen (2020); $u_{*,th}$=surface shear velocity at threshold conditions (m/s); $k_{s,grain}$= equivalent roughness length scale of Nikuradse (1933) related to dynamic grains (Van Rijn, 2011; Van Rijn and Strypsteen, 2020); u_w = local wind velocity at height z_{wind} above the sand surface (m/s); κ= constant of Von Karman (=0.4); α_{ad}= adjustment coefficient related to fetch (maximum 1; Van Rijn and Strypsteen 2020); α_{cf} = reduction coefficient related to the presence of coarse materials (shell/gravel); α_{th}= threshold coefficient (values in the range of 0.07 to 0.11 representing either the static initiation of motion or the dynamic cessation threshold value); α_{slope} = coefficient for sand grains at a sloping surface (Van Rijn and Strypsteen, 2020); α_w= moisture coefficient (=1 for dry sand); α_{veg}= vegetation coefficient (=1 for conditions without vegetation).

Assuming a logarithmic velocity profile for wind flow over the surface, the shear stress is defined by :

$$u_z=(u_*/\kappa)\ln(z/z_o) \qquad (9a)$$

with: u=wind velocity at height z above surface, u_*= shear velocity, z_o=zero velocity level ($\cong k_s/30$), k_s= bed roughness height of Nikuradse (1933), (Van Rijn 2011).
Bagnold (1941) found that the streamwise wind velocity (u_f) is approximately constant at the "focal height z_f" being $\cong$ 2 to 20 mm based on Bagnold and others. Above the near-bed region (>20 mm) with intense saltation and constant wind speed, the wind velocity profile retains the logarithmic velocity distribution with a higher effective bed roughness (z_f). The velocity profile is shifted upward and can be described as:

$$u_z=u_f + (u_*/\kappa)\ln(z/z_f) \qquad (9b)$$

Martin et al. (2013) used Equation (9a) for clean air conditions ($u_*<u_{*th,cessation}$) and Equation (9b) for active saltation conditions ($u_*>u_{*,th,cessation}$) at a field site in California (USA). Based on this approach, three parameters can be determined from measured velocity profiles: cessation threshold $u_{*,th,cessation}$; z_f-value and z_o-value.
Finally, it is noted that Equation (6b) is based on the grain-related shear velocity ($u_{*,grain}$) which is smaller than the overall shear velocity (u_*). This latter parameter may include form drag (eddy/vortex production) which is less important for particle erosion/entrainment. Van Rijn and Strypsteen (2020) have proposed predictive equations for the grain-related shear velocity. Using these equations, a fully predictive model is obtained which only requires the velocity at a certain height above the surface. This can be the velocity measured at a local wind mast at the beach or the velocity from time records measured at a local airport for engineering studies.

2.2 Initiation of motion

Laboratory and field experiments show that sand particles can still be in motion when the shear velocity is smaller than the threshold value for initiation of motion ($u_{*,th,initiation}$; Bagnold 1937, 1941) and only stop when the shear velocity is lower than the threshold for cessation of motion ($u_{*,th,cessation}$). This suggests the coexistence of two distinct threshold values for initiation and cessation of motion. The initiation threshold depends on the properties of the fluid, the gravitational forces and interparticle cohesion forces that oppose the fluid lifting. The cessation (also known as dynamic or impact) threshold shear velocity ($u_{*,th,cessation}$) is the lowest wind shear velocity at which saltation can be sustained after it has been initiated. The cessation threshold is lower than the initiation threshold because moving particles can bring other resting particles into motion through particle impacts (Kok et al., 2012; Martin and Kok, 2018).

Bagnold (1937, 1941) found that $\alpha_{th,initiation} \cong 0.1\text{-}0.11$ and $\alpha_{th,cessation} \cong 0.8\ \alpha_{th,initiation}$. The data of Shao-Lu (2000) and Han et al. (2011) point to a value $\alpha_{th,initiation}=0.1$. Other researchers have found cessation threshold values in the range of $\alpha_{th,cessation} \cong 0.7$ to $0.8\ \alpha_{th,initiation}$ based on analysis of field data (Martin et al., 2013; Martin and Kok, 2017, Martin and Kok, 2018; Martin et al., 2018; Comola et al., 2019). Martin et al. (2013) defined initiation (cessation) as sand transport (no sand transport) occurring after at least 1 second of zero-transport and found $u_{*,th,cessation}/u_{*,th,initiation}=0.76$ based on analysis of measured wind velocity profiles around threshold conditions for a field site in USA. At this site the wind velocity reached a peak value of $u_{initiation} \cong 8.7$ m/s, then declined toward a steady state of about 8.0 m/s for continued sand transport. At cessation conditions, the wind velocity decreased gradually toward a minimum value of $u_{cessation} \cong 6.8$ m/s at the time when transport ceased. Martin and Kok (2017) determined the cessation threshold value from the zero-intercept of the linear fit to saltation flux versus shear stress resulting in cessation threshold shear velocity in the range 0.28 to 0.34 m/s for sand of $d_{50}=0.4$ to 0.53 mm, which was slightly smaller (10%) than the initiation threshold range. Martin and Kok (2018) used a statistical method to derive the initiation and cessation thresholds from high-frequency wind velocity and saltation measurements at three field sites resulting in $\alpha_{th,cessation}/\alpha_{th,initiation}=0.81$, 0.86 and 0.84 for three field sites in Brazil and USA. Their measurements show that when saltation is mostly inactive, its instantaneous occurrence is governed primarily by wind exceedance of the initiation threshold and that the time-averaged saltation flux is primarily governed by the cessation threshold.

It is noted that the transport processes around the threshold value are strongly dominated by the instantaneous turbulent fluctuations resulting in an intermittent transport process. For example, if the mean shear stress is equal to the threshold stress ($\tau_{mean}=\tau_{th}$), there still may be a small net transport due the largest fluctuations ($\tau_{max}>\tau_{th}$), (Stout and Zobeck, 1997). Basically, this can only be represented using a stochastic approach (Kalinske, 1947; Einstein, 1950; Paintal, 1971; Grass, 1970; Van Rijn, 1993; Davidson-Arnott et al., 2008).

2.3 Equilibrium sand transport

Aeolian sand transport across beaches is complex due to the many influential parameters such as grain size, grain sorting, armour layers, bed roughness, beach slope, moisture content and vegetation cover. Mostly, the transport is smaller than the equilibrium transport (or transport capacity) of dry sand. Sand transport is limited by two main effects: transport-limiting effects and supply-limiting effects.

Transport-limiting parameters are wind speed, grain size and roughness which strongly modify/limit the equilibrium transport capacity. The transport capacity increases for increasing wind speed and decreasing grain size. Supply-limiting effects are effects (bed state) which modify/limit the supply of sediment into the air flow. An important supply-limiting effect is the state of the bed surface as modified by moisture, salt crusts, vegetation cover and other bonding agents. This limiting effect partly depends on the strength of the wind speed. Moist particles and/or coarse armour layers consisting of gravels and shells may be immobile at low wind speeds, but may be rather mobile during storm events with high wind speeds. The reduction of sand transport over a moist surface can be determined to some extent by modifying the critical bed-shear velocity.

Limited fetch length being the distance over which the beach is exposed to wind refers to an adjustment process which does not truly falls into either classification, but is herein treated as a supply-limiting effect. The fetch distance is almost infinite for wind parallel to the beach and equal to the beach width beyond the HW-mark for wind normal to the beach. In conditions with onshore wind, there is a progressive increase in sand transport from a zone of no transport at the HW-mark towards a zone of intense transport near the dune foot. In the case of a constant wind speed above the threshold value for initiation of motion, the development of sand transport to the equilibrium (saturated) value for dry sand primarily depends on the upwind fetch distance. The critical fetch distance is the minimum fetch distance to obtain equilibrium sand transport or sand transport capacity of dry sand. The critical fetch distance for dry sand may also be influenced by moisture, shells and vegetation. Based on field data, the critical fetch distance is found the be about 20 to 100 m, depending on the strength and

direction of the wind (Jackson-Cooper 1999; Davidson-Arnott et al., 2005; Bauer et al., 2009, 2012; Delgado-Fernandez, 2010,2011; De Vries et al., 2014). The critical fetch distance is fairly small (<50 m) for low wind speeds.

2.4 Calibration of models for dry sand in wind tunnel

The VR-equation (6b) has been calibrated by the fitting of three coefficients: α_{VR}, β and α_{th} using the data of Belly (1964) measured in a wind tunnel with three fairly uniform diameters (d_{50}=0.44 mm, 0.3 mm and 0.145 mm). The best agreement of measured and computed sand transport rates was found for α_{VR}=1.8, β=0.1 and α_{th}=0.08, see **Figure 1**. Using these values, 92% of the computed transport rates are within a factor of 2 of the measured values (36 out of 39 data points).

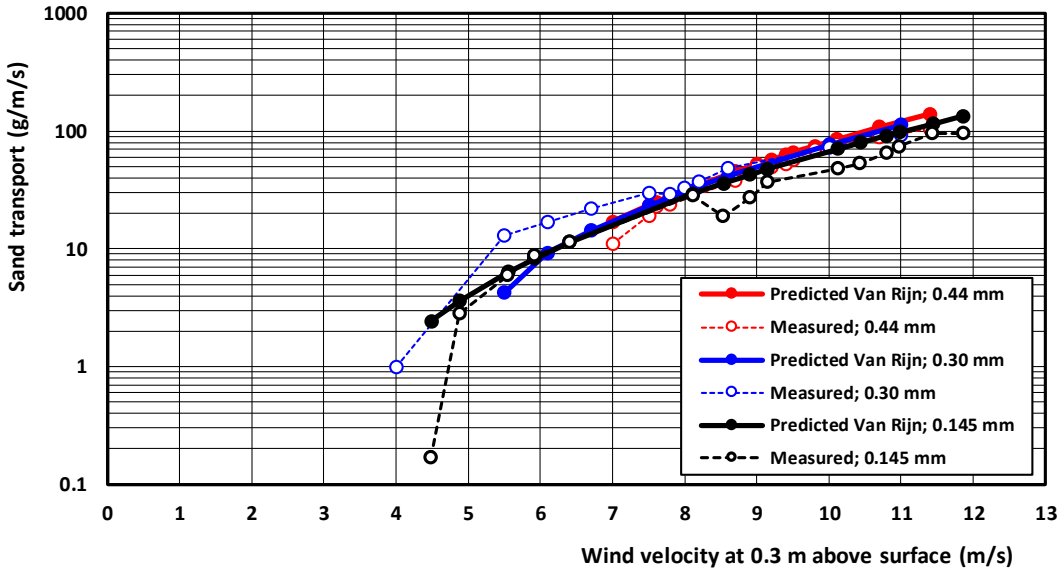

Figure 1 *Predicted and measured wind-blown sand transport; VR-equation (6b) α_{VR}=1.8; β=0.1 and $\alpha_{th,cessation}$=0.08; wind tunnel data of Belly (1964)*

It can be observed that the sand transport strongly increases for increasing wind velocities. The measured transport rates also increase for increasing particle diameter between 0.145 mm and 0.3 mm. The transport rate of sand with d_{50}=0.3 mm is about 50% higher than that of sand with d_{50}=0.145 mm. The transport of sand with d_{50}=0.3 and 0.44 mm is about the same. The power of the relationship between transport and shear velocity is best represented by a value of 3. An extensive discussion on the power of the relationship between transport and shear velocity is given in Part 3 (verification of model). The grain size effect is best represented by β=0.1, which means a weak increase of the transport rate for an increasing grain size. Two values of the α_{th}-coefficient have been used: α_{th}=0.08 representing cessation of motion and α_{th}=0.1 representing initiation of motion. The cessation threshold shear velocity ($\alpha_{th,cessation}$=0.08) yield the best results, because the transport rates at low wind speeds are better predicted.

Similarly, the modified Bagnold-equation using $\alpha_{th,cessation}$=0.08 also yields the best agreement with a score of 90% within a factor of 2 for the data of Belly (1964), see **Figure 2**. The calibration results are slightly less good if the initiation threshold shear velocity ($\alpha_{th,initiation}$= 0.1) is used, see Van Rijn and Strypsteen (2020). The modified Bagnold-equation can represent the measured transport of sand with d_{50}=0.145 and 0.3 mm reasonably well, although the transport of sand with d_{50}=0.145 mm is slightly underpredicted and that of d_{50}=0.44 mm is slightly overpredicted. The effect of the particle diameter is somewhat too strong (β=0.5 somewhat too high) resulting in under- and overprediction of the order for 20% for finer sands and coarser sands.

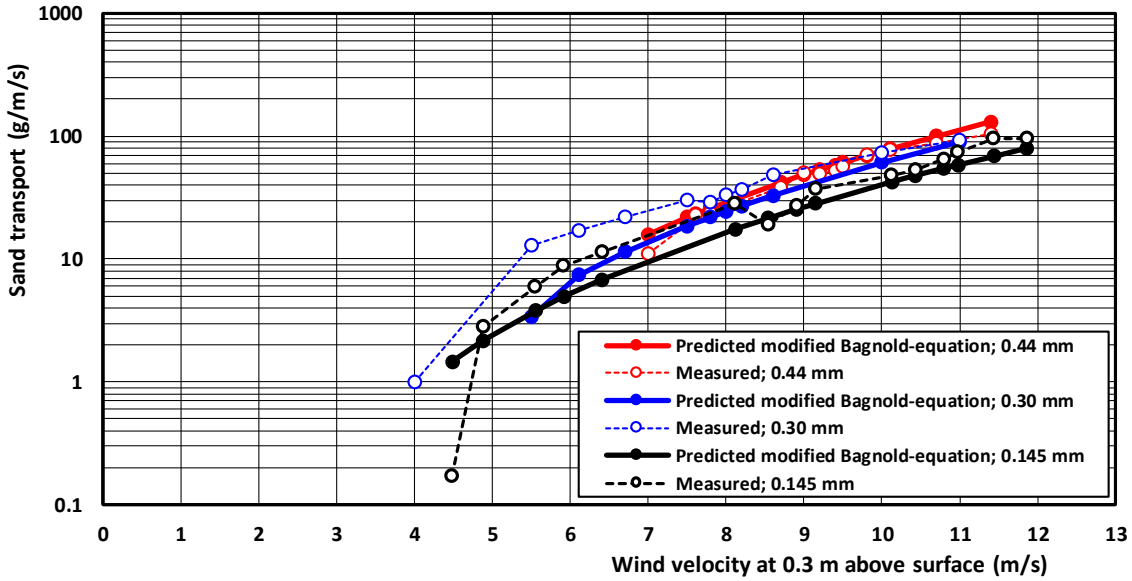

Figure 2 *Predicted and measured wind-blown sand transport; Modified Bagnold equation with α_B=2; and $\alpha_{th,cessation}$=0.08; wind tunnel data of Belly (1964)*

3. Instrumentation and field sites

New laboratory experiments on the effect of moisture and coarse materials have been performed in two mini wind tunnels with a length of 1 m (see **Figure 3**). The bottom and side walls of the tunnels consist of wood (multiplex 18 mm). The tunnel cover is made of transparent material. The internal dimensions of the two tunnels are 50x50 mm² and 60x60 mm². The tunnel height can be reduced by inserting a short wooden ramp in the tunnel to increase the wind velocity. At the downwind end of each tunnel, a small plywood tray filled with sand can be inserted. The top surface of the tray is flush with the top surface of the wooden tunnel bottom. The length of the tray is 250 mm and the height of the tray is 18 mm. The wind flow is generated by a standard hair dryer which can produce wind velocities up to 25 m/s. The hair dryer produces a very steady wind flow with only very minor fluctuations due to turbulence (smaller than 5% of the time-averaged velocity). The wind velocity at the downwind end of the tunnel at an elevation of 30 mm above the surface was measured by a mini wind cup velocity meter with rotor diameter of 22 mm and a cup height of 10 mm (Kaindl-windmaster 2 with inaccuracy < 3%). The wind velocities measured by the Kaindl-instrument have been compared to those of a high-quality wind cup-meter at a short wind mast during a field survey on the island of Texel (Strypsteen et al., 2021) resulting in values within 5% of each-other. The wind velocities in the mini wind tunnel were in the range of 5 to 16 m/s. The wind flow is turbulent as the Reynolds number involved is about $Re=u_w h/\upsilon=10x0.05/0.00001.5=3\ 10^4$.

It is realized that the mini wind tunnels are relatively narrow causing substantial side wall effects. Therefore, special calibration tests have been performed to measure velocity profiles above a flat bottom surface consisting of plywood covered with non-mobile 0.35 mm-sand grains (glued to surface). The measured wind velocity distribution in the middle axis at the end of the tunnel follows a logarithmic profile (R^2=0.99). The bed-shear velocity in the middle axis of the bottom surface is u_*=0.67 m/s for a wind velocity of 10 m/s at z=0.01 m above the bottom surface. The effective roughness of the bottom is k_s=0.00085 m, which is about $2.5d_{50}$. Using this method, a very reasonable estimate of the bed-shear velocity and bed roughness in the middle axis of the bottom section can be obtained. To check this method, another set of calibration tests has been carried out with four types of uniform sand with known threshold shear velocity of initiation of motion (d_{50}=0.17, 0.34, 0.6 and 0.8 mm; $u_{*,initiation}$=0.22, 0.32, 0.42, 0.48 m/s based on Bagnold-equation). The tray was filled with uniform sand and the wind velocity at threshold conditions (some grains moving) was measured. The shear velocity values derived from the measured velocity profiles et the end of the tunnel are about 15% higher than those based on the Bagnold-equation. This systematic difference can be explained by the low level of turbulent fluctuations in the

mini tunnel requiring higher velocities causing initiation of motion (Grass, 1970; De Ruiter, 1983). To account for this deviation a calibration factor of 0.85 is applied. The inaccuracy of the measured bed-shear velocity is estimated to be of the order of 15%.
The sand transport rate at the end of tunnel is determined from the sand mass of the tray before and after each test using a weighing scale accurate to 10 mg. The length of the sand bed in the tray is 0.25 m, which is about 8 times the height of the flow boundary layer. The sand bed is much too short to establish equilibrium sand transport at the end of the tunnel. This is not a real problem as the test results have only been used in a relative way to study the effect of moisture and shells/gravel on the threshold shear velocity and on the sand transport by comparing the results of moist and dry sand under the same wind velocities..

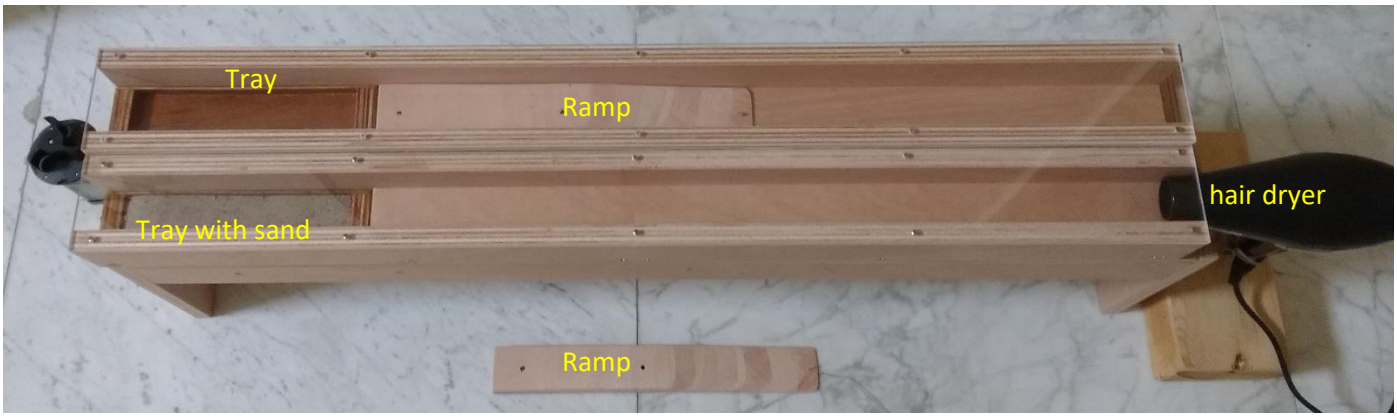

Figure 3 *Mini wind tunnels*

New field data related to the drying of sand after rainfall is obtained from various sites in Belgium (Zeebrugge beach d_{50}=0.2 mm) and in The Netherlands (Schokkerhaven beach d_{50}=0.34 mm and Callantsoog beach d_{50}=0.23 mm). Zeebrugge and Callantsoog are coastal beaches along the North Sea, whereas Schokkerhaven beach is an inland recreational beach along a lake. Detailed information of these beaches is given in Table 1 of Part 3.

4. Effect of moisture content on aeolian transport

4.1 Processes and definitions

Rainfall and related moisture content of the upper layer of beach sand has a strong effect on the mobility and transport of the sand particles. Wind tunnel experiments with dry and moist sand show that wind blown sand transport is strongly reduced with a factor of 2 to 10 for wind velocities in the range of 10 to 20 m/s (Hotta, 1984). Very few field studies on the (time dependent) effect of moisture on sand transport have been done. Drying times and thus the time-dependent moisture content of the beach surface layer strongly depend on the wind speed and the temperature (Horikawa et al., 1982; Jackson and Nordstrom, 1997; Wiggs et al., 2004; Van Dijk et al. 1996; Udo et al. 2008; Davidson-Arnott et al., 2008).
The reduction of sand transport in moist sand conditions is related to cohesion and adhesion effects between particles resulting in an increase of the surface resistance against erosion. Cohesion and adhesion effects may result from the presence of moisture, salt, algae, clay, organic matter and calcareous materials. Even low levels of moisture may effectively reduce the transport rate of dry sand. However, intensive rainfall may also increase the sand transport rate by splash effects promoting saltation processes. An extensive discussion on this is given by Van Rijn and Strypsteen (2020).
The moisture content is generally defined as: w= mass water of sample/mass dry sand of sample (moisture content is moisture fraction x 100%). The moisture content of a saturated sample can be computed by the expression: $w_{saturated}=[\varepsilon/(1-\varepsilon)][\rho/\rho_s]x100\%$ with ε= porosity factor (0.35-0.45 for sand); ρ= water density ($\cong$1000 kg/m^3); ρ_s= sand density ($\cong$2650 kg/m^3), yielding $w_{saturated}$= 20%-30%. Generally, the moisture content of the surface layer of beach sand is in the range of 0 to 10%, as the pores are not fully saturated with water.

Let us assume that a sand particle with diameter D is covered by a thin water film with thickness δ except at the particle contact points; any other pore water is absent.
The volume of the water film is: $V_{wf} = 1.33\pi\ [(0.5D+\delta)^3-(0.5D)^3]$ and the mass is: $M_{wf}=\rho V_{wf}$.
The volume of the sand particle is: $V_{sand}=1.33\pi(0.5D)^3$ and the mass is $M_{sand}=\rho_s V_{sand}$.
The mass ratio of water and dry sand defined as the moisture fraction is:
$w= M_{wf}/M_{sand}= \rho[(0.5D+\delta)^3-(0.5D)^3]/[\rho_s(0.5D)^3]$.
Using: D=200 μm for sand, δ=0.01D=2 μm, it follows that: $w \cong 0.025$ (2.5%).
Thus, a thin water film with thickness equal to 2 μm surrounding a sand particle of 200 μm yields a moisture content of about 2.5%. A water film of 1 μm yields a moisture content of 1%. Dry sand has a moisture content < 0.25% (Han et al., 2011). In conditions with w=10% (near the water line), the surface is so saturated that aeolian transport reduces to almost zero even under very strong winds.
Moist beach surfaces can be differentiated based on the darkness of the surface. Dark surfaces have higher moisture contents, whereas brighter (lighter) surfaces have lower moisture contents. Using this approach, a quick estimate of the percentage moist and dry areas at a particular beach zone can be obtained. The precise moisture content of the moist area can be simply determined by taking samples from the upper layer of the beach surface (drying and weighing). The mid and upper beach areas tend to be the driest areas. Moisture content is relatively high in areas with plant vegetation at the base of the foredune and in areas sheltered from direct solar radiation. To deal with spatial and temporal variability, the moisture content should be determined at many locations in a relatively short period of time. The sampling depth should be of the order of the dominant transport layer thickness. Visual observations from aeolian transport studies reveal that the thickness of the mobile transport layer around initiation of motion is of the order of a few millimeters (Ho, 2012). Mechanical sampling of thin layers of sand is tedious and laborious, both in laboratory and field conditions. Furthermore, the moisture content after rainfall of the thin upper layer can be highly variable, spatially due to topographic variations (bed forms, cusps, runnels, depressions) and temporally due to solar radiation and wind evaporation. In practice, a sampling method based on taking samples of thin layers for analysis in the laboratory (drying end weighing) is not very suitable to cover a wide grid of sampling points in the upwind area of the location where the aeolian transport is studied. A better solution is to use an electronic probe based on measuring conductivity of the sand between pins inserted in the upper sand layer (Atherton et al., 2001; Yang and Davidson-Arnott, 2005). Most probes consist of four stainless steel pins that are inserted into the sand. The difference in impedance/conductivity between the pins and the sand results in a reflection of this signal. The output is a moisture content value which is representative for the sand layer with a thickness equal to the pin length inserted in the sand bed. Accurate determination of the moisture content requires probe-calibration by using in-situ samples. Yang and Davidson-Arnott (2005) have found that a pin insertion length smaller than 20 mm including the calibration procedure taking thin sand samples, reduces the precision and accuracy of the probe substantially. Therefore, a pin length of 20 mm is proposed as the best compromise between accuracy and small layer thickness. However, it should be realized that the moisture content of the most upper mobile sand layer with thickness of a few millimeters is less than that of a layer of 20 mm. This practical field approach focusing on the moisture content of the upper 20 mm is still useful if the threshold shear velocity of the sand can be related to the moisture content of the upper 20 mm.
So far, various laboratory studies have been done in which the threshold velocity is related to the moisture content of the upper 2 to 5 mm of the sands surface (Chepil, 1956; Belly 1964; Hotta et al., 1984; Saleh and Fryrear, 1995; Cornelis and Gabriels 2003; McKenna Neuman and Sanderson, 2008; Han et al. 2011). The relationships between the threshold shear velocity and the moisture content of the upper 2 to 5 mm as found in wind tunnel studies cannot really be used for field conditions as it is problematic to measure the moisture content of the upper 2 to 5 mm at many locations within a short time period. Results from field studies show a large discrepancy compared to those for wind tunnel conditions (Horikawa et al., 1982; Jackson and Nordstrom, 1997; Wiggs et al., 2004; Van Dijk et al., 1996; Davidson-Arnott et al., 2008; Udo et al., 2008). Most likely, this is related to the thickness of the top layer in which the moisture content is measured. Most field data are valid for a top layer with a thickness of about 20 mm, whereas the laboratory data refer to the topmost layer of 2 to 5

mm. The moisture content of the thin top layer of 2 to 5 mm in field conditions will be much lower than the average value over a layer of 20 mm. The field experiments (Davidson-Arnott, 2008) also show that the moisture content at a certain location and thus the critical shear velocity can change rapidly over a period of minutes to hours due to drainage and/or drying by wind and sun.

4.2 Moisture variations during drying of beach sand

The beach sand layer above the ground water table consists of three sublayers (Hird and Bolton, 2017): i) lower layer with capillary water (fully saturated zone), ii) middle layer with funicular water (zone with water droplets coalescing into continuous water filaments) and iii) upper layer with pendular or hanging water (between sand grains) due to adhesive effects. The moisture content in the upper unsaturated layer with hanging water strongly depends on the rainfall intensity and the percolation rate of water in sandy soil. When the rainfall intensity is greater than the percolation rate, the upper sand layer will be become fully saturated with water. However, the rainfall intensity (0.0004 to 0.001 mm/s) at most beaches is much smaller than the percolation rate (0.01 to 0.1 mm/s) resulting in hanging-water conditions in the upper beach layer. Rainwater also disappears through evaporation which is about 1 mm/day in winter to about 8 mm/day in the summer for wind speeds between 3 and 15 m/s (Lin, 2001). However, most water disappears to deeper layers by percolation effects, which is about 100 to 1000 mm/day in sand.

The maximum moisture content in the upper layer where hanging-water prevails, is about 15%. This latter value can easily be determined by an experiment with a layer of beach sand (thickness= 20 mm; d_{50}= 0.34 mm) placed in a tray with perforated bottom plate and soaked with water. After a few minutes, the excess water is drained off through the perforated bottom plate and the moisture content can be found by weighing and drying resulting in moisture values of about 15%. In practice, the moisture content in the upper layer of 20 mm during and immediately after rainfall is found to be much lower with values of about 7% to 10% during normal rainfall intensity based on field tests of this study.

Field and laboratory experiments with moist sand layers have been performed in this study to determine the drying time of moist sand, which is herein defined as the time period after rainfall to get a moisture content of the upper 20 mm below 2 %. The sand surface at a beach is effectively (almost) dry with loose particles when the moisture content of the upper 20 mm is below 2%, because the observations show that the moisture content of the upper 1 to 5 mm is then below approximately 1%.

The laboratory tests consisted of the wetting and drying of a tray (diameter of 150 mm) filled with beach sand (d_{50}= 0.34 mm; thickness of 20 mm). The sand in the tray was wetted using a simple plant sprayer and the moist sand was mixed to get a uniform moisture content. The tray had a perforated bottom to allow water to drain vertically downwards onto a dry towel. The initial moisture content was mostly between 7% and 9%. This range of moisture contents was also observed at field sites immediately after rainfall. The tray was weighed regularly to observe the drying process at temperatures in the range of 5 to 25 ^{o}C. During some tests, the drying process was speed up by placing a ventilator upwind of the tray simulating a light breeze (measured wind velocity of 2.7 to 4.5 m/s at 2 cm above the tray). **Figure 4** shows the decrease of the moisture content of the upper 5 mm (green values) and 20 mm (red values) as function of time for the laboratory experiments. Without wind, the drying process at room temperature proceeds rather slow. All tabulated data are given by Van Rijn (2021).

When the initial moisture content is 8%, the drying time to below 2% is about 30 hours in conditions without wind and a temperature of 20 to 25 °C, about 55 hours for a temperature of 15 to 17 °C and about 120 hours for a temperature of 5 to 10 °C. The drying process during the night-hours is somewhat slower than during the day-hours. When a light wind is present, the drying time reduces substantially to about 5 hours (temperature 20 to 25 °C), 10 hours (15 to 17 °C) and 45 hours (5 to 10 °C). During the final phase of the drying process with moisture content values below 4% (layer of 20 mm), dry spots of lighter color were visible at the sand surface. The grains at these spots could easily be set in motion by blowing gently over the sand surface. The drying time of the upper layer of 5 mm was about 10% to 30% lower in the initial phase of the drying process, and about 50% lower in the final phase of the drying process. When the moisture content of the upper 20 mm layer was about 2% (see green curve with open circles; **Figure 4**), the moisture content of the upper 5 mm was about 1% (almost dry with loose mobile particles). A marked feature during the drying process was the presence of a thin crusty top layer (1 mm thick), which may be formed due to presence of calcareous materials (shell fragments) and very fine cohesive sediments.

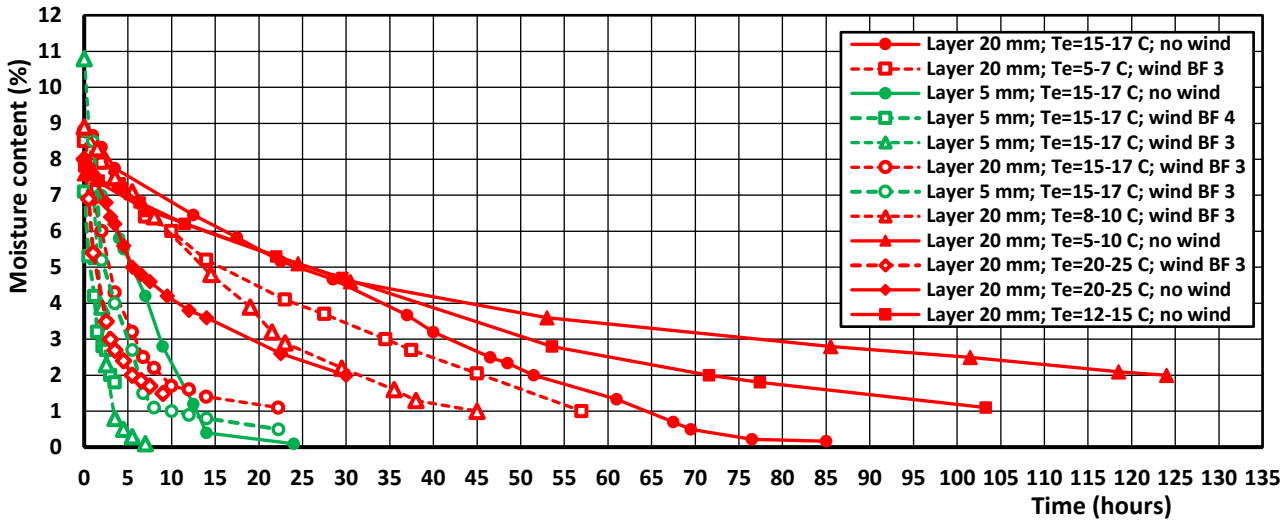

Figure 4 *Moisture content of drying sand (d_{50}=0.34 mm) as function of time in laboratory conditions; initial moisture content of 8% to 9% (upper 20 mm layer)*

The field tests consisted of the sampling and drying of sand from various beach sites. Sand layers with a thickness of 5 mm and 20 mm were scraped from the sand surface at the end of a period with rainfall and at various times during the drying process. The moisture content of the samples was determined by drying (in an oven at temperature of 150 °C) and weighing of the dry samples.

Long-continued rainfall (4 hours of more) produces a relatively thick layer of moist sand (20 to 50 mm), but short-duration rainfall of maximum 1 hour only yields a thin layer of moist sand (5 mm) on top of dry sand, as shown in **Figure 5**. A long period of dry weather (days) at the beach of Callantsoog (Netherlands) in February 2020 had resulted in a dry sand layer with thickness of about 10 to 15 mm. Immediately after rainfall (duration about 1 hour), the moist content of the top layer of 5 mm was about 9.5 %. The moisture content of the upper 20 mm was about 3.5% at about 50 m from the waterline and about 8% at 5 m from the waterline. No wind-induced sand transport was observed at wind velocity of about 6 m/s at z=1.1 m above the surface (Beaufort scale 4).

Figure 5 *Beach surface immediately after rainfall in winter; 8 February 2020; Callantsoog, Netherlands*
Left: vertical cut with moist top layer of 5 mm and dry layer of 10 to 15 mm;
Right: moist layer is removed with spade showing dry sand surface beneath

Field data results of the drying of beach sand are shown in **Figure 6.** All tabulated data are given by Van Rijn (2021). It is found that the total drying time of the upper 20 mm to bring the moisture content below 2% is of the order of about 30 hours in field conditions with moderate winds (< 3 m/s) in the autumn period (5 to 10^{o} C). The moisture content of the upper 5 mm is about 15% to 30% lower than that of the layer of 20 mm during the drying process, except immediately after rainfall (first hour). It was found that the upper 5 mm was almost dry (moisture content <1%) when the moisture content of the upper 20 mm was below 2%.

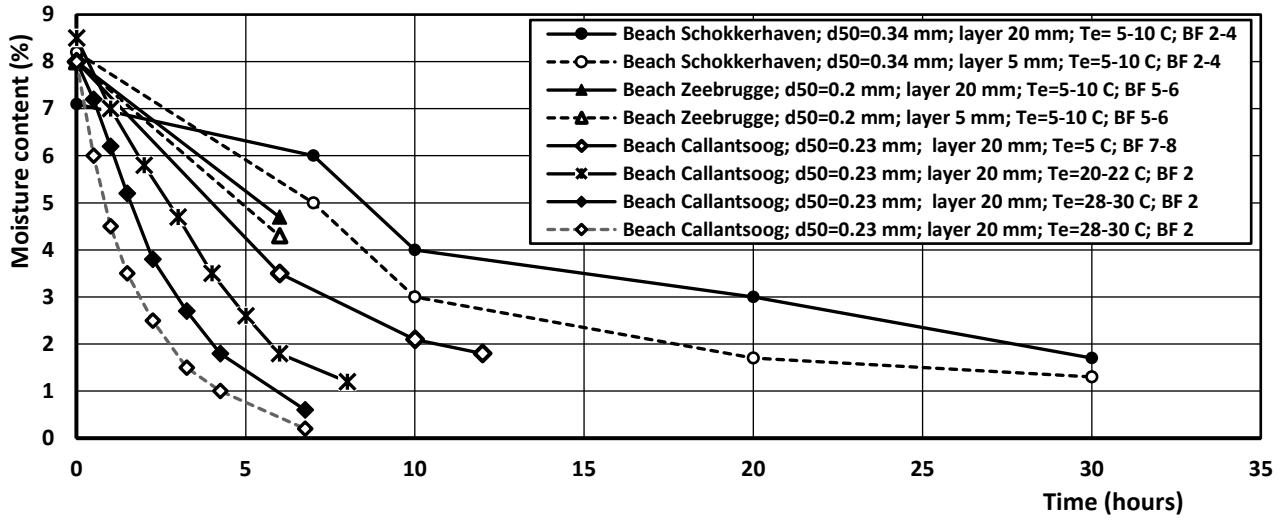

Figure 6 *Moisture content of drying sand as function of time in field conditions;*
initial moisture content of 7% to 9% (upper 20 mm layer)

The drying proceeds much faster in strong winds. At the beach of Callantsoog in February 2020 with temperature of 5^{o} C and a storm wind of 15 m/s (BF7), the moisture content of the top layer of 20 mm reduced from about 8% to 3.5 % in about 6 hours. The sand at the dune top with stronger wind of 18 m/s (BF8) was almost dry after 6 hours.

The drying time from moisture content of 8% to 2% in summer with temperature of almost 30 ^{o}C was about 4 hours. The top layer of 5 mm was almost dry after 2 hours. Hotta et al. (1984) report a drying time of 3 hours for the topmost layer of 3 mm after rainfall in the summer.

Yang and Davidson-Arnott (2005) and Davidson-Arnott et al. (2008) measured the moisture content of beach sand (top layer of 20 mm; 0.26 mm sand) in the period mid-May to Mid-June 2002 at Greenwich Dunes, Prince Edward Island National Park, Canada. They found that the drying of sand is greatest at the mid-beach area; the reduction of moisture content from 5% to 2% was about 3.5 hours in summer conditions. Wiggs et al. (2004) found a decrease from about 7% to about 5% over a period of 5 hours in conditions with a temperature of 15 °C and a gusty wind of BF4 in September 1998, which is in good agreement with the data of Callantsoog beach in The Netherlands, see **Figure 6**.

A remarkable feature of natural beaches is the simultaneous presence of moist and dry spots during the drying process in windy conditions. At the beach of Zeebrugge (Belgium), it was observed that about 60% of the surface was still wet (w_{20mm}= 4.7%) and about 40% was already dry after 6 hours from the last rainfall event in December 2019. Dry mobile sand particles were observed to accumulate in local depressions of the beach surface (lighter color areas). The percentage of dry spots increases rapidly as the drying time increases.

The drying process can be characterized by the time period ($T_{8\%-2\%}$) to bring the moisture content of the topmost layer of 20 mm from 8% immediately after rain fall to below 2%. It is most practical to focus on the upper 20 mm, as the sampling of 20 mm moist sand at field sites is easy with electronic sensors or by taking samples whereas the sampling/scraping of very thin layers (mm's) is problematic. Laboratory and field observations show that the beach surface is almost dry when the moisture content of the upper 20 mm is below 2%. **Figure 7** shows a tentative plot of the drying time scale $T_{8\%-2\%}$ as function of the temperature and the wind velocity (defined at 1 m above the surface) based on the available laboratory and field data. When wind is absent, the $T_{8\%-2\%}$ -value is quite high: 120 hours for temperature in the range of 5-10 °C and 50 hours for 15 to 17 °C and 7 hours for 28 to 30 °C. When light winds are present (BF3), the $T_{8\%-2\%}$ -value decreases to about 30 hours for a temperature of 5 to 10 °C (winter), to 10 hours for 15 to 17 °C (spring) to only 5 hours for a hot summer day with 28 to 30 °C. The characteristic drying time scale for stronger winds (>BF 4) is assumed to be slightly less. The results of this plot are used in Part 3 to include the effect moisture for long term sand transport predictions.

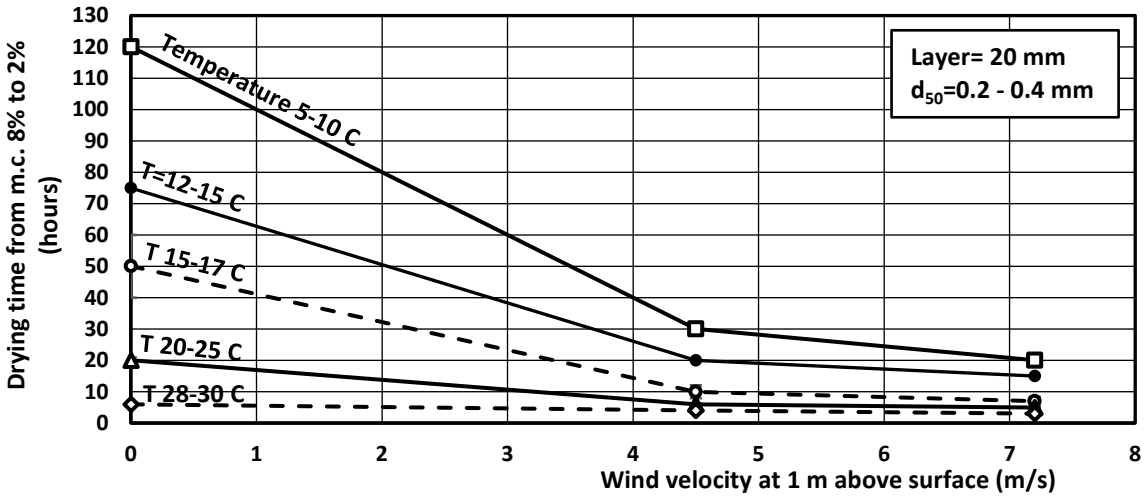

Figure 7 *Characteristic drying time of beach sand (layer 20 mm; m.c.=moisture content); d_{50}= 0.2 to 0.4 mm*

4.3 Effect of moisture content on threshold shear stress and sand transport

Various authors have studied the influence of moisture on the threshold shear velocity of sand particles by wind in wind tunnel conditions (Chepil, 1956; Belly, 1964; Hotta et al., 1984; Saleh and Fryrear, 1995; Cornelis and Gabriels, 2003 and Han et al., 2011) and in field conditions (Davidson-Arnott et al., 2005, 2008; Udo et al., 2008).

The effect of the moisture content on the threshold shear velocity is generally represented by: $u_{*,th,moist}=\alpha_w u_{*,th,o}$ with the α_w-coefficient being strongly dependent on the moisture content and the layer thickness considered. Additional experiments on the influence of the moisture content on the threshold shear velocity have been done in the mini-wind tunnels (see Section 3) focusing on the moisture content of the upper 20 mm. All tabulated data are given by Van Rijn (2021). Dry sand was mixed with tap water and a layer (20 mm) of wet sand was placed in the tray at the end of the mini wind tunnel. Three particle sizes (d_{50}=0.17, 0.34 and 0.8 mm) were used. The wind velocity was raised in steps until particle movement of grains was observed visually. Surface crust formation was observed in the tests with 0.17 mm-sand and 0.34 mm-sand. Individual sand particles and tiny sand balls of clustered particles (3 mm) were observed to be eroded from the crusted sand surface in these tests. Crust formation was not observed in the tests with 0.8 mm-sand; individual sand particles were observed to be rolling along the surface at threshold conditions. The ratio (α_w-coefficient) of the threshold shear velocity value of moist sand and dry sand is shown in **Figure 8**. The α_w-values of 0.8 mm-sand are significantly smaller than those of 0.17 mm-sand. Crust formation resulting in stronger adhesive/cohesive effects was clearly observed for 0.17 and 0.34 mm-sand but not for 0.8 mm-sand.

The data of the present wind tunnel tests and the field data of Davidson-Arnott (2008) can be reasonably well represented by the following expression:

$$\alpha_{w,20mm}= 1+0.1\,(d_{50,ref}/d_{50})\,w_{20mm} \qquad (10)$$

with: w_{20mm}= moisture content in upper 20 mm of surface, $d_{50,ref}$= median particle size of reference sand (0.25 mm), d_{50}=median particle size. Equation (10) which is a slight modified version of that proposed by Van Rijn and Strypsteen (2020) yields higher-values for finer sands as found in the present tunnel tests (crust formation effect). The effect of the grain size on the $\alpha_{w,20mm}$-coefficient is a bit speculative, as not many data points are available. Application of Equation (10) requires input data of the moisture content of the topmost 20 mm of the sand bed, either from measurements or from a prediction model for the moisture content. Equation (10) is used in Part 3 for the prediction of sand transport at moist field beaches.

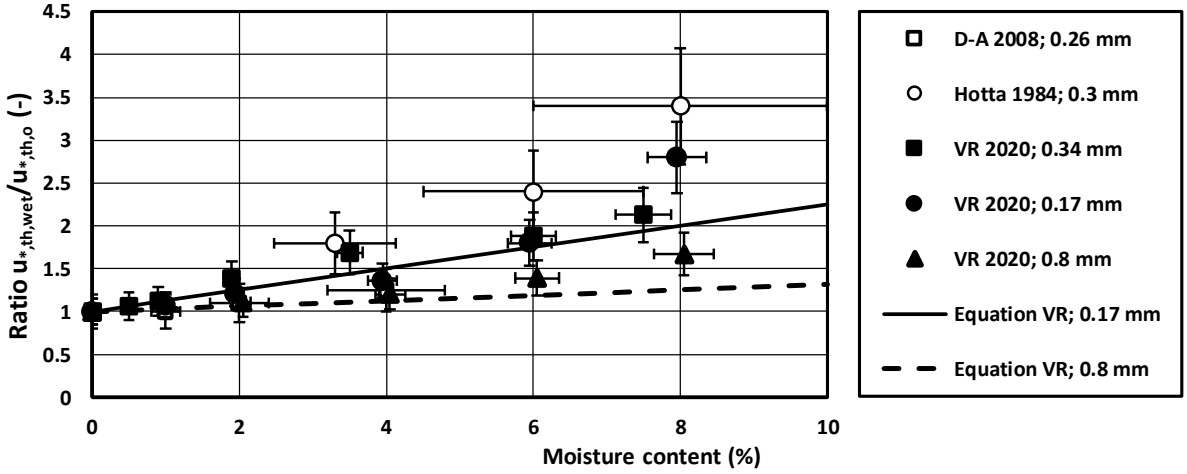

Figure 8 *Threshold shear velocity for initiation of motion as function of particle diameter and moisture content*

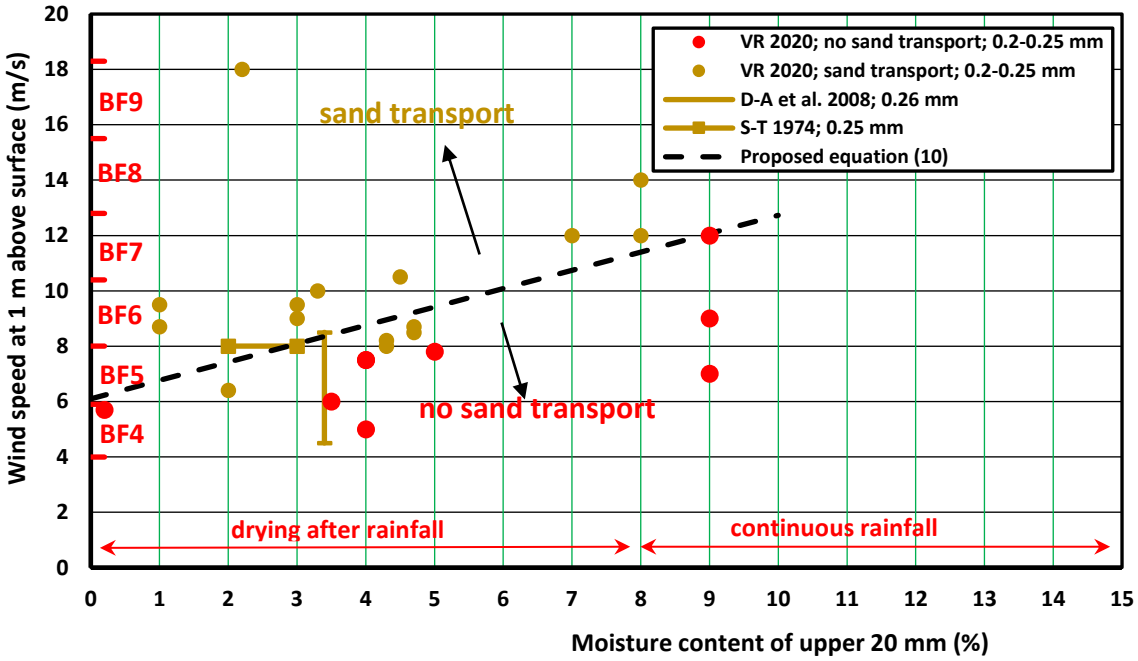

VR=Van Rijn 2020 (this study); D-A=Davidson-Arnott et al. 2008; S-T= Svasek and Terwindt 1974

Figure 9 *Effect of moisture content and wind speed on initiation of sand transport (BF is defined at height of 10 m above surface)*

During the field experiments at the beach of Callantsoog (The Netherlands), many observations of conditions with and without initiation of motion have been made at dry and moist areas on the beach. All basic data are given by Van Rijn (2021). **Figure 9** shows a diagram which can be used to determine the wind speed at which sand transport is initiated for given moisture levels of the upper 20 mm of the beach surface. Initiation of movement of dry sand particles occurs at a critical wind speed (at 1 m above the sand surface) of about 5.7 to 6.3 m/s for grains of 0.2 to 0.3 mm. The critical wind speed increases significantly for increasing moisture levels. After a rainfall event the moisture content of the upper 20 mm is about 8% to 10%, which requires a wind speed of 12 m/s (BF7) to generate sand transport processes. The wind speed of the Beaufort scale is defined at a height of 10 m above the surface. The wind speed at 1 m above the surface is about 75% of that at a height at 10 m, assuming a logarithmic velocity distribution. Data of Svasek and Terwindt (1974) during a summer storm are also shown. The data of Davidson-Arnott et al. (2008) represent the threshold range of sand transport with minimum and maximum wind speeds during which sand movement was observed by a saltiphone-sensor. Equation (10) converted to wind speed gives a very reasonable representation of the separation between transport and no transport (see dashed line in Figure 9). It should be realized that Equation (10) represents a hard transition between transport and no transport, whereas in reality a much more smooth transition will occur.

New experiments have been performed in the mini wind tunnel to qualitatively study the reduction of sand transport for various moisture levels. All tabulated data is given by Van Rijn (2021). Moist sand with d_{50}=0.34 mm was placed in the small tray at the end of the wind tunnel. The sand transport rate at the end of the tray was determined from the sand loss (gram) divided by the product of time period (s) and tray width of 0.05 m. In some tests there was sand feed (dry sand) from upwind boundary, but in most tests there was no sand feed. The initial moisture content was varied in the range of 1% to 8%. Crust formation was observed during all tests with 0.34 mm-sand and moisture content values between 0.5% and 8%.

Figure 10 shows the effect of the moisture content on the measured sand transport rates as a function of the measured wind velocity without upwind sand feed. The inaccuracy of the measured sand transport rates is about 20% to 30% based on repetitive tests. The inaccuracy of the measured wind velocity is less than 5%. The sand

transport rate of dry sand particles increases from about 10 g/m/s at a wind velocity of 10 m/s to about 100 g/m/s at a wind velocity of 16 m/s (factor 10 for velocity increase of factor 1.5) expressing a strong non-linear effect. At a high velocity of 16 m/s (at 0.03 m above the sand surface), the transport is very intensive with continuous movement at all places and the sand mass is completely removed (empty tray) within 30 sec. The measured sand transport rates at the end of the mini tunnels are much smaller than the equilibrium transport rates due to the limited length of the sand tray, the absence of wind gusts and the absence of irregularities (ripples, etc).

No particle movement and sand transport were observed for a moisture content of 7% to 8% for wind velocities up to 16 m/s (at 0.03 m above the sand surface). Similarly, no movement and transport were observed for an initial moisture content of 4% and wind velocities up to 14 m/s. Wind velocity alone over a moist sand surface can only generate minor entrainment of sand particles. Overall, the sand transport process was very minor during these tests with initial moisture content-values (mc) of 1% to 8% and a factor of 100 less than that for dry sand (see **Figure 10**). The smallest mc-value used was mc=0.5% in 2 tests (S22 to S24). The effect of a very minor moisture content was still clearly manifest. The sand was slightly sticky reducing the sand transport at the end of the tray by a factor of 5 to 6 compared to the sand transport of dry sand.

The test results of **Figure 10** show that the sand transport rate is significantly reduced by a wind flow over a moist bed without supply of sand from upwind. This changes markedly when dry sand is fed from the upwind tunnel entrance, which is illustrated in **Figure 11** for moist sand with initial moist percentage of 2%. The wind velocity is 12 m/s at 0.03 m above the sand surface. The sand transport rate is very small during the first 15 minutes and increases slightly to about 0.5 g/m/s in the period 15 to 60 minutes. The sand transport process is highly intermittent due to the ongoing drying process. Layers of dry grains are intermittently removed, but no transport is generated at places where the crust is too strong. It is noted that the transport rate of dry sand for a wind velocity of about 12 m/s is much higher with a value of about 57 g/m/s (**Figure 12**). The sand transport ceases almost completely in the period 60 to 140 min due to the formation of local crusts. The sand surface is irregular with grooves and accumulations (small balls of sand). At time t=140 minutes, the sand feed of about 1 g/m/s was started resulting in very rapid crust breaking and erosion of the sand surface due to the sand blasting effect of the incoming sand particles. The sand transport rate during the last 6 minutes increased from 0 to about 5 g/m/s. The moisture content of the sand remaining in the tray was found to be 1.5%.

Figure 12 shows the relative sand transport (ratio of sand transport and dry sand transport) of tests with and without sand feed and moist sand in the range of 1% to 8%. The wind velocity is 14 m/s at 0.03 m above the sand surface in these tests yielding a sand transport rate of 57 g/m/s for dry sand. The sand transport rate measured at the end of the sand tray is almost none for moist sand of 1% to 8% in conditions without sand feed. The sand transport rate increases markedly (more than factor 10) when dry sand is supplied at the entrance of the tunnel. This is mainly caused by the sand blasting effect of the incoming sand particles. This proves that moist sand is mainly set into motion by the impacts of incoming saltating sand particles. Similar observations were reported by Van Dijk et al. (1996) in a large wind tunnel.

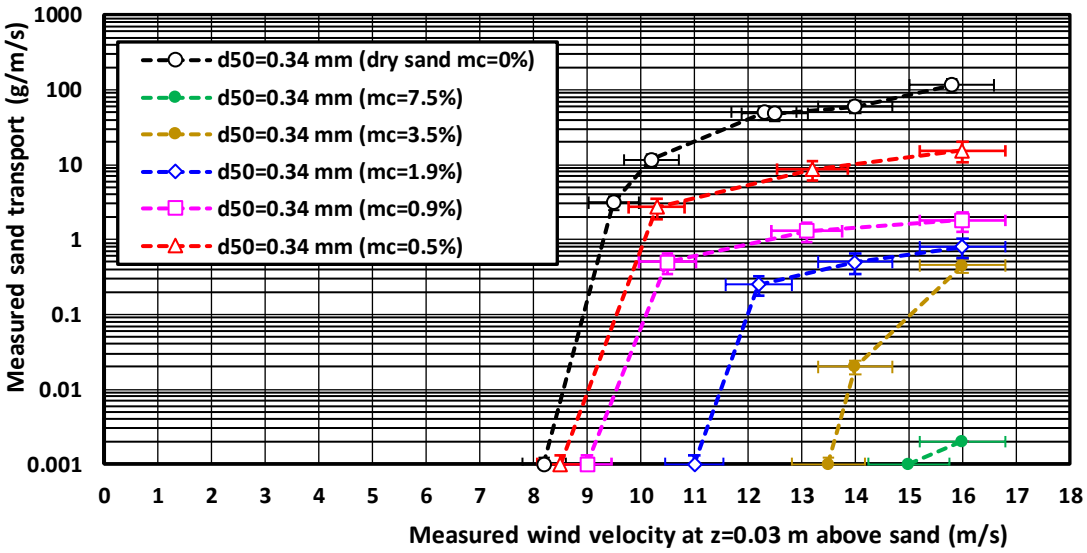

Figure 10 *Measured sand transport as function of wind velocity; effect of moisture content mc (no sand feed)*

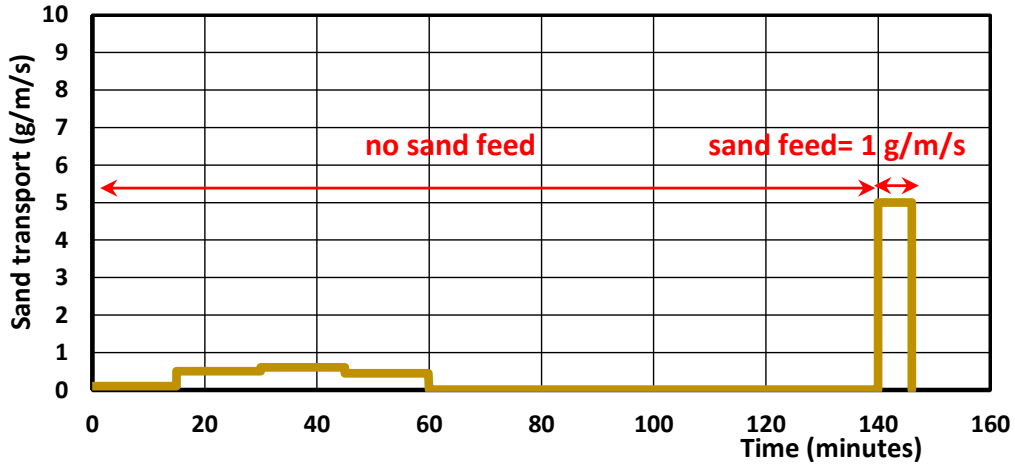

Figure 11 *Measured sand transport as function of time; wind velocity= 12 m/s at 0.03 m above surface*

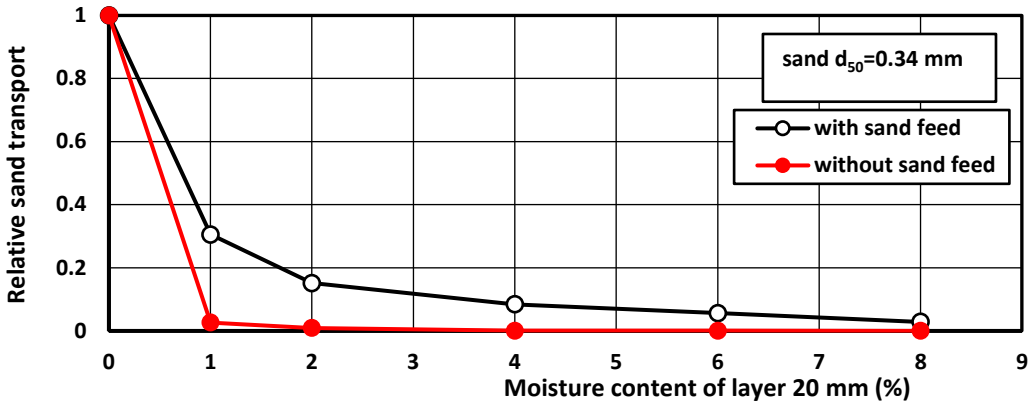

Figure 12 *Measured relative sand transport as function of moisture content with and without sand feed; wind velocity = 14 m/s at z=0.03 m above sand surface; sand transport of dry sand=57 g/m/s*

5. Effect of coarse materials (gravel and shells) on sand transport

Wind-induced sand transport is strongly reduced when the surface is covered with high quantities of coarse materials (gravels and shells) as discussed by Van Rijn and Strypsteen (2020).

Shells (calcium carbonate) and gravels can protect the beach surface against erosion of the sand particles. Large percentages of shell and gravels are mostly found on the upper part of natural beaches outside the wave action zone and on beaches with nourished sand. Literature on this topic is rather scarce and mostly qualitative. The two main effects of coare materials (gravel and shells) on the sand transport process are: i) gravel and shells cover a certain area of the bed which is not available for sand particle erosion and ii) sand particles in the direct vicinity of gravel and shells are less exposed to the wind forces (hiding effect). Observations in wind tunnels and field conditions show that shells of different sizes tend to interlock and form clusters (spatial organization; Mckenna Neuman et al., 2012; Strypsteen 2019). At the Dutch sand motor site south of The Hague, the percentage of shells at the surface is up to 20% resulting in a strong reduction of erosion of sand (De Vries and Hoonhout, 2017; Hoonhout and De Vries, 2017, 2019). At the Dutch Prins Hendrik site on the island of Texel, a new beach and dune system was made and the sand surface was covered with a layer of coarse sand, gravel and shells to reduce the loss of sand due to wind erosion and thus reduce the maintenance costs (Strypsteen et al., 2021). Strypsteen (2019) observed the presence of pronounced shell clusters on Belgium beaches, especially shortly after nourishment activities.

Van der Wal (1998) performed wind tunnel tests to study the effect of coarse materials on the wind-induced transport rate of beach sand (0.21 to 0.35 mm) taken from Dutch sites. The percentage of coarse materials consisting of gravel, stones and shells (> 2 mm) varied in the range 1 to 30%. The sand transport rate without shells was reduced by about 60% for a shell percentage of 7% and by about 80% to 85% for shell percentages of 18% to 32%. Shell pavements were formed during the wind tunnel experiments with shell-rich beach sand. McKenna Neuman et al. (2012) conducted a wind tunnel study on the effect of shells on the erosion of a sand bed. Three types of shells were used: crushed shells with cover percentages between 12% and 22%; small shells < 12.7 mm with cover percentages between 17% and 43% and large shells > 12.7 mm with cover percentages between 14% and 30%. It was observed that the shells were organized into chains and clusters with the long axis of many of the shells appearing to be aligned with the wind flow. The amount of erosion after the test was measured showing almost no erosion for the largest cover values of 40% both for small and large shells. Erosion is reduced by a factor of 5 to 10 by increasing the cover of shell from about 15% to about 30%-40%. Crushed shells are less effective than small/large shells.

Information of the effect of gravel on sand transport can also be obtained from a study of Tan et al. (2013). They studied the change in sand transport from a pure sand bed to a bed covered with gravel (20 to 55 mm) using a mobile wind tunnel operated in the Gobi Desert in China. The sand transport was reduced by about 20% for a gravel coverage of 10%, about 40% for a gravel coverage of 20%. The maximum reduction was about 50% for gravel coverage of 30% up to 70%. The basic cause of the sand transport reduction was the decrease of the wind velocities in the lowest layer of 50 to 100 mm above the sand surface due to the presence of the large gravel particles. As a consequence of the reduced sand transport rates, deposition of sand was observed at the bed covered with gravel particles. Similar findings are given by Gillies et al. (2006), who observed sand transport reductions as large as 90%.

Van Rijn and Strypsteen (2020) have proposed to represent the effect of coarse materials (gravel, shells) on the sand transport rate by a simple reduction coefficient acting on the transport rate. As only few experimental results are available in the literature, new experiments with shells and gravel particles on a sand bed have been done in the mini wind tunnels. The wind velocities were in the range of 10 to 13 m/s. Sand with d_{50}=0.34 mm was used. The tray was filled with sand. Coarse materials (gravels 2-6 mm or shells 8 to 25 mm) were placed on the sand surface of the tray, see **Figure 13**. The percentage of shells was varied in the range of 0% to 60%. The shells were immobile at low wind velocities up to 10 m/s. To prevent the movement of shells at high wind velocities of 12 to 13 m/s, the shells were glued to the sand surface. The loss of sand from the tray was measured by weighing before and after each test. Most tests were repeated to determine the variability. The sand transport rate (in g/m/s) at the end of the tray was determined as the loss of sand divided by the test time and the tray width. Similar tests with gravel have been performed. The mass percentage of gravel was varied in the 10% to

60%. **Figure 14** shows the test results for shells and gravel. The measured sand transport rates at the end of the tray are made dimensionless by dividing by the measured transport rate ($q_{s,o}$) without shells or gravel. The gravel percentage is given in terms of the mass percentage, which is approximately equal (within ±10%) to the area percentage based on detailed analysis of photos of the tray with gravel materials on the surface. The effect of gravel particles is much stronger than that of the shells. The individual shells have a streamlined shape leading to increased velocities around the shells with more intensive erosion. The smaller gravel particles are much more widely spread and create a stronger hiding effect than individual shells.
The effect of shells and gravels can be crudely represented by:

$$\alpha_{cf,shell} = q_s/q_{s,o} = (1-p_{shells}/100)^{1.5} \quad (11a)$$

$$\alpha_{cf,gravel} = q_s/q_{s,o} = (1-2p_{gravel}/100)^3\, q_{s,o} \quad (11b)$$

with: $q_{s,o}$=sand transport without shells or gravel, p_{shells}=percentage of shells, and p_{gravel}=percentage of gravel (%)
For example, p_{shells}=30% gives $q_s \cong 0.6\, q_{s,o}$ (reduction of 40%); p_{gravel}=30% gives $q_s \cong 0.06\, q_{s,o}$ (reduction of 94%).
Equation (11) is very similar to that proposed by Van Rijn and Strypsteen (2020). The results of Van der Wal (1998) and Tan et al. (2013) are also shown in **Figure 14**. The result of Van der Wal (1998) for sand samples with a coarse fraction of gravel and shells are in very good agreement with the gravel results of the mini wind tunnel. This suggests that gravel is the dominant factor with respect to the reduction of sand transport. The result of Tan et al. (2013) for large gravel particles of 20 to 30 mm are more in agreement with the test results of shells. It seems that fewer larger gravel elements offer less hiding and shielding than many smaller gravel particles
Equation (11) is herein used as a supply-limiting factor acting on the sand transport rate to obtain a quick engineering scan of the effect of shells in reducing sand transport on nourished shelly beaches. The gradual development of an armor layer of coarse shells in time cannot be represented in this way, as it requires a more detailed approach. Basically, the simulation of sand transport in conditions with a relatively wide grain size distribution (d_{90}/d_{10}> 10) and significant shell cover values (10% to 30%) requires an approach with multiple fractions including a book-keeping process for each grid cell and vertical sand layer. Hiding and exposure effects must be included as well as roughness variation effects (Raupach 1992; Van Rijn 2007). The present model can be extended to a fractional approach (Van Rijn 2007; Strypsteen et al., 2021). Using such an approach, the changes in surface conditions can be simulated both in space and time (Hoonhout and De Vries, 2017). However, such an approach is far more complex with many coefficients and calibrations involved and may be a bridge too far for engineering purposes (see detailed discussion by McKenna Neuman et al., 2012).

Figure 13 *Laboratory setup with shells and gravel in tray of mini wind tunnel (length of tray=250 mm)*

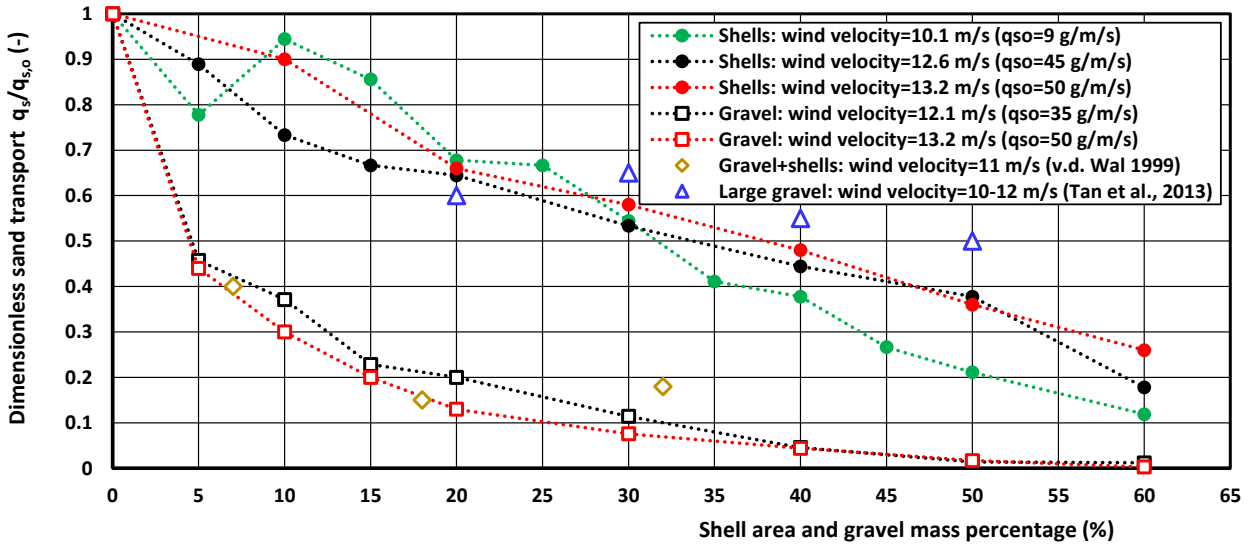

Figure 14 *Effect of shells and gravel on wind-induced sand transport; laboratory tests in mini wind tunnel ($q_{s,o}$= sand transport at percentage 0%)*

6. Summary and conclusions

This paper is a continuation of earlier work (Part 1) on the effect of moisture and coarse materials (gravel and shells) on aeolian transport. Two mini wind tunnels have been designed and used to study the effect of moisture and coarse materials on the threshold shear velocity and on the sand transport rate at wind velocities in the range of 10 to 17 m/s. Extensive attention was given to the determination of the drying time of the beach surface after a period with rainfall.

Two prediction methods for aeolian sand transport were evaluated: the modified Bagnold-transport equation and the new VR-transport equation. Both methods include the effects of sand diameter and the threshold shear stress, which is essential for accurate determination of sand transport at low wind speeds. The grain-related shear velocity is the basic driving parameter. The wind tunnel data of Belly (1964) have been used to calibrate the new VR-sand transport equation.

The main findings of the study are:

- A new VR-sand transport equation is proposed and calibrated based on the wind tunnel data of Belly (1964). The effect of grain size for particles in the range of 0.15 to 0.4 mm is found to be weak. The measured results are best represented for a threshold coefficient of α_{th}=0.08, which represents dynamic (cessation) threshold conditions
- The drying process of beach surface can be characterized as the time period to bring the moisture content of the topmost layer of 20 mm from 8% immediately after rain fall to below 2%. When wind is absent, the drying time is quite high: 70 hours for temperature in the range of 5-10 ^{o}C and 50 hours for 15 to 20 ^{o}C. When light winds are present (BF 3), the drying time decreases to about 30 hours for a temperature of 5 to 10 ^{o}C (winter); to 10 hours for 15 to 20 ^{o}C (spring) and to 5 hours for temperatures of 20 to 25 ^{o}C (summer), see Figure 7.
- The threshold shear velocities of moist sand are much higher than those of dry sand. No particle movement was observed for a moisture content of 7% to 8% and wind velocities below 16 m/s in a mini wind tunnel. Similarly, no movement and transport were observed for an initial moisture content of 4% and wind velocities below 14 m/s. The threshold shear velocity depends on the moisture content of the upper sand layer and the grain size and can be represented by a simple expression, which is also found to be valid for field conditions (Figure 9).
- The entrainment of moist sand is strongly reduced in conditions without upwind supply of sand. The sand transport in the mini wind tunnel was very minor during tests with initial moisture content of 1% to 8% and a factor of 100 less than that for dry sand. Even for a small moisture content of 0.5% the sand transport was reduced by a factor of 5 to 6 compared to the sand transport of dry sand. The sand transport rate in the mini wind tunnel increased markedly (more than factor 10) in tests with sand feed due to the sand blasting effect, which proves that moist sand is mainly set into motion by the impacts of incoming saltating sand particles (Figures 10 to 12).
- Field data of sand transport show that the effect of moisture is minor for storm events with wind velocities higher than 10 m/s at 1 m above surface (BF7), which can be explained by the entrainment of sand from drier spots setting moist sand into motion (sand blasting effect). Sand transport at BF7 and higher is only reduced if the moisture level of the upper 20 mm is higher than 6% (Figure 9)
- The sand transport rate is strongly restricted if the beach surface is covered with a significant amount of coarse materials (gravel and shells). Gravel has a more pronounced effect than shells, Figure 13. The sand transport rate is reduced by about 50% for a gravel percentage of about 10%. A high percentage of gravel will lead to beach armoring, at observed at the Prins Hendrik beach site on the island of Texel.

The findings and equations of Part 2 will be used in Part 3 for verification and application of the new VR-sand transport equation for natural beaches with dry and moist sand based on the collection of many new data using the new LVRS trap-type sampler.

Acknowledgements
The Dutch water board Hoogheemraadschap Hollands Noorderkwartier (HHNK) and the Belgian marine dredging contractor Jan De Nul Group are gratefully acknowledged for providing support and funds for this study.
Prof. B.G. Ruessink and Master Student M. Hoogland of the Department of Physical Geography of the University of Utrecht are gratefully acknowledged for support and execution of laboratory experiments.

References
Atherton, R.J., Baird, A.J. and Wiggs, G.F.S., 2001. Inter-tidal dynamics of surface moisture content on a meso-tidal beach. Journal of Coastal Research, Vol. 17, 482-489
Bagnold, R.A., 1937. The transport of sand by wind. Geographical J. Vol. 89, 409–38
Bagnold, R.A. 1941, 1954. The physics of blown sand and desert dunes. Methuen, New York.
Bauer, B.O., Davidson-Arnott, R.G.D., Hesp, P.A., Namikas, S.L., Ollerhead, J. and Walker, I.J., 2009. Aeolian sediment transport on a beach: surface moisture, wind fetch and mean transport. Geomorphology, Vol. 105, 106-116
Bauer, B.O., Davidson-Arnott, R.G.D., Walker, I.J., Hesp, P.A., Ollerhead, J., 2012, Wind direction and complex sediment transport response across a beach-dune system. Earth Surface Processes and Landforms, 37, 1661–1677. https://doi.org/10.1002/esp.3306
Belly, P.Y., 1964. Sand Movement by Wind. U.S. Army Corps of Engineers, Technical Memorandum No 1, CERC, Washington, DC.
Chepil, W.S., 1956. Influence of moisture on erodibility of soil by wind. Proc. Soil Sci. Soc. Am., 20, 288–292.
Comola, F., Kok, J.F., Chamecki, M. and Martin, R.L., 2019. The intermittency of wind-driven sand transport. Geophysical Research Letters, Vol. 46, 13, 13,430-13,440. Doi: 10.1029/2019GL085739
Cornelis, W.M., Gabriels, D., 2003. The effect of surface moisture on the entrainment of dune sand wind: an evaluation of selected models. Sedimentology Vol. 50, 771–790.
Davidson-Arnott, R.G.D., Bauer, B.O., Ollerhead, J., Hesp, P.A., Namikas, S. and Walker, I.J., 2005. Moisture and fetch effects on aeolian sediment transport rates during a fall storm, Greenwich dunes, Prince Edward Island. Canadian Coastal Conference.
Davidson-Arnott, R.G.D., Yang, Y., Ollerhead, J., Hesp., P.A. and Walker, I.J., 2008. The effects of surface moisture on aeolian sediment transport threshold and mass flux on a beach. Earth Surface Processes and Landforms, Vol. 33, 55-74. Doi:10.1002/esp.1527
Delgado-Fernandez, I., 2010. A review of the application of the fetch effect to modelling sand supply to coastal foredunes. Aeolian Research Vol. 2 (2-3), 61-70
Delgado-Fernandez, I., 2011. Meso-scale modelling of aeolian sediment input to coastal dunes. Geomorphology Vol.130, 230-243
De Ruiter, J.C.C., 1983. Incipient motion and pick-up of sediment as function of local variables. Report R657-XI, Delft Hydraulics, Delft, The Netherlands.
De Vries, S., Arens, S.M., De Schipper, M.A., and Ranasinghe, R., 2014. Aeolian sediment transport on a beach with a varying sediment supply. Aeolian Research Vol. 15, 235-244
De Vries, S. and Hoonhout, B., 2017. Field measurements on spatial variations in aeolian sediment availability at the sand motor mega nourishment. Aeolian Research Vo. 24, 93-104
Einstein, H.A., 1950. The bed-load function for sediment transportation in open channel flow. Technical Bulletin No. 1026, U.S Department of Agriculture, Washington D.C., USA
Gillies, J.A., Nickling, W.G. and King, J., 2006. Aeolian sediment transport through large patches of roughness in the atmospheric inertial layer. Journal of Geophysical Research Vol. 111, F02006. Doi: 10.1029/2005JF000434
Grass, A.J., 1970. Initial instability of fine sand bed. Journal of the Hydraulic Division, ASCE, Vol. 96, No. HY3, 619-632
Han, Q., Qu, J., Liao, K., Zhu, S., Zhang, K., Zu, R. and Niu, Q., 2011. A wind tunnel study of aeolian sand transport on a wetted surface using sands from tropical humid coastal southern China. Environmental Earth Sciences, Vol. 64, 1375-1385; DOI 10.1007/s12665-011-0962-7
Hird, R. and Bolton, M.D., 2017. Clarification of capillary rise in dry sand. Engineering Geology, Vol.20, 77-83

Ho, T., 2012. Experimental study of saltating particles in a turbulent boundary layer. Doctoral Thesis, University of Rennes, France
Hoonhout, B. and De Vries, S., 2017. Aeolian sediment supply at a mega nourishment. Coastal Engineering Vol. 123, 11-20
Hoonhout, B. and De Vries, S., 2019. Simulating spatiotemporal aeolian sediment supply at a mega nourishment. Coastal Engineering Vol. 145, 21-35
Horikawa, K., Hotta, S. and Kubota, S., 1982. Experimental study of blown sand on a wetted sand surface, Coastal Engineering in Japan, Vol. 25, 177-195,
Hotta, S., Kubota, S., Katori, S., Horikawa, K., 1984. Sand transport by wind on a wet sand surface. Proceedings 19th Coastal Engineering Conference. ASCE, New York, 1265–1281.
Jackson, N.L. and Nordstrom, K.F., 1997. Effects of time-dependent moisture content of surface sediments on aeolian transport rates across a beach Wildwood, New Jersey, USA. Earth Surface Processes and Landforms, Vol. 22, 611-621
Jackson, D. and Cooper, J., 1999. Beach fetch distance and aeolian sediment transport. Sedimentology, 517–522.
Kalinske, A.A., 1947. Movement of sediment as bed load in rivers. Trans. American Geophysical Union, Vol. 128, No. 4, USA
Kok, J.F., Parteli, E.J.R., Michaels, T.I. and Karam, D.B.., 2012. The physics of wind-blown sand and dust. Rep. Prog. Phys. Vol. 75, Doi:10.1088/0034-4885/75/10/106901
Lin, S.D., 2001. Water and Wastewater Calculations Manual, 2001, McGraw-Hill, New York.
Martin, R.L. and Kok, J.F., 2017. Wind-invariant saltation heights imply linear scaling of aeolian saltation flux with shear stress. Science Advances Vol. 3 (6). Doi: 10.1126/sciadv.1602569
Martin, R.L. and Kok, J.F., 2018. Distinct thresholds for the initiation and cessation of aeolian saltation from field measurements. Journal of Geophysical Research: Earth Surface, Vol. 123, 1546-1564. Doi: 10.1029/2017JF004416
Martin, R.L., Barchyn, T.E., Hugenholtz, C.H. and Jerolmack, D.J., 2013. Timescale dependence of aeolian sand flux observations under atmospheric turbulence. Journal of Geophysical Research: Atmospheres, Vol. 118, 9078-9092. Doi:10.1002/jgrd.50687
Martin, R.L., Kok, J.F., Barchyn, T.E., and Chamecki, M. 2018. High-frequency measurements of aeolian saltation flux: field-based methodology and applications. Aeolian Research. Doi: 10.1016/j.aeolia.2017.12.003
McKenna Neuman, C. and Sanderson, S., 2008. Humidity control of particle emissions in aeolian systems. Journal of Geophysical Research, Vol. 143, D02S14. Doi:10.1029/2007JF000780
McKenna Neuman, C., Li, B. and Nash, D., 2012. Micro-topographic analysis of shell pavements formed by aeolian transport in a wind tunnel simulation. Journal of Geophysical Research Vol. 117, F04003. Doi: 10.1029/2012JF002381
Meyer-Peter, E. and Mueller, R., 1948. Formulas for bed-load transport. Sec. Int. IAHR Congres, Stockholm, Sweden
Nikuradse, J., 1933. Stromungsgesetz in rauhren rohren, Forschungsheft Arb. Ing. Wesen 361, Germany (English translation: Laws of flow in rough pipes; Tech. Rep. NACA Technical Memorandum, 1292).
Paintal, A.S., 1971. Concept of critical shear stress in loose boundary open channels. Journal of Hydraulic Research, Vol. 9, No. 1
Raupach, M.R., 1992. Drag and drag partition on rough surfaces. Boundary Layer Meteorology Vol. 60, 375–395.
Saleh, A. and Fryrear, D.W., 1995. Threshold wind velocities of wet soils as affected by wind-blown sand. Soil Sci., 160, 304–309.
Shao, Y. P. and Lu, H., 2000 A simple expression for wind erosion threshold friction velocity Journal Geophysical Research Vol. 105, 22437–43
Sherman, D., Ellis, J.T., Li, B., Farrell, E.J., Maia, P. and Granja, H.M., 2013. Recalibrating aeolian sand transport models. Earth Surface and Landforms, Vol. 38, 169-178. Doi: 10.1002/esp.3310
Stout, J. E., and Zobeck, T. M., 1997. Intermittent saltation. Sedimentology, Vol. 44 (5), 959–970

Strypsteen, G., 2019. Monitoring and modelling aeolian sand transport at the Belgian coast. Doctoral Thesis, KU Leuven, Belgium.
Strypsteen, G., Van Rijn, L.C., Hoogland, M.D., Rauwoens, P., Fordeyn, J. and Hijma, M.P. 2021. Reducing aeolian sand transport and beach erosion by using armour layer of coarse materials. Coastal Engineering, Vol. 166, 103871
Svasek, J.N. and Terwindt, J.H.J., 1974. Measurements of sand transport by wind on a natural beach. Sedimentology, Vol. 21, 311-322
Tan, L., Zhang, W., Qu, J., Zhang, K., An, Z. and Wang, X., 2013. Aeolian sand transport over Gobi with different gravel coverages under limited sand supply: a mobile wind tunnel investigation. Aeolian Research 11, 67-74
Udo, K., Kuriyama, Y. and Jackson, D.W.T., 2008. Observations of wind-blown sand under various meteorological conditions at a beach. Journal of Geophysical Research Vol. 113, F04008. Doi: 10.1029/2007JF00936
Van Dijk, P.M., Stroosnijder, L. and De Lima, J.L.M.P., 1996. The influence of rainfall on transport of beach sand by wind. Earth Surface Processes and Landforms, Vol. 21, 341-352
Van der Wal, D., 1998. The impact of the grain-size distribution of nourishment sand on aeolian sand transport. Journal of Coastal Research, 14, 620-631
Van Rijn, L.C., 1993. Principles of sediment transport in rivers, estuaries and coastal seas, Part I and II. AquaPublications, The Netherlands (www.aquapublications.nl)
Van Rijn, L.C., 2007. Unified view of sediment transport by currents and waves, I: Initiation of motion, bed roughness, and bed-load transport. Journal of Hydraulic Engineering, 133(6), 649-667.
Van Rijn, L.C., 2007. Unified view of sediment transport by currents and waves, II: Suspended transport. Journal of Hydraulic Engineering, 133(6), 668-389.
Van Rijn, L.C., 2007. Unified view of sediment transport by currents and waves, III: Graded beds. Journal of Hydraulic Engineering, 133(7), 761-775.
Van Rijn, L.C., 2011. Principles of fluid flow and surface waves in rivers, estuaries and coastal seas. AquaPublications, The Netherlands (www.aquapublications.nl)
Van Rijn, L. C., 2021. Aeolian sand transport; field measurements and model predictions for dry and moist beaches. www.leovanrijn-sediment.com (free download)
Van Rijn, L.C. and Strypsteen, G., 2020. A fully predictive model for aeolian sand transport. Coastal Engineering, Vol. 156
Wiggs, G.F.S., Baird, A.J. and Atherton, R.J., 2004. Thy dynamic effects of moisture on the entrainment and transport of sand by wind. Geomorphology 59, 13-30
Yalin, M.S., 1977. Mechanics of sediment transport. Pergamon Press
Yang, Y. and Davidson-Arnott, R.G.D., 2005. Rapid measurements of surface moisture content on a beach. Journal of Coastal Research, Vol. 21, No. 3, 447-452

A FULLY PREDICTIVE MODEL FOR AEOLIAN SAND TRANSPORT, Part 3: Verification and application of model for natural beaches

by L.C. van Rijn[1]
[1]LVRS-consultancy, Domineeswal 6, 8356D Blokzijl, The Netherlands; info@leovanrijn-sediment.com

Keywords: predictive model for wind-blown sand; supply-limiting effects on wind-blown sand

Abstract
This paper presents extensive research results on the verification of a new transport equation for dry and moist sand at field sites and is a continuation of earlier work (Van Rijn and Strypsteen, 2020). A new trap-type instrument (LVRS-sampler) for measuring the sand transport rate of sliding, rolling and saltating particles was designed and used at many natural beach sites in Belgium and The Netherlands. A short mast equipped with three mini wind cup meters was used to measure the velocity distribution in the lowest 1 m of the boundary layer flow. Many new data sets (81 data) of aeolian sand transport for dry and moist beach surface conditions were obtained using the new equipment and used for verification of the new prediction method. Older field data (48 data points) from the literature were also used for verification. The score of the predicted sand transport based on the new VR-method is 87% within a factor of 2 of measured values for dry sand and 91% for moist sand. The modified Bagnold-transport equation was also used for verification of the available field data with scores of 79% and 67%. As a practical example, the new VR-sand transport equation was applied to calculate the annual aeolian sand transport on a Dutch beach site using wind velocity and rainfall data from a local weather station including rain fall effects (moist sand) and conversion of inland wind velocities to beach velocities (upscaling of results).

1. Introduction

This paper is a continuation of earlier work (Part 1: Van Rijn and Strypsteen 2020) on the development of a complete theory for the prediction of aeolian transport of dry and moist sand including the effects of coarse materials. Van Rijn and Strypsteen (2020) have modified and verified the well-known Bagnold equation for wind-driven sand transport by including the threshold for initiation of motion and the grain-related shear velocity as the main driving parameter instead of the overall shear velocity. A prediction method for the grain-related shear velocity is proposed in Part 1. The effects of moisture and coarse materials on sand transport were also explored in Part 1 based on available data from the literature. In Part 2 (Van Rijn, 2021) a new equation for aeolian sand transport is derived and calibrated (VR-transport equation). New research results on the effect of moisture and coarse materials (gravel and shells) are presented, based on experiments in two mini wind tunnels. Extensive attention is given to the determination of the drying time of the beach surface after a period with rainfall for a range of temperatures and wind conditions.
In this Part 3, the new method for aeolian sand transport as proposed in Part 1 and Part 2 is verified by comparing measured and computed sand transport rates for natural sand beaches in Belgium and The Netherlands. Many new field data were collected at these beaches using a new trap-type sampler. Existing data of aeolian sand transport from the literature were used as well (Sherman et al., 2013). They have presented a high-quality dataset of 32 points of wind-driven sand transport rates, but much more tabulated data based on well-defined parameters can hardly be found in the literature.
The applied models for sand transport are briefly summarized in Section 2. Field sites and laboratory instrumentation are explained in Section 3. Sand transport rates at field sites are analyzed in Section 4. Model verification based on field data only is presented in Section 5. Special attention is given to the verification of the new model for sand transport at low wind velocities around threshold conditions. Finally, the new VR-sand transport equation is applied for annual sand transport predictions in Section 6. A new procedure for the inclusion of moisture effects in sand transport predictions is proposed and discussed.

2. Sand transport equations

The VR-sand transport equation developed in Part 2 is briefly summarized here, as follows:

$$q_{s,eq,VR} = \alpha_{VR}\,\alpha_{ad}\,\alpha_{cf}\,(\rho_{air}/g)\,(D_*)^{\beta}\,[(u_{*,grain})^3 - (u_{*,th})^3] \quad (1)$$

The threshold shear velocity is described by the Bagnold-equation, as follows:

Threshold shear velocity:

$$u_{*,th} = \alpha_w\,\alpha_{slope}\,u_{*,th,B} \quad (2a)$$

$$u_{*,th,B} = \alpha_{th}\,[(\rho_s/\rho_{air}-1)\,g\,d_{50}]^{0.5} \quad \text{for } d_{50} > 100\ \mu m \quad (2b)$$

$$u_{*,th,B} = \alpha_{th}\,u_{*,th,100\ um} \quad \text{for } 32 < d_{50} < 100\ \mu m \quad (2c)$$

Grain-related shear velocity:

$$u_{*,grain} = \kappa\,\alpha_{veg}\,u_w/\ln(30z_{wind}/k_{s,grain}) \quad (3)$$

with: $u_{*,grain}$ = shear velocity related to the dynamic grains (m/s) as proposed by Van Rijn and Strypsteen (2020); $u_{*,th}$=threshold shear velocity (m/s); $k_{s,grain}$= equivalent roughness length scale related to dynamic saltating grains (Van Rijn and Strypsteen, 2020); u_w = local wind velocity at height z_{wind} above the sand surface (m/s); κ= constant of Von Karman (=0.4); α_{ad}= adjustment coefficient related to fetch (maximum 1; Van Rijn and Strypsteen 2020); α_{cf} = reduction coefficient related to the presence of coarse materials (shell/gravel); α_{th}= threshold coefficient; α_{slope} = coefficient for sand grains at a sloping surface; α_w= moisture coefficient (=1 for dry sand); α_{veg}= vegetation coefficient (=1 for conditions without vegetation).

Using the wind tunnel data of Belly (1964), three coefficients were calibrated by fitting of measured and computed transport values resulting in: α_{VR}=1.8, β=0.1 and $\alpha_{th}=\alpha_{th,cessation}$= 0.08. Predictive equations of the α_{cf}-coefficient (effect of shells and coarse materials) and the α_w-coefficient (effect of moisture) are proposed in Part 2. These equations are used in Part 3 for verification of the VR-sand transport equation. The coefficients α_{ad}, α_{slope} and α_{veg} are set to 1.

3. Field sites and instrumentation

3.1 Field sites

Aeolian sand transport measurements have been done at various beaches in Belgium and The Netherlands. Most beaches are relatively wide coastal sand beaches with tidal ranges of 2 to 3 m backed by high foredunes along the coast of The Netherlands and Belgium, except for the sites of Lemmer and Schokkerhaven which are inland recreational beaches in The Netherlands. Most data were collected at the sandy beach of Callantsoog, The Netherlands. The sand composition of 12 beaches is given in **Table 1**. The threshold wind velocity values are also given (based on Equation 2).

Many new field measurements of sand transport have been done at these beaches in the period December 2019 to April 2021 using the LVRS-trap sampler (Section 3.2). Beach conditions were dry, moist and combinations of dry and moist spots. Wind conditions were up to Beaufort scale 9 (BF9=22 m/s at 10 m above surface). The measurement period of the trap sampler was in the range of 5 minutes at high wind speeds to 30 minutes at low speeds. During this period, many 1 minute-averaged wind speeds were measured at 3 heights above the surface at a location within 0.5 m from the mouth of the trap. Sand samples of the upper 20 mm of the surface were taken for determination of sand composition (d_{50}, d_{90}), percentage of coarse materials (> 2 mm) and moisture content (w_{20}). Photographs were taken for determination of bed irregularities (bed forms). At most dates in late spring, summer and early autumn the beach surface was dry. At most dates in winter and autumn, the beach surface was (partly) moist. Sometimes, the beach surface showed combinations of dry (lighter colors) and moist spots (darker colors). The percentage of dry and wet spots upwind of the trap sampler was visually estimated for each measurement date. The elapsed time since the last rainfall period was also estimated. In all, 81 new high-quality field data sets are available for analysis and verification of transport equations (see Section 4).

The field data at the beach of Callantsoog in February 2020 are discussed in more detail as the weather was quite stormy in this month. The storms of 9 February and 15 February hit the coast with peak wind velocities up to 18

m/s at 1 m above the beach surface. Most of the time, the wind was almost parallel (from southwest) to the coast.

Figure 1 shows a typical setup at the beach of Callantsoog in February 2020. Dark-colored moist spots and light-colored dry spots can be observed in front of the trap sampler at the upper beach area.

Location	**Grain size**				**Threshold wind velocity at 1 m above surface at initiation of motion based on Bagnold-equation (m/s)**	
	d_{10} (μm)	d_{50} (μm)	d_{90} (μm)	coarse > 2 mm (%)	cessation (α_{th}=0.08)	initiation of motion (α_{th}=0.1)
Lemmer (NL); inland, recreational beach	150	300	900	<5	5.3	6.6
Schokkerhaven (NL); inland, recreational beach	205	340	700	<3	5.6	7.0
Callantsoog (NL); coastal, tidal beach	160	230	400	<3	4.6	5.8
Groote Keeten (NL); coastal, tidal beach	150	240	450	<1	4.7	5.9
Zandvoort (NL); coastal, tidal beach	150	250	400	<1	4.8	6.0
Texel-Den Hoorn; coastal, tidal beach	180	270	450	<1	5.0	6.2
Texel- Prins Hendrik; Wadden Sea, dry tidal beach	140	260	500	<3	4.9	6.1
Texel-Prins Hendrik; Wadden Sea, wet intertidal beach	200	400	1000	<5	6.1	7.6
Zeebrugge (BE); coastal, tidal beach	140	200	400	<3	4.3	5.4
Koksijde (BE); coastal, tidal beach	150	230	400	<5	4.6	5.8
Oostende (BE); coastal, tidal beach	180	300	500	<5	5.3	6.6
Mariakerke (BE); coastal, tidal beach	170	310	600	<3	5.4	6.7

Table 1 *Sand characteristics of beaches in Belgium and The Netherlands*

Figure 1 *Wind transport at beach of Callantsoog; minor storm BF 6/7; 15 February 2020 (mc=moisture content)*

3.2 Field instrumentation

At present, the simple mechanical trap-type samplers intercepting the moving particles of the saltation layer are the most reliable instruments to obtain field data for calibration of transport models. Sampling times should be sufficiently long (say 10 to 30 minutes) to integrate over fluctuations due to turbulence and wind gusts. Many samplings should be done at the "same" location to reduce variability due to small transverse and streamwise gradients. Field experiments have been done by the author using a new trap-type sampler (LVRS-sampler). The equipment consists of a short stainless steel mast (length=1.5 m) with three wind cup velocity meters (cup-type sensors) and several traps attached to the mast and a separate bed load trap (see also inset **Figure 1**) placed close to the mast location. The wind velocity was measured by using three JDC-wind cup meters (type eole) with averaging time interval of 1 minute. The accuracy of the instrument specified by the manufacturer is $\pm$3%. Based on comparison to wind velocity data of other wind cup meters during a field survey on the island of Texel, the practical inaccuracy of the JDC-meters is estimated to be about 10% (Strypsteen et al., 2021). The bed load trap consists of a rectangular steel tube with internal width of 93 mm and internal height of 71 mm and a 70 μm-bag for the trapping of sand. The circular traps consist of steel tubes with internal diameter of 36 mm (equivalent square diameter of 32 mm) and 70 μm-bags. The traps are placed in the wind direction (as indicated by a small red vane attached to the mast; inset of Figure 1) and can be deployed in 5 minutes. The bed-load and suspended sand traps can not follow the changes in wind direction during the measuring period. The LVRS-sampler is very similar to the Sherman streamer trap (SST; Sherman et al., 2014). The trap efficiency of these types of traps is close to 1. No scour was observed around the corners of the instrument during all types of wind events. Comparison with results from other trap type samplers (Campos, 2018; Sarre, 1988; see also Section 5) shows fairly good agreement without any systematic errors (Van Rijn 2021).

The total transport of sand can be determined by summation of the transport data of the bottom trap with vertical height of 71 mm and the circular tube -type traps placed at various near-bed elevations (range of 100 to 300 mm above the surface; almost no transport above 300 mm). Based on practical experience, the transport of sand in the layer 0 to 71 mm measured by the bottom trap is mostly about 70% of the total transport for high wind speeds to about 100% for low wind speeds (Ho, 2012). About 30% of the total transport takes place in the layers above the bottom trap and can be derived by exponential interpolation from the measured fluxes which are defined in the center points of the tube-type traps (Ellis et al., 2009). Small interpolation errors may occur to determine the transport of sand in the unmeasured layers between the tube-type traps. The overall error of the total transport is estimated to be less than 15%.

The regression coefficients of logarithmic fits of the measured velocities at three heights of the short mast are higher than 0.95 in all cases of the present study ($R^2 > 0.95$), which supports the assumption of logarithmic velocity profiles in the lowest 1 m. It is noted that the wind velocities of the short mast (and not the bed shear velocities) are used to drive the sand transport model proposed by Van Rijn and Strypsteen (2020). This model only requires the specification of one velocity at a given height above the surface, and the bed roughness is fully predicted (see Part 2).

4. Analysis of field data

In all, 81 new high-quality field data sets are available for analysis and verification of transport equations. **Table 2** shows an example of the field data measured at the beach of Callantsoog (The Netherlands) during the storm month of February 2020. Many more of these detailed tables with all data (including shear velocity u_* and bed roughness k_s derived from measured velocity profiles) are reported by Van Rijn (2021). Most of the data sets (75% for dry sand and 85% for moist sand) have wind velocities $u > 1.5\ u_{th,initiation}$ with $u_{th,initation}$=threshold wind velocity at 1 m above surface for initiation of motion (see Table 1), which means continuous transport conditions (Stout and Zobeck, 1997). In 15% to 25% of the cases, the transport conditions are intermittent ($u_{th,cessation} < u < u_{th,\ initiation}$). The fetch length of each measurement is accurately known. Most data refer to winds almost parallel to the beach with fetch length > 500 m, see **Table 2**.

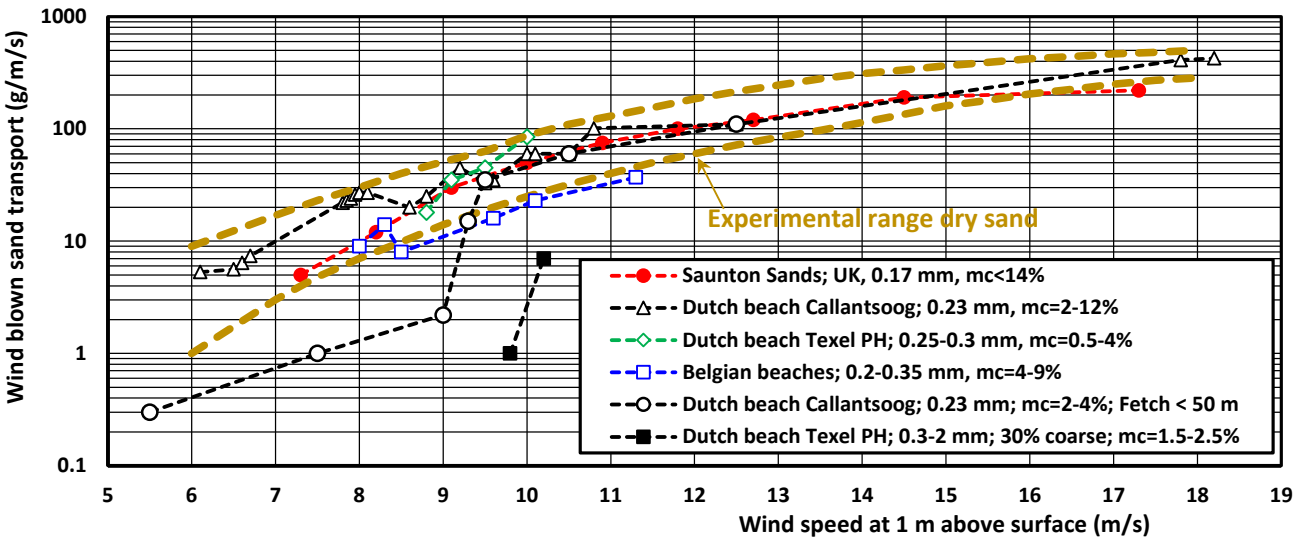

Figure 2 *Effect of fetch, moisture and coarse materials on transport (mc=moisture content upper 20 mm)*

Location Date Duration	Beach		Moisture (%)			Wind conditions		Wind transport (g/m/s) and test duration (s)
	$d_{50};d_{90}$ (mm) p_{shell}	Description	upper 5mm	upper 20mm	p_m (%)	height (m) and velocity (m/s);	direction and fetch length (m)	
9 February 2020; dry	0.23; 0.4 <3%	flat middle beach	2%; 10 hrs(alr)	2%; 10 hrs(alr)	80%	z=1.43; u= 18.7±1.5 Te= 8° C; BF9	almost parallel FL> 500 m	total: 410/425 (mt=240s)
9 February 2020; dry	0.23; 0.4 <3%	flat middle beach	2% 10 hrs	2% 10 hrs	80%	z=1.43; u= 19.0±1.5 Te= 8° C; BF9	almost parallel FL> 500 m	total: 435 (mt=150 s)
11 February 2020; dry	0.23; 0.4 <3%	dune foot; flat surface upwind	4.0% 5 hrs	4.0% 5 hrs	100 %	z=1.15; u=7.7 ±0.5 Te= 5° C; BF7 to 8	angle=20° to shore normal; FL= 10 m	layer 0-71: 1 g/m/s (mt=1320 s)
15 February 2020 dry	0.23; 0.4 <3%	flat middle beach;	1% to 17% 10 hrs	1% to 17% 10 hrs	70%	z=1.13; u=9.5 ±0.5 Te=12° C; BF6 to 7	almost parallel FL> 500	total: 45 (mt=600 s) (mc= 0.5-1%)
15 February 2020; dry	0.23; 0.4 <3%	flat middle beach; ripples (0-20 mm)	1% to 17% 10 hrs	1% to 17% 10 hrs	70%	z=1.13; u=10.5 ±0.7 Te=12° C; BF6 to 7	almost parallel FL> 500	total: 60 (mt=600 s) (mc=0.5-1%)
22 February 2020; dry	0.23; 0.4 <3%	upper beach near dune toe	nm	3.3% 4 hours	50%	z=1.48; u=11 ±1 Te=10° C; BF 7/8	oblique angle 45° FL=50	total: 60 (mt=300 s) (mc<1%)
22 February 2020; dry	0.23; 0.4 <3%	upper beach near dune toe	nm	3% 4 hours	50%	z=1.48; u=10 ±1 Te=10° C; BF 7/8	oblique angle 45° FL=50	total: 35 (mt=480 s) (mc<1%)
22 February 2020; rainy;	0.23; 0.4 <3%	upper beach near dune toe	8%	5% during rainfall	100 %	z=1.48; u=13 ±1 Te=10° C; BF 8	oblique angle 45° FL=50	total: 110 (mt=360 s) (mc<1%)

BF=Beaufort wind scale; p_{shell}= percentage shells at beach surface; alr=after last rainfall; Te= temperature
FL= fetch length; p_m= percentage of beach surface with moist appearance at measurement location; z= height above bed; u= wind velocity at height z; mt=measuring time sand transport; mc= moisture content; nm=not measured

Table 2 *Wind transport data at beaches of Callantsoog, The Netherlands, February 2020*

The new measured field data of dry and moist sand of the present study are plotted as function of the measured wind velocity at 1 m above the surface in **Figure 2**. For clearness, only the experimental range of the dry sand data (based on 71 data points with FL > 500 m) are shown. These latter data for dry sand shows a clear nonlinear relationship between sand transport and velocity, although there is substantial scatter. The sand transport rate is proportional to velocity to the power of 3 to 4, which means shear stress to power of 1.5 to 2. The scatter is most likely related to the relatively large variations in bed roughness values at different sites and at different dates (flat bed, ripples, runnels, shell clusters, beach debris) and to variations in particle diameter.
The field data at the beach of Callantsoog in February 2020 are discussed in more detail as the weather was quite stormy on 9 February and 15 February with peak velocities up to 18 m/s at 1 m and 22 m/s at 10 m (BF9), see **Figure 3**. The wind strength distribution over 20 days between 9 and 29 February was approximately: 50% BF6 (11 m/s at z=10 m); 15% BF7 (15 m/s), 5% BF8 (19 m/s) and 2% B9 (22 m/s). On 9 February, a record sand transport measurement of 425 g/m/s at a wind speed of 18 m/s at 1 m above the surface was done, see open triangles in **Figure 2**. Moisture due to rainfall may have a strong effect on aeolian sand transport as described in many papers (see Pye and Tsoar, 2009). About 20 rainfall events did occur in the period between 9 and 29 February 2020. The maximum rain intensity was about 5 mm/hour. The total duration of the rainfall in February 2020 was about 90 hours (about 13% of the time; twice the normal value). The duration of the rainfall events was in the range of 0.5 hour to 16 hours with an average duration of about 4.5 hours. The periods with dry weather (dry time) after rainfall varied between 1 hour and maximum 36 hours for the period between 9 and 29 February. Most of the dry time was in the range of 10 to 20 hours which is less than the required dry time of 30 hours (Part 2) to obtain a fairly dry surface in wintertime. Many beach samples were taken and mostly the moisture content at the upper beach was higher than about 2%. Sand transport was intense in this period as long the wind speed was higher than BF6. Sand grains were in the air up to a height of several meters above the surface at high wind speeds. Morphological deposition of the order of 3 to 5 m^3/m over a period of 3 weeks was observed at various dune foot locations, particularly around the beach entrances/exits for visitors.
Most of the new data refer to conditions with a very long fetch as the wind was almost parallel to the beach. At some dates in February 2020, the wind was oblique to normal from the sea and the distance between the wet intertidal beach and the measurement location was in the range of 5 to 50 m resulting in relatively small, non-saturated (non-equilibrium) sand transport rates. The fetch-related reduction effect is minor (factor 1.5) for relatively high wind speeds> 10 m/s, but major (factor 5 to 10) for relatively low wind speeds < 9 m/s, see open circles in **Figure 2**.

Figure 3 *Wind transport at beach of Callantsoog; major storm BF 9 (18 m/s) on 9 February 2020 (lighter colours represent is a thin, dense layer of saltating grains with continuous transport)*

Most of the measured sand transport values in moist conditions are within the experimental range of the dry transport values, particularly for the higher wind speeds > 10 m/s. For low wind speeds < 9 m/s, the sand transport rates are slightly reduced in moist conditions. The field data at Saunton Sands in **Figure 2** (red dots) are taken from the plots of Sarre (1988) and refer to moist conditions up to 14%. His data are in excellent agreement with the moist data of Callantsoog (open triangles), which contributes to the confidence in the new data. The intense transport of sand at higher wind speeds in moist conditions can be explained by the entrainment of sand from the drier spots which are always there (between vegetation at the dune front, behind obstacles and from beneath the beach houses on piles). The presence of dry spots with lighter colour was a very prominent feature during measurements in moist conditions (a few hours after the last rainfall) at the beach of Callantsoog and other beaches. Most likely, these dry spots consist of sand particles carried along the beach surface and deposited in depressions at the surface (see inset upper left corner of **Figure 1**).
Finally, the effect of coarse materials is discussed. **Figure 2** shows 2 data points (solid squares) from a beach with a coarse armor layer (Van Rijn 2021; Strypsteen et al., 2021), where sand transport was very low at a wind speed of about 10 m/s (factor 10 lower than the values of the experimental range). The α_{cf}-equation (Part 2) yields a reduction of 95% for a gravel percentage of 30% in agreement with the field data.

5. Verification of transport equations

5.1 Verification and discussion of sand transport equations

The new VR-sand transport model (Section 2 and Part 2) has been verified using old and new field data sets. The input data are: the measured wind velocity and height at which the wind velocity is measured, the d_{50} and d_{90}-values and percentage of coarse materials; the percentage of dry (p_d) and moist (p_m) spots upwind of the sampling location and the moisture content of the upper 20 mm of the moist spots (w_{20mm}), see **Table 2.**
The transport rates for moist sand conditions are computed as: $q_s=(1-p_m/100)q_{s,d} + p_m/100\ q_{s,m}$, with: $q_{s,d}$= sand transport at dry spots; $q_{s,m}$=sand transport at moist spots; p_d= percentage of dry spots; p_m=percentage of dry spots at the beach upwind of the measurement location ($p_m+p_d=100\%$). The p_m and p_d values are not known for the literature data, but are estimated as good as possible based on the available information. Other parameters are: κ=0.4; ρ_{air}=1.2 kg/m³; ρ_{sand}=2650 kg/m³; α_B=2; α_{VR}=1.8; $\alpha_{th,ces}$=0.08 (cessation threshold); $d_{50,ref}$=0.00025 m.
Various data sets from the literature and the new field data sets of beaches in Belgium and The Netherlands have been used for verification of the proposed transport equations. The old data sets from the literature (48 data points) refer the existing data sets of Sherman et al. (2013), Campos (2018) and Strypsteen (2019) for dry beach sand conditions and the data sets of Sarre (1988), Jackson and Nordstrom (1997) and Wiggs et al. (2004) for moist sand conditions. The new data sets refer to dry and moist beach sand conditions (81 data points at 10 beaches in Belgium and The Netherlands). Detailed tabulated data of all new field data sets are given in Van Rijn (2021). In all, 129 high-quality data sets have been used for verification. All tabulated data used for verification can be found in Van Rijn (2021).
The field data of Sarre (1988), Jackson and Nordstorm (1997), Wiggs et al. (2004) are briefly described here. The other literature data have been described by Van Rijn and Strypsteen (2020) and can be found in Van Rijn (2021).
Sarre (1988) measured wind transport at a British intertidal site using a vertical sand trap, together with simultaneous monitoring of wind speed and moisture levels up 18% in the top 1-2 mm surface layers of sand (beach sand of 0.17 mm). Measured transport rates were in the range of 0.1 to 220 kg/m/s. The beach site was Saunton Sands bordering the Bristol Channel, located within Barnstaple Bay, SW England. The beach is a wide, low-angle intertidal plain backed by dunes. The many data points of Sarre were taken from his original plot and clustered into 10 representative data points.

Jackson and Nordstrom (1997) studied (8 to 19 March 1994) the influence of changes in surface moisture content on sand entrainment and transport on the beach of Wildwood, New Yersey, USA. The field site is located near the north end of a 10 km long barrier island. The mean tidal range is 1.25 m; mean spring range is 1.5 m. Beach sediments are very well-sorted, fine sand (d_{50}≅0.165 mm). Sand transport was measured using 4 Leatherman traps placed vertically in the bed. Three data points were taken from the plots.
Wiggs et al. (2004) studied the influence of changes in surface moisture content on sand entrainment and transport on the meso-tidal Aberffraw beach with d_{50}=0.2 mm in Anglesey, North Wales. High frequency (1 Hz) wind velocities measured with hot-wire anemometers were combined with grain impact data from a Sensit monitor and mass flux measurements from a standard sand trap. Surface and near-surface moisture contents were measured gravimetrically from surface sand scrapes.

Figure 4left shows measured and predicted transport rates of the dry sand for the new VR-transport equation. The VR-equation has a score of 87% of the predicted data within a factor of 2 of the measured values. The measured transport rates are slightly overpredicted for stronger wind conditions. The modified Bagnold-equations produces a score of 79%

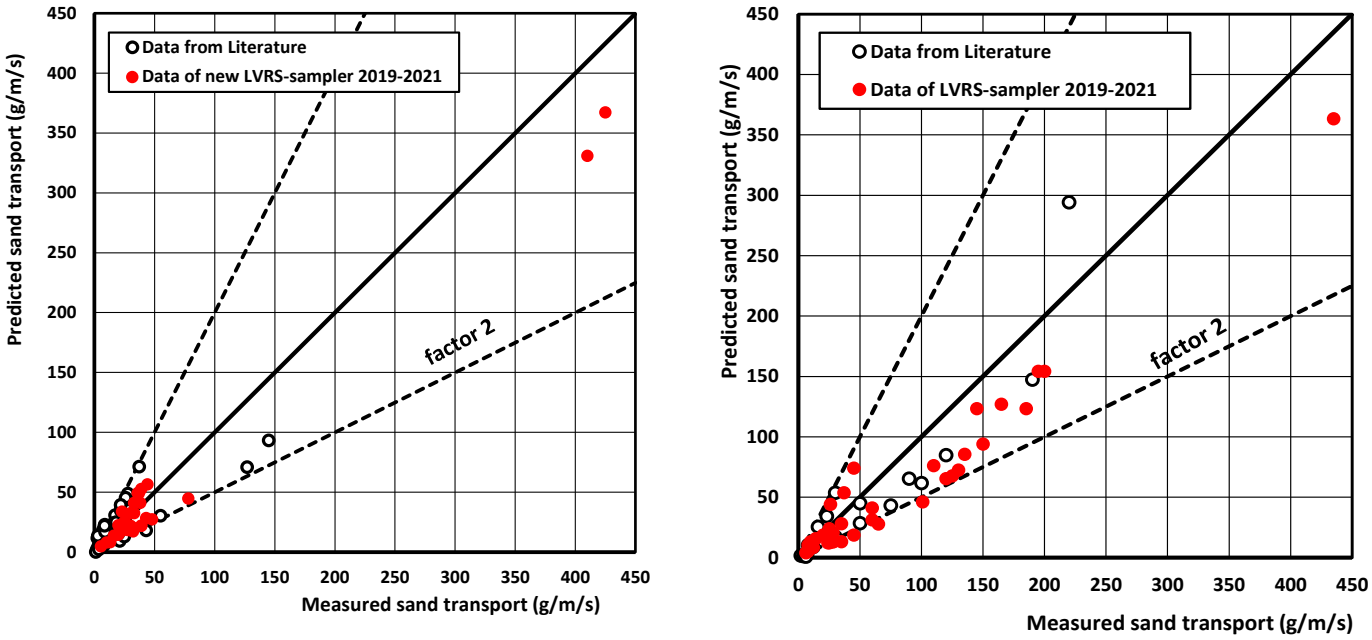

Figure 4 *Comparison of measured and predicted sand transport; VR-transport equations*
Left: dry beach surface (71 data points); Right: moist beach surface (58 data points)

Figure 4right shows a similar comparison for moist sand. Now 91% of the predicted data of the VR-method are within a factor of 2 of the measured values. The Modified Bagnold-equation produces a score of 67%. The high scores of the VR-method are obtained for α_{VR}=1.8, β=0.1 (power of grain size) and $\alpha_{th,cessation}$=0.08 (threshold coefficient), which also gave the best results for the wind tunnel data of Belly (1964), see Part 2. Thus, the field data seem to confirm that the influence of the grain size in the range of 0.15 to 0.4 mm is minor and is better represented by a power of 0.1 (VR-equation) than 0.5 (Bagnold-equation). Three very high transport rates were measured on 9 February 2020 during a storm with high wind velocities of 18 to 19 m/s (BF 9). The bag of the bed load sampler was full in 4 minutes. These record transport rates with values in the range of 400 to 450 g/m/s reveal that the transport rate depends on a strongly nonlinear relationship up to wind velocities of about 20 m/s. However, this conclusion is not very solid as only a few data points are available in the high wind velocity range of 13 to 20 m/s (BF 7 to 9). This emphasizes the need for more data in this range. The VR-method (and also the modified Bagnold-equation) seems to underpredict for wind velocities > 10 m/s, which is most likely caused by the wind gustiness effect. The field transport measurements are strongly influenced by short-duration (30 s) wind gusts within the measuring period of say 10 minutes, whereas the predicted transport is based on a time-averaged wind velocity neglecting the gust effect. A method to solve this may be the introduction of a gust coefficient in the range 1.05 to 1.1 acting on the time-averaged wind velocity. More research is required to define an appropriate gust coefficient.

Figure 5 shows the ratio of measured and predicted sand transport as function of the wind speed for the new VR-transport equation. It can easily be counted that 10 (11%) of the 128 data points are outside the range of a factor of 2 and thus 89% are within a factor of 2. As regards the dry sand data points, about 50% of the data points are above and under the ratio of 1 (no bias). As regards the moist sand data points, most values are above the ratio of 1 indicating underprediction. Most likely, the effect of moist sand on the predicted sand transport is somewhat too strong. The new VR-sand transport equation seems to work well for low very wind speeds (5 to 7 m/s) and very high wind speeds (15 to 20 m/s).

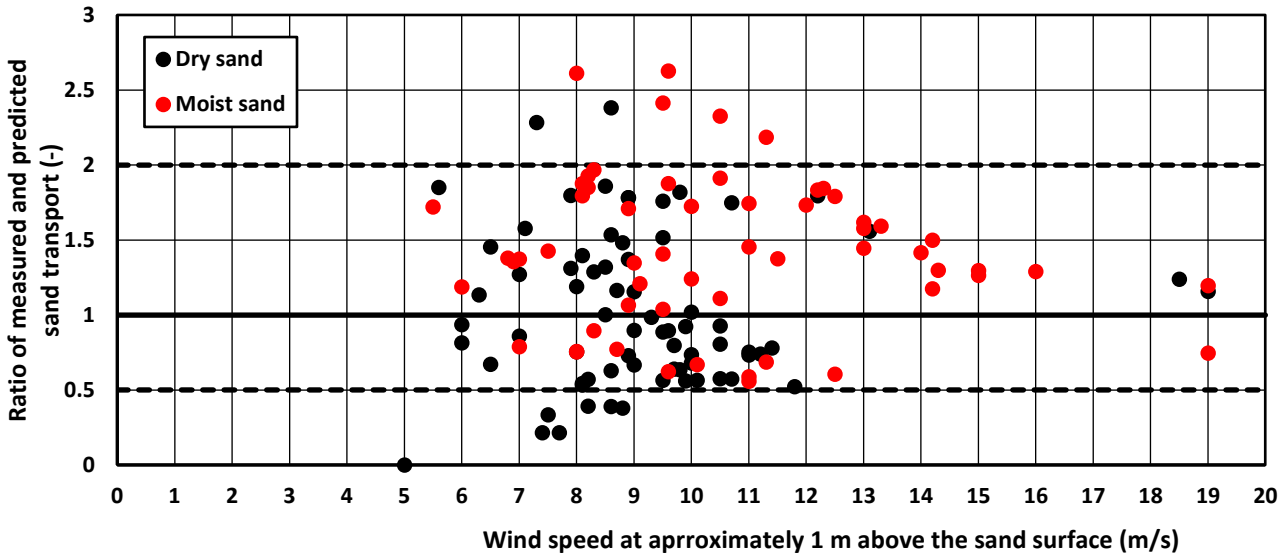

Figure 5 *Ratio of measured and predicted sand transport for new VR-transport equation*

The classical models of Bagnold (1941) for sand transport in air and Meyer-Peter & Müller (1948) for sand transport in water close to the bed have a nonlinear relationship between transport and shear stress ($\gamma \cong 1.5$), which is based on the assumption that the particle speed scales with the shear velocity (u_*), supported by the work of Kawamura (1951) and Owen (1964) for wind transport. However, recent studies based on numerical modelling of sand transport in the low shear stress range with intermittent to continuous saltation transport (rolling, sliding and saltating particles including rebounds at the bed) suggest that the saltation height and speed are almost constant and independent of the shear velocity resulting in a linear relationship between wind-driven sand transport and shear stress (Ungar and Haff, 1987; Durán et al., 2011; Kok et al. 2012; Martin et al., 2013; Martin and Kok, 2018). This model approach with grain-dominated particle entrainment and constant saltation characteristics in the lower shear stress range (say: $u_*<1.5$ to $2u_{*,th,c}$) is supported by measured saltation fluxes at various field sites (Martin et al. 2013; Martin and Kok, 2018; Martin et al., 2018). The dimensionless saltation height (δ_s/d_{50}) was found to be in the range 140 to 220 and independent of u_*. The data of Martin et al. (2013) suggest a linear relationship between transport and shear stress in the lower shear stress range near initiation of motion (0.15-0.25 Pa), but a nonlinear relationship (γ=1.5) is also found to be plausible in this shear stress range. Measured fluxes at high shear stresses (storms, τ>0.45 Pa; fluxes > 60 g/m/s) are still missing.
A practical sand flux equation can be derived by approximating: $q_s=u_{eff}\, M_{load}$ with u_{eff}= effective streamwise speed of the saltating particles (m/s) and M_{load}= mass load of particles in motion per unit area (kg/m^2). Based on the work of Durán et al. (2011); Martin et al. (2013); Pähtz and Durán (2020), two regimes can be distinguished:

- low shear velocity regime ($u_*<1.5$ to $2u_{*,th,c}$): $u_{eff}=C_1 u_{*,th,c}$ and $M_{load}=C_2(\tau-\tau_{th,c})$ giving $q_s=C_3\, u_{*,th,c}\,(\tau-\tau_{th,c})$;
- high shear velocity regime ($u_*>1.5$ to $2u_{*,th,c}$): $u_{eff}=C_4\, u_*$, and $M_{load}=C_5(\tau-\tau_{th,c})$ giving $q_s=C_6\, u_*(\tau-\tau_{th,c}) \cong C_7(\tau)^{1.5}$.

with: q_s= equilibrium sand transport (kg/m/s) $\tau_{th,c} = \rho_a u_{*,th,c}^2$=cessation (impact) threshold shear stress at cessation of transport (Pa), ρ_a= air density (kg/m^3), C= calibration coefficient, C_3= calibration factor of the order of 5 to 8 based on field data (Kok et al., 2012; Martin and Kok, 2017). This approach shows a nonlinear relationship in the high shear velocity regime.
Finally, It is noted that the sand transport equations used in this study are deterministic equations, which are by definition not accurate around threshold conditions with intermittent transport of rolling, sliding and saltating particles (Grass, 1970; Paintal, 1971; Stout and Zobeck, 1997 and others). Sand transport in turbulent wind conditions around the threshold for initiation of motion is an intermittent process with the wind velocity often falling below the threshold wind speed. Stout and Zobeck (1997) measured the instantaneous wind velocity and saltation intensity close to the surface and determined the intermittency factor (γ_p) defined as the fraction of time with saltating particles ($0<\gamma_p<1$). They showed that turbulent wind around threshold conditions at a field site in the USA had an almost perfect normal (Gaussian) probability distribution. The threshold wind velocity (u_{th}) was defined as the mean wind speed giving an intermittency factor γ_p=0.5. This means that sand transport occurs during 50% of the time when the wind speed > u_{th} and no sand transport occurs during the other 50% of the time when the wind speed < u_{th}. Thus, sand transport occurs when the mean wind speed (or shear stress) is equal to the threshold wind speed (or threshold shear stress). This cannot be represented by a deterministic sand transport equation which always gives zero transport for $u=u_{th}$. Based on the work of Stout and Zobeck (1997), sand transport is almost zero ($\gamma_p<0.05$) for a mean wind speed of about $0.7u_{th}$ (cessation threshold); sand transport is continuous ($\gamma_p>0.9$) for a mean wind speed of about $1.5u_{th}$. Using a lower threshold value (impact or cessation threshold value) in a deterministic sand transport equation improves the predicting ability (Durán et al. 2011, Kok et al. 2012). Comola et al. (2019) have tried to overcome the problem by introducing an intermittency factor in a deterministic transport equation, which however requires information of the cumulative probability density function of the wind speed around threshold conditions. Another approach is the application of fully stochastic sand transport formulations to estimate the sand transport at conditions with intermittent particle motions (Kalinske, 1947; Einstein, 1950; Van Rijn 1993). However, these types of equations are less easy to apply than deterministic equations.
Summarizing, the present study of deterministic transport equations suggests a nonlinear relationship (power 1.5) between sand transport and shear stress in agreement with the classical work of Bagnold (1937, 1941),

rather than a linear relationship as proposed in various recent studies (Durán et al., 2011; Kok et al. 2012; Martin et al., 2013; Martin and Kok, 2017, 2018; Pähtz and Durán, 2018, 2020**;** Pähtz et al., 2021).

5.2 Verification of sand transport around threshold conditions

Special attention is given to the transport of dry sand just beyond the threshold value based on measurements at two beaches (The Netherlands) and in the mini wind tunnel (Part 2).

Very small transport rates at low velocities are of less practical importance, but it is interesting to assess the type of relationship between transport and shear stress around the threshold conditions and to determine the predicting ability of available deterministic transport equations for low shear stresses with intermittent transport conditions.

The field tests were performed at the beach of De Hors on the island of Texel (summer and autumn of 2000) and the beach of Callantsoog in The Netherlands (29 February, 13 April and 24 October 2020) in conditions with fairly dry sand during wind velocities of 5 to 8 m/s. (BF 4 to 6). The particle size characteristics of Callantsoog beach are d_{10}=0.17$\pm$ 0.02 mm, d_{50}=0.23$\pm$ 0.03 mm, d_{90}=0.35$\pm$ 0.05 mm. In addition, a series of tests has been done in a mini wind tunnel (length=1 m ; width=0.06 m, see Part 2) to measure the sand transport rate of dry particles at low wind velocities just above the threshold conditions. The wind flow with a constant velocity (without gusts) is generated by a commercial hair dryer. The wind velocity can be increased gradually by placing the hair dryer closer to the tunnel entrance. The sand transport rate was determined from the mass difference of the tunnel tray (length of 0.2 m) with sand before and after the test. The effective transport width at the sand surface of the tray is 0.03 m based on visual observations of the scour marks. The test duration was in the range of 40 to 100 s. Some tests were done with a flat sand surface, but most tests were done with an irregular sand surface ($\cong$ 5 mm high) at the sand surface. Four types of uniform (dry) sand with diameters 0.17, 0.35, 0.6 and 0.8 mm were used, see **Table 3**. In addition, two sand samples (C1, C2) from the beach of Callantsoog (The Netherlands) were used. Sample C1 is the original beach sand with $d_{50}\cong$0.23 mm excluding coarse gravel materials and shell fragments (removed using a sieve of 1 mm). Sample C2 is taken from trapped sand of the bed load sampler (Section 3) and consists of slightly finer sand with $d_{50}\cong$0.2 m without coarse materials.

The wind velocity ($u_{0.03}$) was measured in the axis of the tunnel at 0.03 m above the sand surface at the end of the tray using a miniature wind velocity meter (Kaindl windmaster2; miniature cup-rotor of 25 mm wide and 10 mm high). It is noted that the wind velocity in the tunnel is a constant wind velocity without gusts as present in nature. To compare the wind tunnel data to field data, the wind $u_{0.03}$ has been converted to a virtual wind velocity u_1 at 1 m above the surface using the equation $u_1=\alpha_{log}u_{0.03}$ with α_{log}= coefficient related to logarithmic velocity profile ($\cong$1.5 for a bed roughness of about 0.5 mm; velocity at 1 m is about 50 % higher than that at 0.03 m), see values in the last column of **Table 3**.

First, the instantaneous threshold wind velocities of the sand samples used in the mini wind tunnel are discussed. **Figure 6** shows that the measured threshold velocities derived from the mini tunnel tests are higher (15% to 20%) than the predicted values based on the Bagnold-equation with $\alpha_{th,\ initiation}$=0.1. The time-averaged (over 10 minutes) threshold wind velocity measured at the beach of Callantsoog with d_{50}=0.23 mm is about 6 m/s (at z=1 m above surface; open circle in **Figure 6**). The same sand in the mini tunnel requires a velocity of 7.7 m/s for initiation of motion. The measured threshold velocity at the beach of Callantsoog is close to the predicted value of the Bagnold-equation with coefficient=0.1. The threshold wind velocity measured at the beach of Callantsoog (6 m/s) represents the time-averaged velocity including wind gusts. The peak velocities in field conditions over a short period of say 10 minutes can be represented by $u_{peak}=u_{mean}+\sigma_U$ with σ_U =0.15-0.2u_{mean} (Stout and Zobeck, 1997). Thus, the peak velocities (instantaneous velocity) causing initiation of particle motion at the beach are about 15% to 20% higher resulting in values in the range of 7.1 to 7.5 m/s which is fairly close to the value of 7.7 m/s measured in the tunnel. The wind velocities measured in the tunnel are almost constant with very minor turbulent fluctuations (<3%) and can therefore be seen as instantaneous velocities. The instantaneous threshold

velocity can be represented by the Bagnold-equation with a coefficient α_{th}=0.12. The threshold velocity for cessation of motion is much smaller (Part 2), see **Figure 6**.

Sand	**Instantaneous threshold wind velocity at z=0.03 m above bed for initiation of motion measured in mini wind tunnel $u_{0.03}$ (m/s)**	**Instantaneous threshold wind velocity at 1 m above bed for initiation of motion u_1=1.5$u_{0.03}$ (m/s)**
Uniform: d_{50}=0.17 mm (0.1-0.3 mm)	4.3	6.5
Uniform: d_{50}=0.35 mm (0.3-0.5 mm)	6.7	8.7
Uniform: d_{50}=0.6 mm (0.4-0.8 mm)	7.1	10.7
Uniform: d_{50}=0.8 mm (0.5-1 mm)	8.4	12.6
C1 Callantsoog beach d_{50}=0.23 mm; without coarse materials	5.1	7.7
C2 Callantsoog beach d_{50}=0.2 mm; no coarse materials	4.8	7.2

Table 3 *Threshold wind velocities of various types of sand in mini wind tunnel*

The results of the sand transport experiments at low velocities at the beach of Callantsoog on 29 February, 13 April and 24 October 2020 using the LVRS-bed load sampler (Section 3) are shown in **Figure 7**. Earlier results measured at the beach of De Hors on the island of Texel are also shown (Strypsteen et al., 2021). The transport rates of sand with d_{50}=0.23 mm were measured in the velocity range of 6 to 8 m/s (time-averaged values over 10 minutes). Predicted transport rates are shown for different values of the cessation threshold coefficient ($\alpha_{th,cessation}$=0.07 and 0.08). The predicted values for $\alpha_{th,cessation}$=0.07 (green curve) are quite good for velocities in the range of 6 to 7.5 m/s, but somewhat too small for the velocity range of 7.5 to 8 m/s. The predicted transport rates are somewhat too small for $\alpha_{th,cessation}$=0.08 (red curve). Two effects are important in the low velocity regime: i) sand transport ceases at a much lower velocity (≅4.5 to 5 m/s) than that for initiation of erosion (≅ 6 to 6.5 m/s, see **Figure 8**) and ii) the finer sand particles (< 0.15 mm) are more easily winnowed from the sand surface resulting in higher transport rates. The sand trapped in the bed load sampler at the beach of Callantsoog was finer (d_{50} ≅ 0.2 mm) than the original bed material (d_{50}≅0.23 mm). The representation of these processes by a deterministic transport equation requires a relatively small threshold value ($\alpha_{th,cessation}$=0.07).

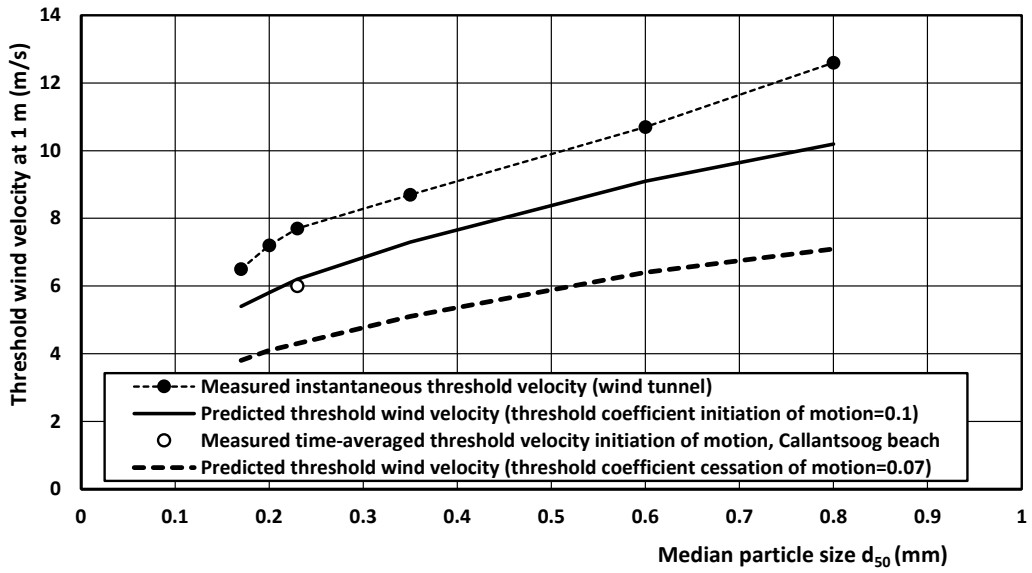

Figure 6 *Threshold wind velocity of sand bed*

Figure 7 also shows predicted values of the Multi-Fraction (MF) method using the VR-transport equation (see Strypsteen et al., 2021) for 7 fractions: 5% of 0.06-0.1 mm; 10% of 0.1-0.15 mm; 20% of 0.15-0.2 mm; 25% of 0.2-0.25 mm; 20% of 0.25-3 mm; 15% of 0.3-0.35 mm and 5% of 0.35-0.4 mm (d_{50}=0.23 mm) and hiding-exposure coefficient equal to 1. The results of the MF-method are almost the same as those of the Single-Fraction (SF) method. The MF-method is most suitable for widely graded sediments with a substantial coarse fraction, but has no added value for fine almost uniform sediments.
The measured sand transport rates of dry sand in the mini wind tunnel at low velocities are given in **Figure 8**. The error range of the measured transport rates is about ±30% based on the variation of repetitive tests. It can be observed that the measured sand transport rates at low velocities are strongly related to the particle size and the associated threshold wind velocity. Larger particles have a higher threshold velocity and thus a lower transport rate at the same velocity.

Figure 9 shows the results of the tunnel tests and the field experiments plotted as function of an excess shear stress parameter u_{1m}^2-$u_{th,cessation}^2$, with $u_{th,cessation}$= threshold velocity at cessation of transport ($u_{th,cessation}$ ≅5 m/s for d_{50}=0.23 mm; transport=0). Sand transport is assumed to be intermittent for u_{1m} < 1.5 $u_{th,cessation}$. Sand transport is clearly higher for sand of 0.17 mm than for 0.23 mm, but the results of particles in the range of 0.35 to 0.8 mm are somewhat scattered without a clear trend. The measured sand transport data suggests a nonlinear relationship between transport and shear stress, particularly the field data at the transition from intermittent to continuous transport at velocities > 7.5 m/s (excess parameter > 40). The measured field data of Callantsoog beach can be reasonably well represented by the VR-sand transport equation with TC=$\alpha_{th,cessation}$=0.07, which is based on a nonlinear relationship (power 1.5) between transport and shear stress . Using TC=$\alpha_{th,initiation}$=0.10, the predicted sand transport values are much too small. Based on this, it is concluded that the threshold value for a deterministic sand transport equation can be best represented by the cessation threshold value.

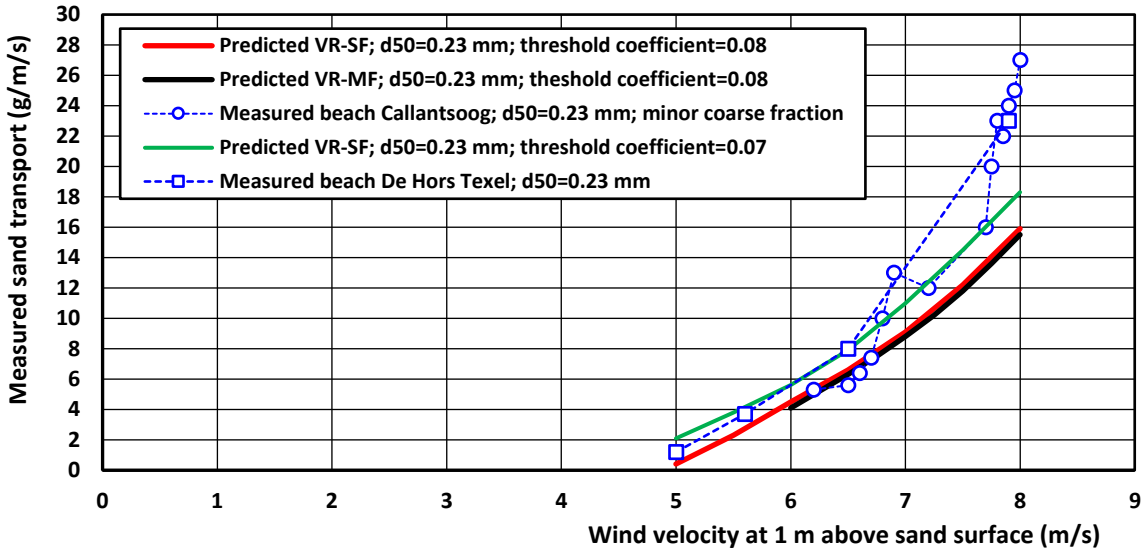

Figure 7 *Sand transport at low velocities at natural beaches, The Netherlands*
VR-SF= Van Rijn equation based on Single Fraction method; MF= Multi-Fraction method

It is noted that the measurements in the mini wind tunnel should be seen as exploring as it is questionable whether the measured transport rates in the mini tunnel represent equilibrium conditions given the short length (0.2 m) of the sand tray, although only low wind velocities have been used. The adjustment length for establishing equilibrium sand transport with only rolling particles is most likely fairly small, but its proper value is unknown. More research is required to better determine the effect of particle diameter on the transport rates at low velocities.

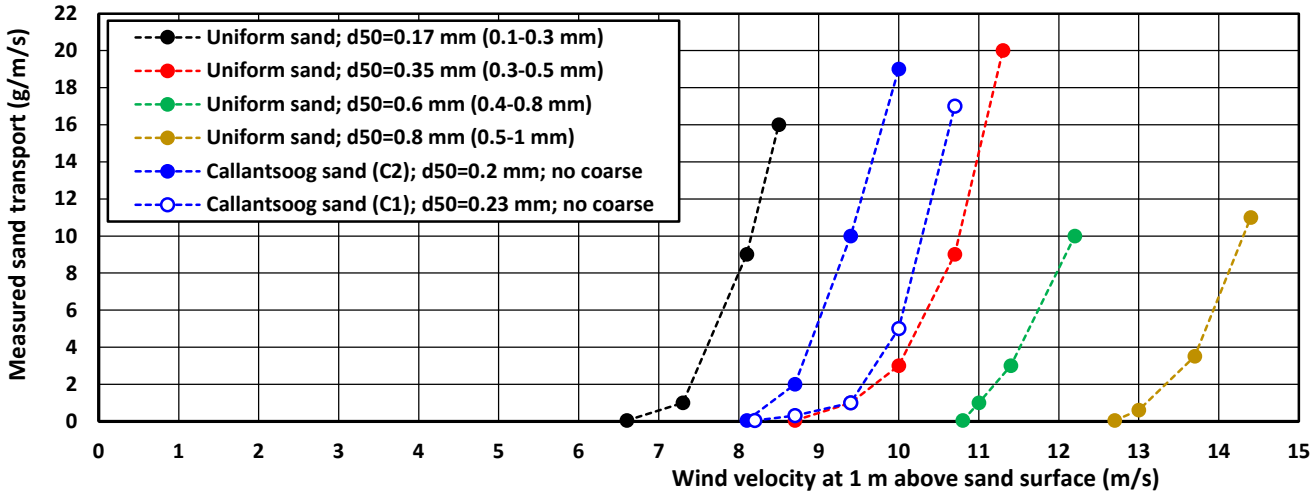

Figure 8 *Sand transport at low velocities in mini wind tunnel*

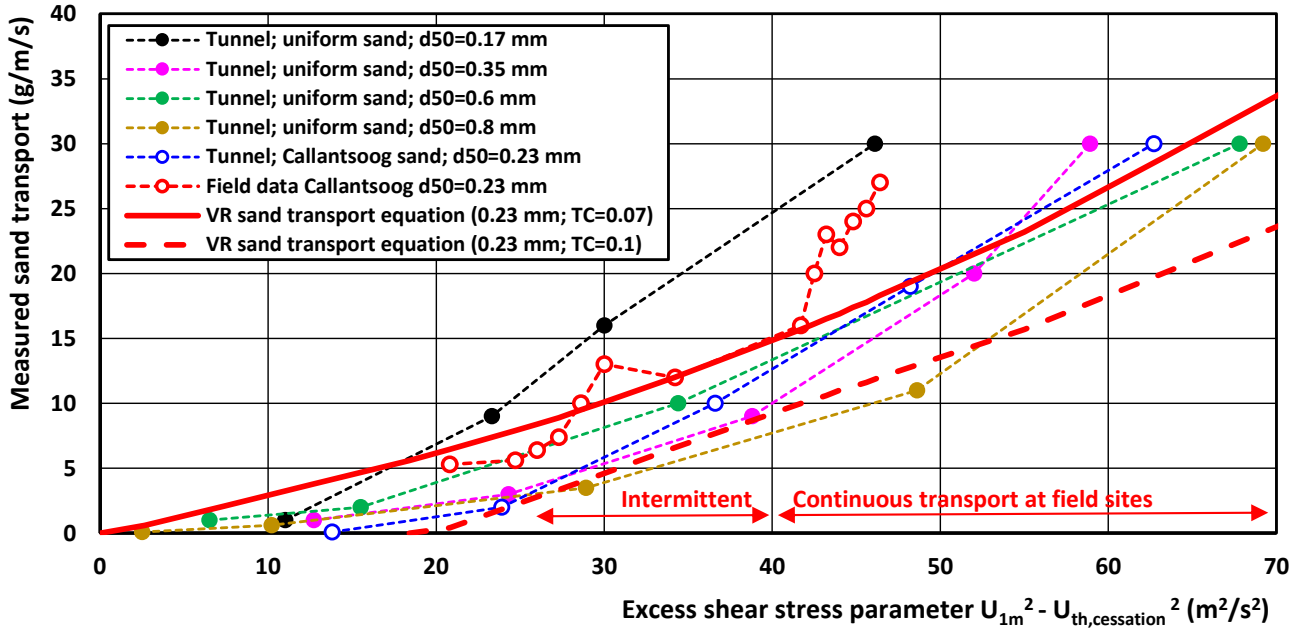

Figure 9 *Sand transport at low velocities as function of excess shear stress parameter*

6. Applications of sand transport equations for long term predictions of dry and moist sand

6.1 General

For historical studies and engineering projects in coastal aeras often long-term predictions of aeolian sand transport are required. The Dutch dune system consists of dunes with heights in the range of 10 to 20 m, created in the period between 800 and 1600 AD (Jelgerma et al., 1970). Pool and Van der Valk (1988) have shown that the development of this (ancient) dune system can be explained by a long term annual onshore wind transport of about 50 m³/m/year. Nowadays, the annual wind transport rates are much lower of the order of 10 to 20 m^3/m/year, which can be derived from measured dune migration rates (dune height≅15 m; migration rates≅ 1 m/year; Mulder and Tonnon, 2011). To get realistic sand transport rates of the order of 15 m^3/m/year, the effect of rainfall and moisture has to be included in long term predictions (Section 6.2). Another problem is the availability of long term wind velocity data at the beach. Long term wind transport predictions at beaches are mostly based on wind velocities measured at regional weather or airport stations. Usually, the wind velocity at such a station is measured at a long mast open to all directions. The wind velocity and direction measured there are not the same as those on the nearby beach backed by high dunes. Two effects are important and need to be taken into account (Section 6.3): i) higher wind speed at beach than at an inland wind station and ii) lower wind speed at beaches backed by high dunes (De winter et al., 2020)

6.2 Inclusion of moist due to rainfall

The proposed sand transport equation (Section 2) can be used to predict the wind-driven sand transport rate in dry beach conditions. A general method to include moisture effect due to rainfall events is not yet available. Herein, a new method to include moisture effects is proposed. **Table 4** summarizes the sand transport restrictions for various combinations of wind strength and rain fall intensity in a fairly wet and windy climate as present along the beaches in Belgium and The Netherlands based on the experiences of the author during many field trips/visits.

Rain→	**No rain**			**Light rain < 1 mm/hour**	**Medium rain 1-5 mm/hour**	**Strong rain > 10 mm/hour**
Wind ↓	**m.c. <2%**	**2-8%**	**8-15%**	**m.c.=4-8%**	**8-10%**	**10-15%**
Light wind 5-8 m/s (< BF4)	unrestricted transport p_o=50%	slightly restricted p_o=5-10%	restricted transport p_o=5-10%	restricted transport p_o=5-10%	very restricted; minor splash-type transport may occur p_o=3-5%	very restricted; minor splash-type transport may occur p_o<1%
Strong wind 8-15 m/s (BF5 to 7)	unrestricted transport p_o=10%	wind ⊥: restricted wind//: unrestricted p_o=5-10%	wind ⊥: restricted wind//: slightly restricted p_o=3-5%	wind ⊥: restricted wind//: unrestricted p_o=3-5%	wind ⊥: restricted some splash-type tr. wind//: unrestricted tr. and splash-type tr. p_o<1%	wind ⊥: very restricted; splash-type transport wind//: slightly restricted; splash-type transport p_o<1%
Storm wind > 15 m/s (BF8 to 10)	unrestricted transport p_o<1%	wind ⊥: restricted wind//: unrestricted p_o<1%	wind ⊥: restricted wind//: slightly restricted p_o<1%	wind ⊥: restricted wind//: unrestricted p_o<1%	wind ⊥: slightly restricted only splash-type tr. wind//: unrestricted tr. and splash-type tr. p_o<1%	wind ⊥: slightly restricted only splash-type transport wind//: unrestricted and splash-type tr. p_o<1%

m.c.= moisture content; p_o= percentage of time of that conditions occur; wind ⊥ = wind normal to beach (often supply-limited as beach width usually< 100 m); wind//= wind parallel to beach (no supply-limitation as upwind sources are abundant; fetch length > 1000 m)

Table 4 *Effect of rainfall and wind on type of sand transport at exposed beach sites*

During rainfall with strong to stormy winds parallel to the beach, sand transport does not cease but continues. Splash-type transport may be dominant in strong rains and mild winds. Severely restricted transport occurs during light rainfall and immediately after rain fall with light winds (about 20% of the time). Sand transport is restricted in conditions with a drying beach surface after rainfall and light winds (about 30% of the time).

Moisture effects are found to be very minor for strong winds parallel to the beach because the fetch is then almost infinite and dry sand is always available at some spots. Moisture effects reduce sand transport severely for winds oblique or normal to the shore. In the latter case the fetch over the wet lower intertidal zone and the moist upper beach is generally too short for the development of equilibrium sand transport conditions resulting in underloading conditions. Supply-limited conditions due to rainfall were clearly observed during various events at the Dutch beach of Callantsoog. On 16 February 2020, the wind parallel to the beach dropped suddenly from BF7 (15 m/s) to BF5 (9 m/s) and sand transport ceased in conditions with moisture levels of 9 to 12% at the upper beach. On 24 February 2020, the wind speed parallel to the beach suddenly increased to BF7 (15 m/s) after a rainfall event; no sand transport was visually observed at the moist upper beach. On another date with BF7, the sand transport was intense and continued when rainfall started. Thus, the chronology of wind speed and rainfall is rather important. An increasing strong wind up to BF7 over a wet surface leads to supply-limited conditions, but sand transport due a strong steady wind (BF7) is not reduced (limited) by rainfall creating a wet surface.

Based on field observations during and after rainfall events, three types of transport periods are distinguished:

- rainfall period with almost wet sand surface and moisture levels of about 8% in the upper 20 mm of the sand bed; no or minor sand transport for low wind velocities < 10 m/s; continuous transport during storm events (> 15 m/s);
- drying period with wet and dry spots; moisture levels gradually reduce from 8% to 2% and;
- almost dry period when moisture levels of the upper 20 mm are below 2% (mc-levels of upper 1 to 5 mm are below 1%; see Part 2); mostly occurring in late spring, summer and early autumn.

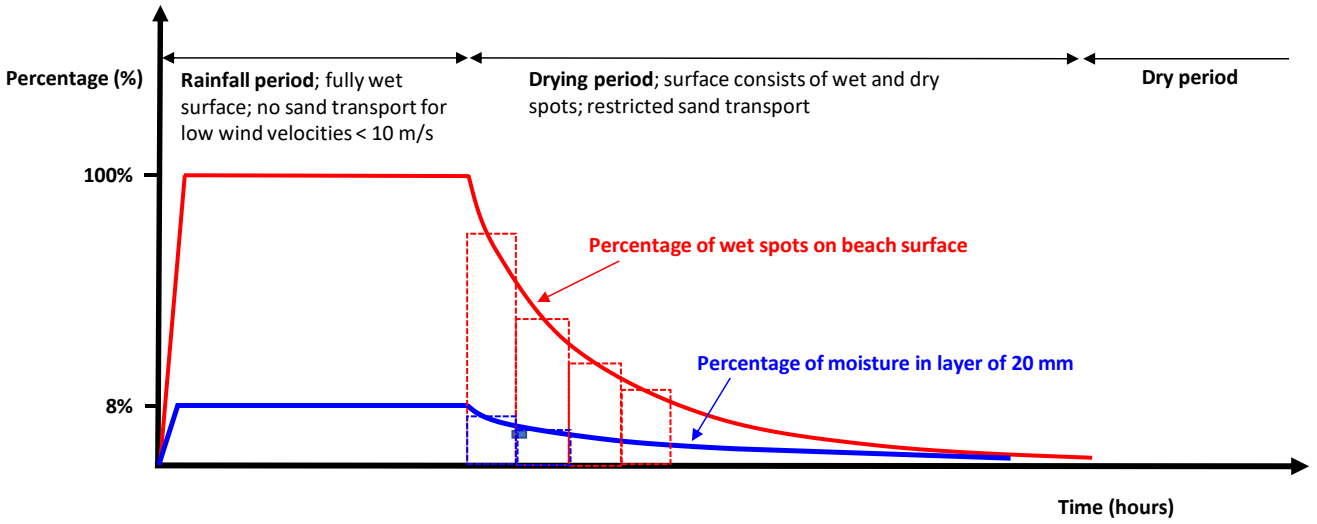

Figure 10 *Beach surface conditions during and after rainfall event*

The duration of the drying period strongly depends on the wind strength and the air temperature (Part 2). The drying period can be schematized in a series of blocks (histograms) with decreasing values of the moisture percentage and decreasing percentage of wet spots, see **Figure 10**. For example, six hours after the last rainfall event at the beach of Zeebrugge (Belgium) in December 2019, the percentage of wet spots was still about 50% with a moisture level of 4%, but the measured sand transport rates were only slightly reduced compared to that of dry sand at the same wind speed.

To predict the sand transport rate in conditions with dry and wet spots, it proposed to consider the transport in each period separately and then make a summation over all wet and dry conditions. This can be formulated as follows:

$$q_{s,total}= \sum^{N} [(\alpha_r q_{s,m,i})t_{r,i} + \{(1-p_{m,i}/100)\ q_{s,d,i} + (p_{m,i}/100)\ q_{s,m,i}\}\ T_{8\%-2\%,i} + (q_{s,d,i})t_{d,i}]/\rho_{d,sand} \quad (4)$$

with:

$q_{s,total}$= total volumetric sand transport over a series of events (m^3/m/events); $q_{s,d,i}$ = mass transport of sand (kg/m/s) over dry surface in event i; $q_{s,m,i}$ = mass transport of sand over moist surface (spot) in event i; α_r = reduction coefficient = 1 for wind velocities (at 1 m above surface) > 10 m/s and α_r = 0 for low wind velocities < 10 m/s; $t_{w,i}$ = duration of event i with a constant wind velocity $u_{w,i}$ and angle of of incidence θ_i; $t_{r,i}$ = duration of rainfall period in event i; $T_{8\%-2\%,i}$= duration of drying period after rainfall (Part 2) in event i; $T_{8\%-2\%,i}=t_{w,i}-t_{r,i}$ if $t_{w,i}-t_{r,i}<T_{8\%-2\%,i}$; $t_{d,i}=t_{w,i} - t_{r,i} - T_{8\%-2\%,i}$= duration of period with dry surface in event i; p_d=percentage of dry spots, p_m= percentage of moist spots in the drying period (p_m+p_d=100%), $\rho_{d,sand}$ = dry bulk density of sand , N= total number of events.

Equation (4) consists of three terms. The first term represents the sand transport during periods with rainfall including splash-type transport (latter component is neglected in this study). Sand transport during rainfall is assumed to be absent for low wind velocities (at 1 m above surface) < 10 m/s and continues for wind velocities > 10 m/s. The middle term represents the combined (restricted) transport over dry and wet spots during the drying period (Part 2). The last term represents the transport of sand in dry beach conditions. The parameters to be specified as input data are: $t_{w,i}$, $t_{r,i}$, $T_{8\%-2\%,i}$, $p_{m,i}$, $w_{20mm,i}$. The effect of rainfall on sand transport is zero by setting $t_{r,i}=T_{8\%-2\%,i}=p_{m,i}$= 0. These parameters are all known based on field measurements for the present data set (Van Rijn, 2021). Equations (1) to (4) are implemented in the spreadsheet model AEOL-ST (freely available).

6.3 Wind modification effects

When the beach is backed by high foredunes (> 10 m), the wind velocity in the lower boundary layer at midbeach may be reduced due to the obstacle effect created by the foredunes, particularly for shore-normal wind conditions. Due to pressure buildup in front of the foredune, the wind streamlines near the beach surface are gradually pushed upwards resulting in lower wind velocities (Wiggs et al., 1996; Hesp et al., 2005; Bauer et al., 2012; De Winter et al., 2020). This obstacle effect reducing the wind velocity at mid-beach is stronger for higher and steeper foredunes, but is less for oblique winds and almost absent for shore-parallel winds.

De winter et al. (2020) measured wind velocities at height of 0.9 m above the sand using ultrasonic anemometers in a cross-shore array from the waterline to the dune foot (spacing of about 10 m) at the beach of Egmond aan Zee (The Netherlands), which is backed by high dunes (up to 22 m). Regional wind speed and direction were measured at the meteorological station in IJmuiden-harbour, which is about 15 km south of the beach site. These (regional) wind velocities (at height of 10 m) were converted to a velocity at 0.9 m above the surface (assumed roughness k_s=0.03 m; yielding: $u_{reg,0.9m}$=0,.74 $u_{reg,10m}$). Measured results show that the ratio of beach and regional wind speed ($u_{w,beach}/u_{w,regional}$) is mostly < 1, except for velocities smaller than 3.0 to 4.0 m/s. This ratio is about 0.4 at mid-beach when the wind direction is normal to the dunes. Close to the dune foot the wind speeds are smaller than at mid beach for winds normal to the dune, promoting deposition. This effect is less for shore-parallel winds. The ratio $u_{w,beach}/u_{w,regional}$ increases with increasing obliquity towards almost 1 for alongshore winds. The wind direction of local winds at mid-beach are almost the same as those of the regional winds.

Deviation of the wind velocity (wind steering) only occurs at the dune foot and is the largest (about 13˚ larger than the incoming wind angle) with oblique approaching winds of 40˚ from the dune normal. Perpendicular and nearly alongshore winds do not show any steering near the dune foot. The measured results of De Winter et al. (2020) are herein described by a simple linear function, as follows:

$$u_{w,midbeach} = f_r\, f_o\, u_{w,regional} \quad (5a)$$

$$f_o = f_{o,m}\,[1-abs(\theta)/90] + abs(\theta)/90 \quad (5b)$$

with: θ= wind incidence angle to the shore-normal (degrees); f_r= conversion factor for wind velocity from inland to beach (1.0 to 1.2); f_o= obstacle factor related to dunes (0 to 1); $f_{o,m}$= minimum value of f_o-coefficient (input value depending on obstacle height; range of 0.5 to 1).
Equation (5) yields values between $f_{o,m}$ and 1 depending on the wind incidence angle; $f_o = f_{m,o}$ for shore normal wind (angle=0) and f_o=1 for shore-parallel wind (angle=90).

6.4 Annual sand transport predictions for beach of Callantsoog, The Netherlands

The total sand transport at mid-beach is computed in 4 typical months representing the 4 seasons of spring (May), summer (August), autumn (December) and winter (February). The shore normal at Callantsoog makes a positive angle of 97° to North. The beach is backed by high foredunes (height up to 15 m). The beach consists of sand with d_{50}= 0.23 mm. The representative wind and rain conditions ((annual-average values over 2009-2019) have been taken from a weather station at 5 km inland (De Kooy near Den Helder). **Figure 11** shows the annual wind, rain and dry time roses. These roses present the distribution of the wind speed, rainfall and dry time periods without rainfall over specific classes and wind directions. The direction of rainfall and dry time are assumed to be equal to those of the wind speed. The dominant wind directions are from south to west. The dry periods with duration longer than 30 hours are dominant resulting in a decreasing moisture content (upper layer of 20 mm) to below 2%. The annual-average rainfall at weather station De Kooy near the beach of Callantsoog is about 763 mm in about 585 hours (about 7% of the total time per year). Thus, the annual-average rainfall intensity is 763/585=1.3 mm/hour. There are about 200 rainfall events per year (evenly spread over the seasons) with average duration of 585/200≅3 hours. Wind and rain data in February, May, August and December are given in **Table 5**.

Month	**Duration of wind in 4 classes**				**Rainfall data**			
	0-5 m/s	**5-9 m/s**	**9-15 m/s**	**> 15 m/s**	**total mm**	**duration hours**	**dry time > 5 hrs**	**dry time > 30 hrs**
February (673 hrs)	310 hrs 46%	270 hrs 40%	85 hrs 13%	4.7 hr 0.7%	44 mm	57 hrs 8%	480 hrs 70%	245 hrs 35%
May (736 hrs)	450 60%	255 35%	35 5%	0 0%	59	34 5%	575 80%	360 50%
August (735 hrs)	465 63%	230 30%	35 5%	0.6 <1%	92	45 6%	540 75%	300 40%
December 740 hrs)	310 42%	275 37%	150 20%	6.1 0.8%	73	70 10%	455 60%	190 25%

Table 5 *Wind and rain data of 4 characteristic months (February, May, August and December); Station De Kooy (2009-2019)*

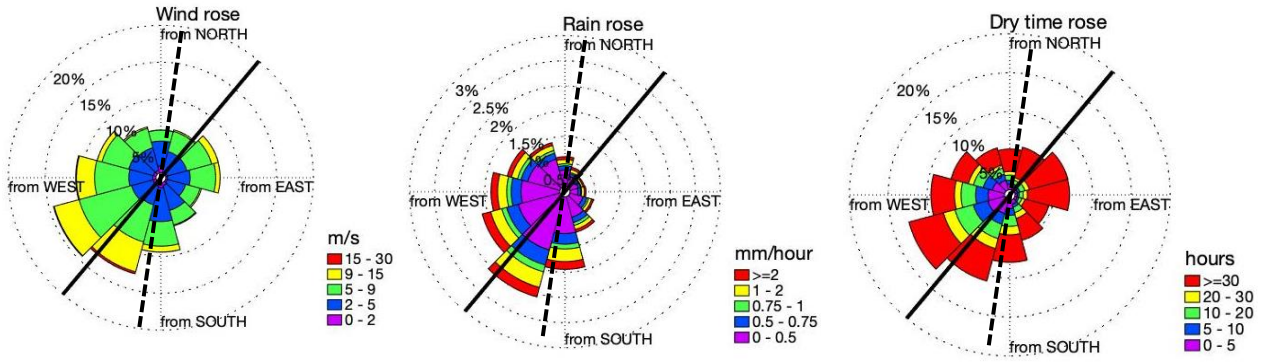

Figure 11 *Wind, rain and dry time roses; annual-average values 2009-2019; Station De Kooy, The Netherlands (black dashed line is local coastline line at Callantsoog beach)*

The rainfall intensity (mm) is lowest in February and highest in August. The duration of the rainfall is lowest (5% of the time) in May, and highest (10% of the time) in December. In the winter month February, the periods with dry weather longer than 30 hours (required to reduce the moisture content of the upper beach layer of 20 mm to 2%) occur during about 35% of the time. Thus, reasonably dry beach sand available for wind transport occurs during about 35% of the time in February. In the summer month August, the periods with dry weather longer than 5 hours (required to reduce the moisture content of the upper beach layer of 20 mm to 2%) occur during about 75% of the time. Thus, reasonably dry beach sand available for wind transport occurs during 75% of the time in August

The percentage of time over a full year with restricted transport can be determined as follows. There are about 200 rainfall events (per year) with duration of about 3 hours; each rainfall event is followed by a drying period of 5 to 10 hours in spring to summer and 20 to 30 hours in autumn to winter resulting in a total period with restricted sand transport of 200/2x(3+0.5(5+10)) + 200/2x(3+0.5(20+30))=3850 hours (with moisture levels in the range of 2% to 8%). Thus, the percentage of time over a full year with restricted sand transport is about 3850/(365x24) x 100%≅45%. This means that the effect of rainfall on wind transport is meaningful, but not dominant. Most of the time (55%), the beach is sufficiently dry for unrestricted or slightly restricted sand transport.

The wind and rain climate for each of the 4 months are schematized in 24 events with constant wind velocity, direction and rainfall based on available data (Van Rijn 2021). The rainfall intensity is not used, as it is assumed that the splash-type sand transport during rainfall is negligibly small. Unknown parameters are the duration of the drying period, the percentage of dry and moist spots at the beach in the drying period, and the moisture content of the moist spots. The effect of these parameters was studied by defining various scenarios given in **Table 6**. Annual-integrated values are obtained by assuming that each month is representative for a season of 3 months.

Case 0 is the base case assuming dry sand during all seasons resulting in a dune-ward sand transport of 36 m^3/m/year. A similar run based on a more detailed wind table with 96 wind conditions yields a value of 35 m^3/m/day, which means that the simplified wind table with 24 events is sufficiently accurate.

Case 1A assumes that there is no transport during rainfall and no restricted sand transport in the drying period resulting in a transport reduction of about 10%.

Case 3A is an extremely conservative case resulting in a transport reduction up to 35%. The transport reductions are relatively high in the wetter months and smaller in the drier months of May and August. The net annual dune-ward transport is about 36 m^3/year for the base case (neglecting rainfall effects) and about 23 m^3/year for the most conservative case (scenario). The net annual alongshore transport to the North is about 52 m^3/m/year for the base case and 33 m^3/m/year for Case 3A. The net alongshore transport is significantly higher than the dune-ward transport of sand, which is caused by the dominant winds from the south-west direction.

Measured annual deposition values at the dune front due to onshore-directed wind transport at the beach of Callantsoog are in the range of 7.5 to 15 m³/year based on annual dune migration rates of 0.5 to 1 m/year and dune height of 15 m (Mulder and Tonnon, 2011). Thus, the predicted onshore values in the range of 23 to 33 m³/m/year are somewhat too high (over-predicted). Overprediction may occur as the wind data have been taken from an inland station neglecting the wind modification effects as represented by Equation (5). De winter et al. (2020) have shown that the onshore winds at a beach backed by high foredunes are substantially reduced.
Finally, these wind speed modification effects are included (Cases 1B to 3C) based on Equation (5). The beach winds are higher than those from an inland regional station and lower due to presence of the high foredune (obstacle effect). The wind velocities at the beach are assumed to be 10% higher than those at the inland station De Kooy (f_r=1.1). The $f_{o,m}$ value related to the obstacle effect is varied in the range of 0.7 (strong effect) to 1 (no effect). The annual dune-ward transport reduces significantly (about 35% to 70%) for the Cases 1B, 2B and 3B by including the wind modification effects. The obstacle effect alone gives a reduction of about 50% from 23 (Case 3A) to 11 (Case 3C) m^3/m/year. This reduction of 50% is much stronger than the maximum reduction of 35% related to moisture effects (Case 0 and Case 3A). The reduction of about 50% related to the obstacle effect emphasizes the importance of long term wind measurements at the beach for accurate estimations of the annual wind transport towards the dunes. Wind data taken from an inland station without corrections lead to significant errors (overprediction of 50%). The most realistic case is 3B yielding a net dune-ward sand transport of 17 m^3/m/year at Callantsoog beach, which is somewhat higher than the sand transport rate associated with annual dune migration (7.5 to 15 m^3/m/year).
Similar computations have been made for the storm month of February 2002 (Van Rijn 2021). The dune-ward sand transport in the storm month February 2020 is found to be 5 to 10 m³/m/month (including all effects), which is much higher (factor 5) than the value of about 1 to 2 m^3/m/month in a normal month of February. During the field measurements in February 2020 at the beach of Callantsoog, observed local deposition values at the dune toe were in the range of 3 to 5 m³/m over 3 weeks, which is of the same order of magnitude as the predicted duneward sand transport.

Cases	**Predicted annual sand transport in duneward direction (m³/m/year)**	**Predicted net annual sand transport in alongshore direction (m³/m/year)**
0. No effect of rainfall and moisture; no wind modification	36	52
1A. Rainfall effect: no transport during rainfall and no restricted sand transport in the drying period; no wind modification (f_r=1; $f_{o,m}$=1)	33 (-10%)	45 (-15%)
2A. Rainfall effect: relatively short drying period; low percentage of moist spots (<50%); low moisture levels (<4%) during the drying period; no wind modification (f_r=1; $f_{o,m}$=1)	26 (-25%)	37 (-30%)
3A Rainfall effect: relatively long drying period; high percentage of wet spots (>50%); high moisture levels (>4%) during the drying period; no wind modification (f_r=1; $f_{o,m}$=1)	23 (-35%)	33 (-35%)
1B. Rainfall same as Case 1A + wind modification effects (f_r=1.1; $f_{o,m}$=0.7)	24 (-35%)	49 (-2%)
2B. Rainfall same as Case 2A + wind modification effects (f_r=1.1; $f_{o,m}$=0.7)	20 (-45%)	42 (-20%)
3B. Rainfall same as Case 3A + wind modification effects (f_r=1.1; $f_{o,m}$=0.7)	17 (-50%)	39 (-20%)
3C. Rainfall same as Case 3A + wind modification effects (f_r=1.0; $f_{o,m}$=0.7)	11 (-70%)	25 (-50%)

Table 6 *Predicted annual sand transport for various cases at beach Callantsoog*

7. Summary and conclusions

This paper is a continuation of earlier work (part 1 and part 2) on the prediction of sand transport of dry and moist sand at natural beaches. A new trap-type instrument (LVRS-sampler) for measuring the sand transport rate of sliding, rolling and saltating particles at beaches was designed and used at many sites in Belgium and The Netherlands. The instrument functioned well without any signs of scour influencing the trapping of moving particles. A short mast equipped with three mini wind cup meters was used to measure the velocity distribution in the lowest 1 m of the boundary layer. In all, 81 new data sets of aeolian sand transport for dry and moist beach surface conditions were obtained using the new equipment. Two prediction methods were evaluated: the modified Bagnold-transport equation and the new VR-transport equation. The wind tunnel data of Belly (1964) have been used to calibrate this latter new method (Part 2). The new field data (81) and older field data (48) from the literature were used to determine the prediction skills of the two methods. Finally, the new VR-method was applied to calculate the annual aeolian sand transport on a Dutch beach using data of wind velocities and rainfall intensity from a local weather station.
The main findings of the study are:

- The new LVRS-trap sampler was used to measure aeolian transport at dry and moist beaches in conditions with wind speeds up to 19 m/s (BF9). The new data are in good agreement with the older data of Sarre (1988). The power of 3 relationship between transport and wind speed is proved to be valid for low and high wind speeds.
- Field data of sand transport show that the effect of moisture is minor for storm events with wind velocities higher than 10 m/s, which can be explained by the entrainment of sand from drier spots setting moist sand into motion (sand blasting effect). For wind speeds below 10 m/s the sand transport at field sites is slightly restricted in moist conditions.
- The sand transport rate is strongly reduced when the beach surface is covered with a significant amount of coarse materials (gravel and shells). Gravel has a more pronounced effect than shells. A high percentage of gravel will lead to beach armoring, at observed at the Prins Hendrik beach site on the island of Texel.
- The results of new VR-sand transport equation show good agreement with the measured sand transport rates in field conditions. About 87% of the predicted values are within a factor of 2 of the measured values for dry sand and about 91% for moist sand using the same calibration coefficients as found for the laboratory data of Belly (1964).
- A new method for the inclusion of moisture effects during and after rainfall is proposed and used for the calculation of annual aeolian transport at a Dutch beach based on measured wind speed, direction and rainfall from a nearby weather station. The annual transport to the dunes is reduced by about 35% by including the moisture effect due to rainfall. The annual transport towards the dunes is reduced by about 50% by including wind modification effects and by about 70% if both effects (moisture and wind modification) are included.

Finally, some recommendations are given with respect to the parameters to be measured during field work: at least three wind velocities at defined heights above the surface; fetch length; time period since last rainfall; d_{50}, d_{90} and percentage of coarse materials (> 2 mm) of local sand surface; bed form height and length; percentage of moist spots (darker colour) in upwind area (100x100 m^2); moist content of upper 20 mm of moist spots (space-averaged value); vegetation cover and vegetation height in upwind area (100x100 m^2).

Acknowledgements
The Dutch water board Hoogheemraadschap Hollands Noorderkwartier (HHNK) and the Belgian marine contractor Jan De Nul Group are gratefully acknowledged for providing funds and logistics for this study.

References

Bagnold, R.A., 1937. The transport of sand by wind. Geographical J. Vol. 89, 409–38

Bagnold, R.A. 1941, 1954, 1973. The physics of blown sand and desert dunes. Methuen, New York.

Bauer, B.O., Davidson-Arnott, R.G.D., Walker, I.J., Hesp, P.A., Ollerhead, J., 2012, Wind direction and complex sedi-ment transport response across a beach-dune system. Earth Surface Processes and Landforms, 37, 1661–1677. https://doi.org/10.1002/esp.3306

Belly, P.Y., 1964. Sand Movement by Wind. U.S. Army Corps of Engineers, Technical Memorandum No 1, CERC, Washington, DC.

Campos, L.A.D., 2018. Quantification methods for aeolian sand transport on beaches. Doctoral Thesis, University of Twente, The Netherlands. Doi: 10.3990/1.9789036546676

Comola, F., Kok, J.F., Chamecki, M. and Martin, R.L., 2019. The intermittency of wind-driven sand transport. Geophysical Research Letters, Vol. 46, 13, 13,430-13,440. Doi: 10.1029/2019GL085739

De Winter, W., Donker, J., Sterk, G., Van Beem, J. and Ruessink, G., 2020. Regional versus local wind speed and direction at a narrow beach with a high and steep foredune. PlosOne (15(1) e-0226983; doi.org/10.1371/journal.pone.0226983

Durán, O., Claudin, P. and Andreotti, B. 2011. On aeolian transport: grain-scale interactions, dynamical mechanisms and scaling laws. Aeolian Research. Vol. 3, 243–70

Einstein, H.A., 1950. The bed-load function for sediment transportation in open channel flow. Technical Bulletin No. 1026, U.S Department of Agriculture, Washington D.C., USA

Ellis, J.T., Li, B., Farrell, E.J. and Sherman, D.J., 2009. Protocols for characterizing aeolian mass-flux profiles. Aeolian Research 1, 19-26

Grass, A.J., 1970. Initial instability of fine sand bed. Journal of the Hydraulic Division, ASCE, Vol. 96, No. HY3, 619, 632

Ho, T., 2012. Experimental study of saltating particles in a turbulent boundary layer. Doctoral Thesis, University of Rennes, France

Hesp, P.A., Davidson-Arnott, R.G.D., Walker, I. Ollerhead, J., 2005. Flow dynamics over a foredune at Prince Edward Island, Canada. Geomorphology, 65, 71–84. https://doi.org/10.1016/j.geomorph.2004. 08.001

Jackston, N.L. and Nordstrom, K.F., 1997. Effects of time-dependent moisture content of surface sediments on aeolian transport rates across a beach Wildwood, New Yersey, USA. Earth Surface Processes and Landforms, Vol. 22, 611-621

Jelgersma. S, De Jong, J, Zagwijn, W.H. and Van Regteren Altena, J.F., 1970. The coastal dunes of the western Netherlands; Geology, Vegetational history and Archaeology. Rijks Geologische Dienst RGD, Mededelingen Nieuwe Serie Vol. 21, 93-167

Kalinske, A.A., 1947. Movement of sediment as bed load in rivers. Trans. American Geophysical Union, Vol. 128, No. 4, USA

Kawamura, R., 1951. Study of sand movement by wind. Rep. Inst. Sci. Technol. Vol. 5, 95–112.

Kok, J.F., Parteli, E.J.R., Michaels, T.I. and Karam, D.B.., 2012. The physics of wind-blown sand and dust. Rep. Prog. Phys. Vol. 75, Doi:10.1088/0034-4885/75/10/106901

Martin, R.L., Barchyn, T.E., Hugenholtz, C.H. and Jerolmack, D.J., 2013. Timescale dependence of aeolian sand flux observations under atmospheric turbulence. Journal of Geophysical Research: Atmospheres, Vol. 118, 9078-9092. Doi:10.1002/jgrd.50687

Martin, R.L. and Kok, J.F., 2017. Wind-invariant saltation heights imply linear scaling of aeolian saltation flux with shear stress. Science Advances Vol. 3 (6). Doi: 10.1126/sciadv.1602569

Martin, R.L. and Kok, J.F., 2018. Distinct thresholds for the initiation and cessation of aeolian saltation from field measurements. Journal of Geophysical Research: Earth Surface, Vol. 123, 1546-1564. Doi: 10.1029/2017JF004416

Martin, R.L., Kok, J.F., Barchyn, T.E., and Chamecki, M. 2018. High-frequency measurements of aeolian saltation flux: field-based methodology and applications. Aeolian Research. Doi: 10.1016/j.aeolia.2017.12.003

Meyer-Peter, E. and Mueller, R., 1948. Formulas for bed-load transport. Sec. Int. IAHR Congress, Stockholm, Sweden
Mulder, J. and Tonnon, P.K. 2011. Sand engine: background and design of a mega-nourishment pilot in The Netherlands. www.researchgate.net/publication/49115511
Owen, P.R., 1964. Saltation of uniform grains in air. Journal of Fluid Mechanics, Vol. 20, 225-242
Pähtz, T. and Durán, O., 2018. The cessation threshold of non suspended sediment transport across aeolian and fluvial environments. Journal of Geophysical Research: Earth Surface, Vol. 123, 1638–1666. Doi.org/10.1029/2017JF004580
Pähtz, T. and Durán, O., 2020. Unification of aeolian and fluvial sediment transport rate from granular physics. Physical Review Letters. Doi: 10.1103/PhysRevLett.124.168001
Pähtz, T., Liu, Y., Xia, Y., Hu, P., He, Z. and Tholen, K., 2021. Unified model of sediment transport threshold and rate across weak and intense subaqueous bedload, windblown sand, and windblown snow. Journal of Geophysical Research: Earth Surface, Vol. 126. Doi. org/10.1029/2020JF005859
Paintal, A.S., 1971. Concept of critical shear stress in loose boundary open channels. Journal of Hydraulic Research, Vol. 9, No. 1
Pool, M.A. and Van der Valk, L., 1988. Volume computation of the Holland and Zeeland young dunes (in Dutch). Kustgenese, Taskgroup 1000, Report BP10705, RGD, Haarlem, The Netherlands
Pye, K. and Tsoar, H., 2009. Aeolian sand and sand dunes. Springer. Doi: 10.1007/978-3-540-85909-3
Sarre, R.D., 1988. Evaluation of aeolian sand transport equations using intertidal zone measurements, Saunton Sands, England, Sedimentology, Vol. 35, 671-679
Sherman, D., Ellis, J.T., Li, B., Farrell, E.J., Maia, P. and Granja, H.M., 2013. Recalibrating aeolian sand transport models. Earth Surface and Landforms, Vol. 38, 169-178. Doi: 10.1002/esp.3310
Sherman, D.J., Swann, C. and Barron, J.D., 2014. A low-cost aeolian sand trap. Aeolian Research, Vol. 13, 31-34.
Stout, J. E., and Zobeck, T. M., 1997. Intermittent saltation. Sedimentology, Vol. 44 (5), 959–970
Strypsteen, G., 2019. Monitoring and modelling aeolian sand transport at the Belgian coast. Doctoral Thesis, KU Leuven, Belgium.
Strypsteen, G., Van Rijn, L.C., Hoogland, M.D., Rauwoens, P., Fordeyn, J. and Hijma, M.P. 2021. Reducing aeolian sand transport and beach erosion by using armour layer of coarse materials. Coastal Engineering, Vol. 166, 103871
Ungar, J.E. and Haff, P.K., 1987. Steady state saltation in air. Sedimentology, Vol. 34, 289-299
Van Rijn, L.C., 1993. Principles of sediment transport in rivers, estuaries and coastal seas, Part I and II. AquaPublications, The Netherlands (www.aquapublications.nl)
Van Rijn, L. C., 2021. Aeolian sand transport; field measurements and model predictions for dry and moist beaches. www.leovanrijn-sediment.com (free download)
Van Rijn, L.C. and Strypsteen, G., 2020. A fully predictive model for aeolian sand transport. Coastal Engineering, Vol. 156
Wiggs, G.F.S., Livingstone, I., Warren A., 1996. The role of streamline curvature in sand dune dynamics: evidence from field and wind tunnel measurements. Geomorphology,17,29–46. https://doi.org/10.1016/ 0169-555X(95)00093-K
Wiggs, G.F.S., Baird, A.J. and Atherton, R.J., 2004. Thy dynamic effects of moisture on the entrainment and transport of sand by wind. Geomorphology 59, 13-30